AN ACTIVE SYSTEM FOR THE DETECTION OF SPECIAL FISSILE MATERIAL IN SMALL WATERCRAFT

A Thesis

by

NORMAN ALFAN JOHANSEN, III

Submitted to the Office of Graduate Studies of
Texas A&M University
in partial fulfillment of the requirements for the degree of

MASTER OF SCIENCE

August 2006

Major Subject: Nuclear Engineering

AN ACTIVE SYSTEM FOR THE DETECTION OF SPECIAL FISSILE MATERIAL IN SMALL WATERCRAFT

A Thesis

by

NORMAN ALFAN JOHANSEN, III

Submitted to the Office of Graduate Studies of
Texas A&M University
in partial fulfillment of the requirements for the degree of

MASTER OF SCIENCE

Approved by:

Chair of Committee,	William S. Charlton
Committee Members,	Ron R. Hart
	Donald G. Naugle
Head of Department,	William E. Burchill

August 2006

Major Subject: Nuclear Engineering

ABSTRACT

An Active System for the Detection of Special Fissile Material in Small Watercraft.

(August 2006)

Norman Alfan Johansen, III, B.S., The University of Tennessee

Chair of Advisory Committee: Dr. William S. Charlton

Due to increasing terrorist threats and illegal proliferation of nuclear material and technology, there is a need for increased research in the area of detection of smuggled fissile material, some of which is designated by the International Atomic Energy Agency as special fissile material. This thesis focuses on a hypothetical scenario in which a terrorist organization has managed to smuggle an amount of special fissile material onto a personal recreational watercraft and sail it into a marina. If the boat could be forced to go through a detector system, then the contents could be interrogated and a determination made of whether any special fissile material was aboard. This thesis examines the hypothesis that active interrogation may be used successfully in the detection of special fissile material in such an environment. It shows that it is feasible to use an active neutron system to detect a significant quantity of special fissile material onboard a small boat via the differential die-away technique. The MCNP Monte Carlo transport code was used to simulate the use of a pulsed neutron generator to induce fission in the fissile material and then estimate the detector response. The detector modeled was based on elastic scattering-induced recoil protons using pure hydrogen gas. There was a significant difference between the system with and without the presence of fissile material, and the estimated detector response for

the system with fissile material present was shown to be sufficiently greater than the response due to background radiation only. Additionally, dose was estimated and found to be small enough that the system would not likely pose a significant radiological health risk to passengers on the boat.

ACKNOWLEDGMENTS

First, I would like to thank my family and friends back home for their years of encouragement and support, often giving me a lot more credit than I thought I deserved.

Next, I thank my advisor, Dr. Bill Charlton, for his guidance and patience with me. Thanks for helping me get through this research and for taking me on as a student.

I would like to thank my committee members, Drs. Ron Hart and Don Naugle, for being a part of this work.

Special thanks goes to Dr. Ron Hart and the former Department Head of Nuclear Engineering at Texas A&M, Dr. Alan Waltar. It is because of them that I chose to come to Texas A&M.

I also owe a great deal of appreciation to a number of my friends since coming to A&M. I'd like to thank Alex for spending many long hours in discussion with me about this research… a few of your ideas actually worked. For studying with me at all hours of the day and night, and helping fill in the gaps of my understanding of baseball, college football, and nuclear engineering, thank you, Teresa. I also thank my friends for their help in a variety of ways: Jon, Vittorio, Luca, Avery, Amy & Alex, and Cable.

This research was performed under appointment to the U.S. Department of Energy Nuclear Engineering and Health Physics Fellowship Program sponsored by the U.S. Department of Energy's Office of Nuclear Energy, Science, and Technology.

NOMENCLATURE

DDT	Differential die-away technique
eV	Electronvolt
FM	Fissile material
HEU	Highly enriched uranium
IAEA	International Atomic Energy Agency
keV	kiloelectronvolt
kV	kilovolt
MCNP	Monte Carlo N-Particle
MeV	Megaelectronvolt
NAA	Neutron activation analysis
NDA	Non-destructive analysis
PNG	Pulsed neutron generator
SF	Spontaneous fission
SFM	Special fissile material
SQ	Significant quantity
WG	Weapons-grade

TABLE OF CONTENTS

Page

Page

Page

LIST OF FIGURES

Page

Page

Page

LIST OF TABLES

Page

Page

CHAPTER I

INTRODUCTION

Due to increasing terrorist threats and illegal proliferation of nuclear material and technology, there is a need for increased research in the area of detection of smuggled fissile material (FM), some of which is designated special fissile material (SFM). Such SFM, as defined by the International Atomic Energy Agency (IAEA) [1], includes uranium enriched greater than 20 percent of ^{235}U and any amount of ^{239}Pu. One of the most common methods to detect SFM is non-destructive analysis (NDA), where materials may be interrogated and identified without destroying the container in which they are enclosed. One such technique uses neutrons to react with the material and then analyzes the resulting neutron radiation from the reactions. Such techniques are already in use for SFM detection in laboratory settings as well as some controlled environments such as cargo container [2] and package [3, 4] screening, but there is another scenario on which this thesis research focuses. This scenario involves field detection of smuggled SFM on small watercraft.

I.1. A brief discussion of nuclear smuggling

The threat of nuclear smuggling is serious and very real. The end of the Cold War has seen an unfortunate decline in nuclear materials safeguards and accountability in Russia and the other former Soviet republics. These fledgling independent nations have been the targets of rogue nations and terrorist organizations seeking to acquire the knowledge and materials to build nuclear weapons. Economic decline in these states has also spurred illegal sales and transportation of radioactive material by turning scientists, workers, and even

This thesis follows the style of Nuclear Instrumentation and Methods in Physics Research B.

security personnel, whose jobs it had been to protect nuclear materials, into purveyors of nuclear weapons. These conditions have created a lucrative market where someone with access to nuclear materials can easily sell their holdings to anyone with sufficient money and temerity to make a purchase.

There have been several examples of lax security and records of theft of nuclear material from the former Soviet republics. One prominent example of the legacy of abandoned nuclear materials occurred between 1992 and 1994 at the Ulba Metallurgy Plant in Ust-Kamenogorsk, Kazakhstan, culminating in the execution of a secret operation known as Operation Sapphire [5]. During the Soviet regime, the plant had manufactured nuclear fuel for the Soviet navy. In the late 1980's, when the Soviets vacated the facility, the site was left largely unattended. Then in 1992, during a trip to the plant, the newly-appointed Kazakhstani Atomic Energy Director Vladimir Shkolnik discovered a cache of discarded highly-enriched uranium (HEU) estimated at 1,278 pounds. After first contacting their counterparts in Russia to return the material, the Kazakhstanis then informed the U.S. ambassador to Kazakhstan, Bill Courtney, in 1993 of the situation and requested help from the United States. The U.S. agreed and in October-November 1994 sent teams from the Departments of State, Defense, and Energy to the defunct metallurgy plant to remove the HEU and bring it back to the Y-12 plant at Oak Ridge National Laboratory in Tennessee at a cost of $25 million, $20 million of which went directly to the Kazakhstani government.

Upon arriving in Ust-Kamenogorsk, the teams found security woefully absent and were able to enter the site using an ordinary bolt cutter. The HEU was loaded into 1,300 canisters, placed onboard U.S. Air Force C-5 Galaxy cargo planes, and flown back to the United States. As an example of how poorly the accounting of material was, upon arrival at

Oak Ridge, U.S. Department of Energy personnel tallied more than 120 pounds of material greater than what the Kazakhstanis had declared. In the nearly two years between the discovery of the unguarded, abandoned material and its transportation back to the U.S., there was an ample window of opportunity for material to have been stolen and transported out of Kazakhstan.

Another example of nuclear theft is the account of Leonid "Yuri" Smirnov, a worker at the Luch Scientific Production plant. Located twenty-five miles south of Moscow, Luch was a facility that produced reactors for the former Soviet Union space program. Over a period of four months in 1992, Smirnov pocketed 50-70 grams of HEU at a time in vials that he took home with him everyday. In a 1996 interview with *Frontline* on PBS [6], he said he concocted the idea for stealing and selling the HEU after reading an article in a local newspaper in which thieves had managed to steal 1,200 grams of uranium. There were certain "irretrievable losses" the plant management expected and therefore accepted as lost material. One of Smirnov's duties at the plant was to weigh and track material moving through the line. Thus, he knew the amount of unaccounted material at any given time and removed only enough material to stay within those limits. When asked if he ever felt in danger of being caught, he replied, "No… who would suspect me? Such an idea never occurred to any of our workers… The vial was so small and no one searched our bags. No detectors." When asked why he stole the HEU, he said that he thought he could get about $500 for it, enough to buy a new refrigerator, stove, and other items for his family. It may not seem like a lot of money, "but that was [his] salary for two years."

His arrest at the train station in Podolsk was purely coincidental, but serendipitous nonetheless. At the station, he happened upon his neighbor with a group of friends from

their factory. The police at the station received a tip that the men had stolen batteries from the factory at which they worked and arrested them along with Smirnov, though he had no part in the battery scheme. During questioning, the police were drawn to his lead containers, at which time he immediately confessed his plan. He served a few weeks in jail and was sentenced to three years probation. In total, Smirnov had about 1.5 kilograms of 90 percent enriched uranium with him.

There have been literally thousands of instances of attempted smuggling of nuclear material throughout the world, and these are only the reported cases. In July 1994, a Russian navy captain and his civilian brother were arrested while attempting to sell ten pounds of Russian naval reactor HEU [5]. In May 1994, German police found 5.6 grams of supergrade plutonium (greater than 97 percent ^{239}Pu) in the garage of a suspected counterfeiter. It was determined the material likely came from a Russian weapons laboratory. In the first three years after the fall of the Soviet Union, German authorities reported more than seven hundred cases of attempted sales of nuclear materials, with only sixty of those involving seizures of nuclear materials [5]. Russian customs officials reported more than five hundred instances of illegal transportation of nuclear and radioactive materials across Russian borders in 2000 alone [5]. In 2002, enough material for three nuclear weapons was recovered from the largely vacated Vinca Institute of Nuclear Science where workers would clock in at the beginning of the day and then sneak out to work second jobs [5]. Not even the United States is immune to the loss of nuclear material. Although an accurate figure has never been disclosed, the Department of Defense has admitted to a number of accidents, including loss, involving nuclear weapons [5].

In total, there are tens of thousands of nuclear weapons and millions of pounds of nuclear material under weakened, insufficient, or even non-existent security measures. Even under excellent material accountability of greater than 99 percent, there is still potential for the loss of hundreds of weapons worth of weapons-usable material. To ignore the possibility that terrorists or other rogue nations could steal material, manufacture it into even a crude, but working, nuclear weapon and smuggle it into the United States by any means available would be a grave mistake.

I.2. Statement of problem and research objectives

This thesis centers around a hypothetical scenario in which a terrorist group has managed to smuggle an amount of SFM onto a seagoing cargo ship. The terrorist group has someone with access to a personal recreational watercraft (such as a sailboat or small powerboat) go to the cargo ship, load the material onto the small boat, and sail it back into a marina, thus successfully smuggling the material ashore. If the boat could be forced to go near a detector system, the contents could be interrogated and a determination made of whether any SFM were aboard.

The overall objective of the research is to test the hypothesis that active interrogation may be successfully used in the detection of SFM in personal recreational watercraft, such as sailboats and small powerboats. For active interrogation to be feasible there must be a statistically significant difference between the radiation signatures that are to be measured from the system with and without the presence of a quantity of SFM. The

SFM quantities of interest here is slightly less than one significant quantity (SQ[1]) of highly enriched uranium or plutonium. The SQ definition is based on an estimated minimum amount of material needed to make a nuclear weapon, but it is possible to make a usable device using less than one SQ of material. This research also attempts to differentiate between HEU and plutonium in the hypothetical scenario posed.

There are several potential barriers to the success of this research. First, the geometry of the configuration presents a substantial problem. The source is isotropic, or evenly distributed in all directions away from the source location. The SFM was modeled in a spherical shape with diameters of 8.5 cm and 13.5 cm for plutonium and uranium, respectively. Given the isotropic source, and assuming isotropic neutron scattering, the result is that only a small percentage of the source neutrons will interact with the SFM sphere. Then, assuming isotropic fissioning in the SFM sphere, only a small percentage of the fission neutrons will pass through the detector.

Another hindrance comes from the source itself. A large fraction of the source particles never interact with the SFM but make it through the boat and water into the detectors. The source effectively becomes the driver of background radiation in the system since it produces neutrons that individually are indistinguishable from those coming from the SFM.

Another obstacle discussed here is the role of thermalization in the system. The source neutrons are high-energy (either 2.5 MeV from D-D reactions or 14 MeV from D-T reactions), so they can penetrate the water between the source and the walls of the boat.

---

[1] The IAEA defines 1 SQ of SFM as 8 kg of Pu or any amount of HEU containing at least 25 kg ^{235}U [1].

Ideally, the source neutrons would be thermalized to maximize fission production, but that may not be possible in field application, and higher energy neutrons would be required to penetrate other materials that would be present in a real world scenario. The cross section for most neutron reactions in most detector materials is orders of magnitude greater for thermal than for fast neutrons, thus in most detection scenarios it would be beneficial to thermalize the fission neutrons, since the average energy of prompt fission neutrons is about 2 MeV. Water, however, tends to attenuate neutrons as well as thermalize them, so higher energy neutrons increase the chance of neutrons reaching the detectors. Since these competing mechanisms complicate the design of such a system, some sort of optimization is necessary and is discussed later.

The final complication is the natural presence of background neutrons from cosmic ray interactions in the atmosphere. Though the total flux is low compared to the active source considered in the current research, its contribution to the neutron field after the source neutrons have escaped the system may be comparable, and thus significant, to that of the fission neutrons being detected.

I.3. Comparison of NDA techniques

There are two general categories of NDA: passive and active. A comparison of these methods favors active detection in the posed scenario, though a combination of both could also prove beneficial. Passive interrogation utilizes the natural radioactivity of material for detection. As such, passive methods are often preferred because they require less equipment, usually only a detector setup, and pose less of a radiological hazard to the personnel operating the equipment. Active interrogation, however, requires the use of a

radiation source that can be unwieldy and pose a greater radiological hazard thus often prohibiting field application. Neutron generators require power supplies and a compliment of electronics to run the system. As such, a generator used in the field would be subject to collisions and environmental damage and would have to be rugged enough to withstand its environment, which usually results in the system being even larger. There are, however, currently available portable neutron generators weighing as little as 25 pounds, and with some modification may be suitable in the situation posed by this thesis. The primary benefit of active NDA is that far more particles are created in a much shorter amount of time, allowing for rapid detection and response capabilities where passive NDA would otherwise not be able to make any determination.

Both uranium and plutonium are naturally radioactive making each a potential candidate for passive interrogation methods. On the other hand, both materials respond to neutron bombardment by emitting additional neutron radiation making active interrogation a good possibility. A detailed discussion of the naturally occurring and induced radioactivity of both elements is included in Section *II.5*.

A common method of active interrogation is neutron activation analysis. This method uses a neutron source directed at the material under investigation to induce some reaction. The most likely reaction of use for HEU and plutonium is fission, in which additional neutrons are produced.

Neutron detection can utilize the fact that most prompt fission neutrons are slowed down by scattering reactions and are slightly delayed in reaching the detector. This delay allows SFM to be detected rapidly – on the order of milliseconds – with relatively little activation of the material, the exposures lasting on the order of microseconds. For example,

a series of 10 μs bursts of neutrons could be shot at a package containing SFM with a delay time of several milliseconds between each pulse. The prompt fission neutrons would still be emitted hundreds of microseconds or even milliseconds after each burst ended due to the slowing down time of the source neutrons. The neutrons detected between such pulses are known as die-away neutrons, and such a method is known as the differential die-away technique, or DDT.

I.4. Literature review

Currently, there have been developed several NDA techniques for the detection of SFM, but there is little information regarding the detection of SFM in a marine environment. For the rapid inspection of small packages, such as personal luggage at an airport or delivery packages, there have been systems developed utilizing active neutron analysis [3,4]. These systems used a pulsed neutron generator (PNG) to induce fission and then counted the resulting prompt fission neutrons. Additionally, there are systems that utilize passive methods of NDA for the detection and assay of SFM [7] and others that use a combination of active and passive techniques [8].

The combined passive/active system presented by Veilleux [8] proved very sensitive, detecting SFM quantities down to 0.1 g, but required several minutes of time to assay the target. The passive system presented by Armitage *et al* [7] offered adequate detection of SFM, but it also required several detectors surrounding a container to greatly increase the detection area, a feature likely unavailable in the hypothetical scenario. Of all the systems presented, only the active neutron package monitor proved accurate detection

in an acceptable amount of time, less than 30 seconds in some cases [3]. Given the current research, a combination of active and passive techniques may prove useful.

I.5. Theory

This section discusses the various methods used for neutron radiation detection as well as a description of the differential die-away technique commonly used in the detection of SFM. Specifically, three methods of fast neutron detection are discussed, including each method's applicability to the posed scenario, from which a determination is made for a specific detection method to model.

I.5.1. Fast neutron detection

There are three general methods for detecting fast neutrons. First are counters based on neutron moderation. Next are detectors based on fast neutron induced reactions. Lastly are detectors that utilize fast neutron scattering. What follows is a brief discussion of each method along with its potential practical use in the proposed scenario.

I.5.1.1. Detection based on neutron moderation

The first category of fast neutron detection contains methods based on neutron moderation. Most fast neutron detectors are inherently less efficient than thermal neutron detectors due to the rapidly decreasing interaction cross sections with increased neutron energy. Hydrogenous material surrounding a slow neutron detector system could slow down the fast neutrons to a speed at which the detection efficiency is much greater. It would seem reasonable to think increasing the thickness of the moderator material would subsequently increase the overall detection efficiency. However, this is not the case, since competing with thermalization of the fast neutrons is absorption of the neutrons in the

moderating material. Slow neutrons are easily absorbed in the moderating material, so if enough moderating material is present, then eventually none of the impinging neutrons will reach the detector. Thus, the thickness of moderator can be optimized to maximize the detection efficiency based on the energy of impinging neutrons. This optimal thickness, however, pertains only to a given energy. For neutrons within an energy continuum, an optimum thickness is more difficult to obtain and may preclude the possibility of using such a method in practical field applications.

Another hindrance to the thermalization method is the time it takes to collect counts. Fast neutrons must first undergo several collisions before becoming thermalized, and then must diffuse as thermal neutrons and face absorption in the moderating material. Because of these physical processes, more time is required to accumulate counts than if the neutrons were being detected directly. Since rapid detection is important in the posed scenario, the additional time adds to the difficulty of implementing this particular method.

I.5.1.2. Detection based on fast neutron induced reactions

Fast neutron induced reactions make use of direct nuclear reactions between fast neutrons and the target nuclei of the detector. As such, they do not have the time delay associated with "transforming" the fast neutron into a thermal neutron. However, the great disadvantage of this method is that the associated cross sections tend to be orders of magnitude less than the corresponding thermal counterparts. The two major reactions of this type are the $^{6}Li(n,\alpha)$ and $^{3}He(n,p)$ reactions. Lithium may be used in a variety of arrangements, all of which involve either a glass or a crystal configuration. These rather brittle configurations, while well suited for a laboratory environment, are likely too sensitive to the hazards of the field environment in which they would be employed, and as such are

not considered here. The second reaction based on helium could perhaps be utilized in such an application. However, because of the ubiquitous presence of water in the system, there would be a very large thermal neutron flux across the detector, and the cross section for the ^{3}He(n,p) is nearly one thousand times larger in the thermal region, and there would likely be little chance of discerning fast from thermal neutrons, rendering this method ineffective in the posed scenario.

I.5.1.3. Detection based on fast neutron scattering

Perhaps the most common method for fast neutron detection is based on fast neutron elastic scattering. Due to the kinematics of scattering interactions, light nuclei are preferred as targets so the energy transfer from fast neutrons is maximal, and the most preferred nucleus is the single proton in hydrogen. The nuclei in this case are called recoil protons. Another beneficial characteristic of elastic scattering is a relatively constant cross section over a wide range of neutron energies, as seen in Figure 1.

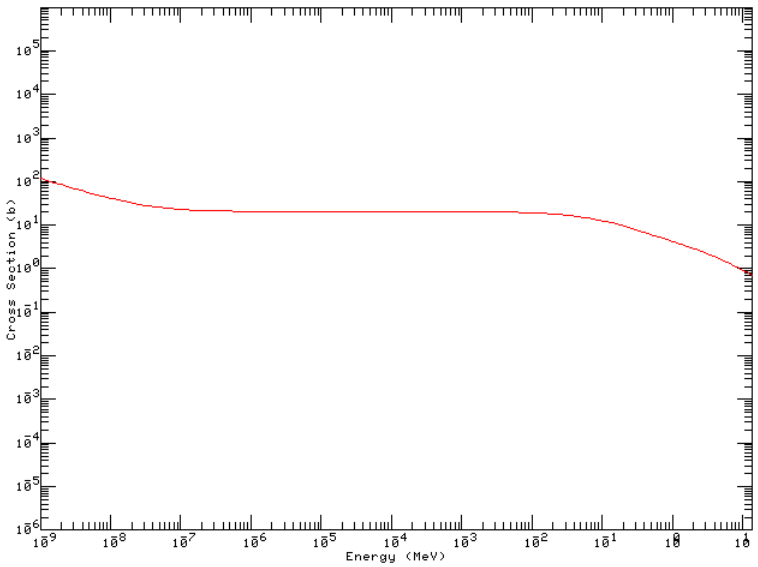

Figure 1. Elastic Scattering Cross Section for ^{1}H [9].

Due to the electronics of such proton recoil detectors, this method is effectively insensitive to thermal neutrons. In practical applications, the lowest energy of neutrons that may be detected is about 100 eV. As mentioned previously, there is a high thermal neutron flux in the system, and ability to filter out thermal neutrons makes proton recoil the method of choice for practical applications.

The two types of detectors utilizing recoil protons are scintillators and gas proportional counters. Scintillators typically use an organic compound containing hydrogen in either liquid or plastic form, whereas proportional counters typically use pure hydrogen or methane gas. Each detector type has its advantages and disadvantages, but the relative insensitivity to gamma radiation makes gas proportional counters the detector of choice in the posed scenario as is typical in most practical applications.

I.5.2. The differential die-away technique

One of the methods used in active interrogation for the detection of fissile materials is the differential die-away technique (DDT). A typical DDT system uses neutrons from a PNG to induce fissions in fissile material, and then it uses neutron detectors coupled with a timing device, typically a multichannel scaler, to differentiate between source and prompt fission neutrons. In many DDT applications, the source neutrons are produced in 10-15 μs pulses with 20 ms between pulses, and the measurement of the die-away neutrons occurs between 200 μs and 10 ms [10, 11]. Moderating materials may also be used to thermalize neutrons and maximize the number of induced fissions [12, 13]. The PNG source strength used in typical applications ranges between 10^7 and 10^9 n/s.

DDT is able to differentiate between source and fission neutrons due to the slowing down time of source neutrons primarily through such moderating material as polyethylene.

An example of a DDT detector setup is shown in Figure 2. When the neutron generator pulses, it emits an amount of neutrons, typically on the order of 10^6. In the absence of fissile material, most of these neutrons scatter throughout the system and are eventually detected in the ^{3}He tubes imbedded in the walls of the system. The cadmium covers around the tubes shields the tubes from most thermal neutrons due to the epithermal peak in the cadmium absorption cross section at about 0.18 eV (Figure 3).

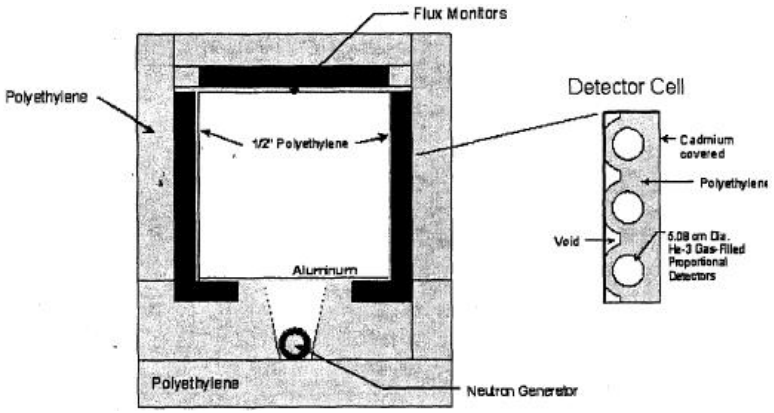

Figure 2. Example DDT Detector Setup [3].

The detector response due to the source neutrons tends to be a simple exponential decay, and in the absence of fissile material, the count rate in the detector would rapidly increase and then rapidly decrease to normal background levels. The time characteristic of this exponential decay is called the *die-away* time of the source neutrons. In the presence of fissile material, however, the decrease in the count rate is much slower. The source neutrons take time to scatter, losing about half their energy in each scattering reaction. Eventually, some neutrons reach thermal levels (around 0.025 eV) and cause fissions in the fissile material. The resulting fission neutrons are emitted from the fissile material, and then they are detected in the ^{3}He tubes similarly as the source neutrons were. The time required for the source neutrons to thermalize and induce fission is called the *die-away* time for fission,

and the resulting neutrons that are emitted are called *die-away neutrons*. The *differential die-away technique* compares the difference between the two die-away times to determine the presence of fissile material in a system. A multichannel scaler is then used to accumulate counts from the detector after each pulse in series of pulses from a neutron generator. Figure 4 shows an example of DDT in calculated and experimentally measured results.

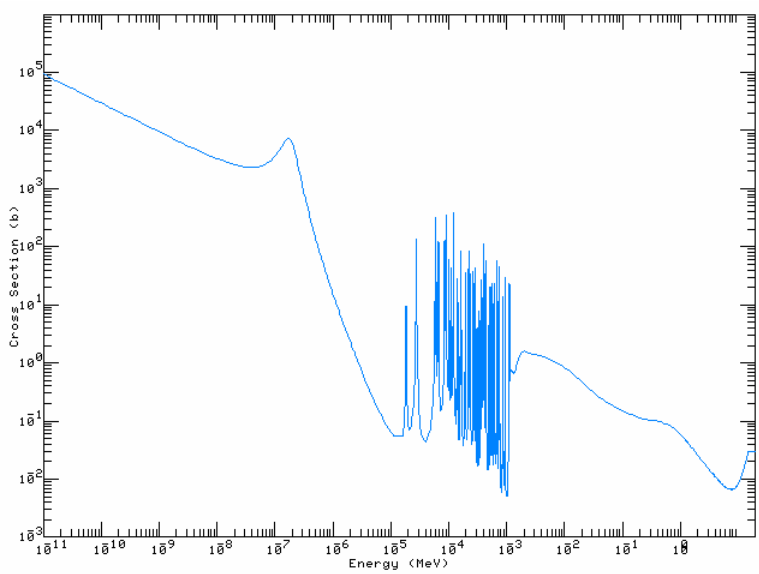

Figure 3. Cadmium Absorption Cross Section [9].

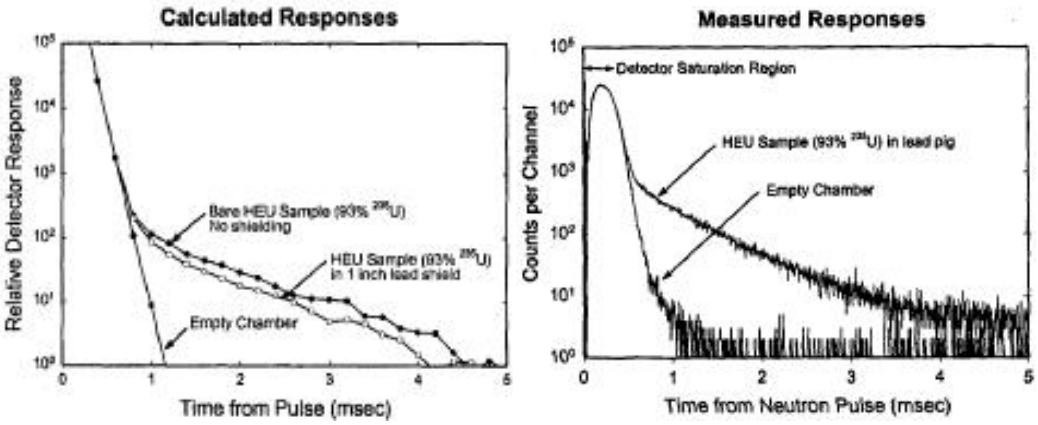

Figure 4. Example DDT Calculated and Measured Detector Response [3].

CHAPTER II

SETTING UP THE PROBLEM

In this Chapter, the selection of a boat design is given followed by the detector and neutron source modeled. Then, a description of the fissile materials used in the simulation is presented. Lastly, a discussion of the radiation signatures of the SFM is included.

II.1. Selection of a watercraft

The selection of a boat design to model was based on a boat that a person might easily be able to rent from a marina and sail several miles offshore to a waiting cargo ship. As for the specific design chosen, there were no exact measurement or size criteria; all that was needed were approximate dimensions and shapes that could easily be modeled within MCNP. The boat design chosen was the MacGregor 26, a 26-foot sailboat designed by MacGregor Sailboats of Marina del Rey, California. A schematic of the boat is shown in Figure 5 below. The surfaces of the boat are all fiberglass using the specifications given in Section *III.1.1*.

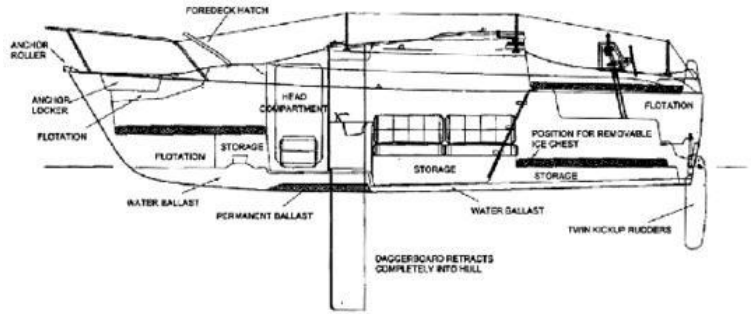

Figure 5. Schematic of MacGregor 26 Sailboat [14].

II.2. Description of the detector

Since fast neutron radiation is being analyzed, an appropriate detector is needed. As mentioned previously, the detector of choice is the pure hydrogen gas filled proportional counter. While there are many different commercial models of such detectors available, it is common for experimenters to design and build detectors suited to a specific purpose. As such, a 3m x 2.5m x 0.3m detector surrounded by a one-eighth-inch-thick layer of stainless steel (SS-304) was chosen. In reality, a single detector of such a large size would be impractical, if not altogether impossible, to build. A more practical approach would be to stack together many small detectors into a desired size and shape, and then connect the associated electronics so they act effectively as one, large detector. The detector is oriented such that the 3 m by 2.5 m face is parallel to the boat face with the 3 m side running along the length of the boat. The detector is also partially submerged with 1 m below the waterline. The fill gas is pure ^{1}H at a pressure of 20 atmospheres with an equivalent density of 0.00178 g/cm^{3}.

II.3. Interrogation source

The neutron source simulated in this research is the deuterium-tritium, or D-T, reaction. In accelerator-based neutron generators, an accelerating potential between 80 and 180 kV is used to fuse deuterium and tritium nuclei to produce helium and neutrons. The reaction yields monoenergetic neutrons at 14.2 MeV. The neutron generators may also use their electronics to create pulses of neutrons so that there are periods of low background noise between bursts of neutrons.

Other neutron sources, known as isotopic sources, utilize either spontaneous fission or the (α, n) reaction. These sources have the advantage of not requiring external power to create an accelerating potential, but they have several disadvantages which render them unsuitable for the application presented in this thesis. Since isotopic sources are naturally radioactive, the reaction cannot be turned off, thus shielding is required for radiological safety when the source is not in use. Isotopic sources are generally only useful for low-flux applications. The neutrons from isotopic sources are emitted over broad energy ranges and cannot be pulsed.

II.4. Description of the SFM

The spheres of SFM used in the simulation are slightly smaller than one SQ as described in Chapter I. Geometrically they are simple and in a configuration that minimizes the amount of material required to make a critical mass. For the purposes of this research, it is assumed the terrorist group has been able to acquire weapon grades of both plutonium and HEU. Some of the isotopes that would otherwise be present in a real-world scenario have been neglected because their contributions to the results of the simulation are sufficiently minor compared to the primary isotopes of interest.

The WG plutonium sphere is comprised of 94 percent ^{239}Pu and 6 percent ^{240}Pu with a mass of 5 kg. Absent are the isotopes ^{238}Pu, ^{241}Pu, and ^{242}Pu. Although ^{241}Am builds up through decay processes in stockpiles of plutonium at a rate of about 0.5 percent per year, it is plausible that in a relatively new batch of plutonium, the amount would be negligible, and so it is ignored here. This assumption also adds conservatism to the analysis as a sphere of WG plutonium could more easily be detected with enough ^{241}Am present.

The HEU sphere is comprised of 95 percent ^{235}U and 5 percent ^{238}U with a mass of 25 kg. Notably missing from the HEU sphere is the isotope ^{234}U, which again might be present in a real world scenario, but its contribution to the overall results is sufficiently small to warrant exclusion.

II.5. Radiation signatures

Both uranium and plutonium have radioactive properties that lend themselves to the types of analyses considered in this thesis. Below is a discussion of the natures of uranium and plutonium that allow for both passive and active analysis of SFM.

II.5.1. Properties of uranium

Some of the uranium isotopes decay via spontaneous fission (SF), thus possibly allowing for detection via passive detection methods. Unfortunately, the activity level of this mode of decay for uranium tends to be rather small. Table 1 lists the SF rates for uranium and compares the emission of neutrons via SF for natural and WG HEU.

Table 1. Spontaneous Fission Rates from Uranium [15].

Isotope	25 kg Natural Uranium		25 kg HEU	
	weight %	SF rate (n/s)	weight %	SF rate (n/s)
^{234}U	0.0049	0.00	1.032	2.5
^{235}U	0.7108	0.00	97.65	7.5
^{236}U	0.00	0.00	0.2523	0.0
^{238}U	99.28	338	1.07	2.5

As can be seen in the Table 1, as the enrichment in ^{235}U increases the SF rate decreases, making detection of HEU based on passive neutron measurement very difficult. For example, in a 25 kg mass of HEU, the expected number of neutrons emitted per second is

only about 12.5, making passive detection of HEU based on SF highly unlikely in a short amount of time.

In addition to passive radiation, uranium also responds to bombardment by neutrons. The primary reaction of interest in this research is neutron-induced fission. In this case, the neutrons yield a spectrum of energies with an average of 2 MeV. Of greatest concern here, however, are the energies of the fission-inducing neutrons. ^{235}U responds favorably to thermal neutrons with a cross section of about 507 b [9], but reduces greatly to only a few barns at fast energies, as seen in Figure 6. ^{238}U responds poorly to neutron-induced fission in general. Thermal fission is effectively negligible, and at fast energies, its cross section is only a few tenths of a barn and thus is barely useful (see Figure 7 below).

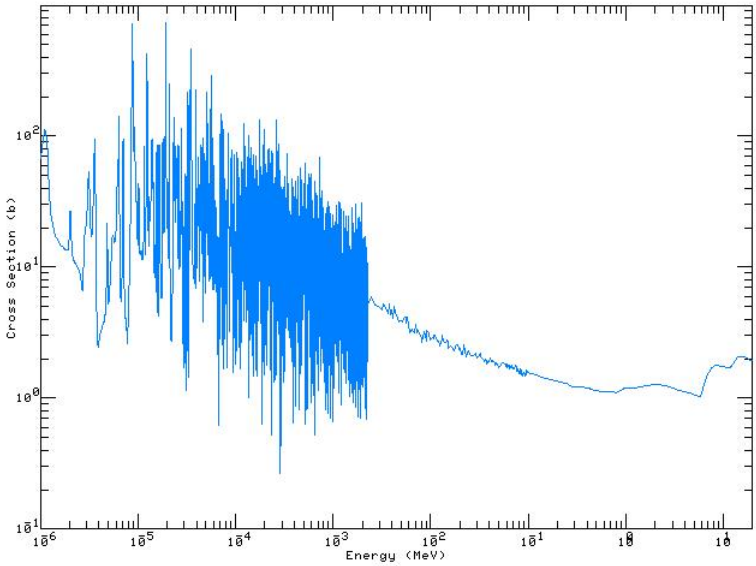

Figure 6. Fission Cross Section of ^{235}U [9].

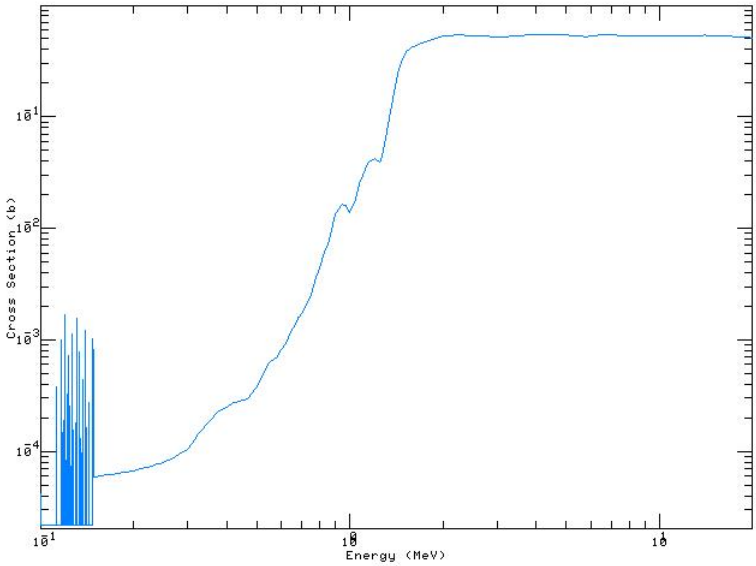

Figure 7. Fission Cross Section for ^{238}U [9].

II.5.2. Properties of plutonium

Plutonium tends to emit several neutrons via spontaneous fission. The activity levels of this mode of decay tend to be larger and more useful to passive detection of plutonium. Table 2 lists the SF rates for some plutonium isotopes. As can be seen in Table 2, the SF rate is much greater for plutonium than for uranium. In the case of 5 kg of WG plutonium, there can be expected about 300,000 SF neutrons per second, and thus it may be possible to detect plutonium based on SF in a short amount of time.

Table 2. Spontaneous Fission Rates from WG Plutonium [15, 16].

Isotope (wt %)[2]	SF of 5kg WG Pu (n/s)
^{238}Pu (0.012)	1550
^{239}Pu (93.8)	105
^{240}Pu (6)	3.0E+5
^{241}Pu (0.35)	0.0
^{242}Pu (0.022)	1890

[2] Values calculated based on isotopic composition from Mozley, p. 65.

In addition to passive radiation, plutonium also responds to bombardment by neutrons. The primary reaction of interest is again neutron-induced fission. For plutonium, the neutrons yielded have average energies slightly greater than those of uranium, around 2.1 MeV. ^{239}Pu has a thermal cross section of about 698 b [9] and again drops off greatly to only a few barns at fast energies, as seen in Figure 8. ^{240}Pu has a more favorable response to neutron-induced fission than its ^{238}U counterpart does. Thermal fission is weak but worth noting at about 53 mb, and at fast neutron energies, its cross section climbs to a few barns, making it nearly comparable to ^{239}Pu for fast energies (see Figure 9 below).

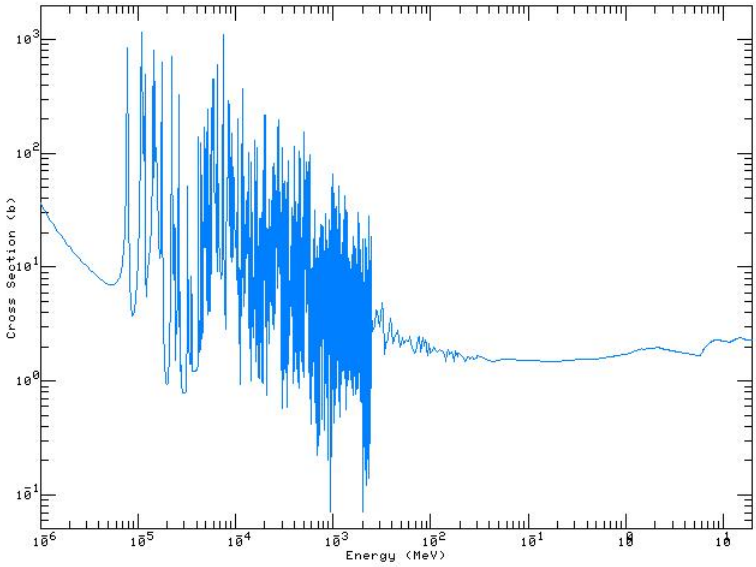

Figure 8. Fission Cross Section for ^{239}Pu [9].

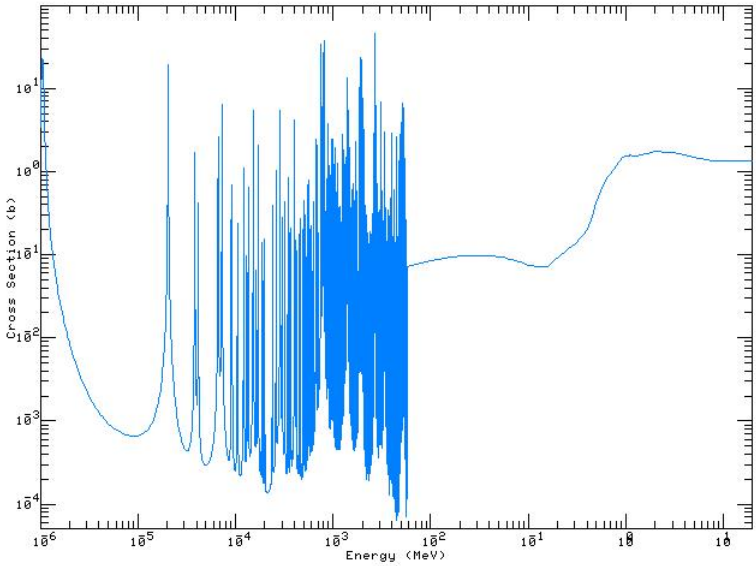

Figure 9. Fission Cross Section for ^{240}Pu [9].

CHAPTER III

MODELS AND SIMULATIONS

Presented here is the development of the computational model based on the physical scenario, description of the measured parameters of the model, and conditions of the simulations being run.

III.1. Building the model in MCNP

In building the computational model, a number of simplifications and assumptions were necessary for several reasons. For example, in a real-world scenario, a sailboat would have thousands of individual components ranging from hull material, wiring, interior fixtures, sails, cables, a mast, nuts, bolts, and so on. Incorporating all of these features would likely result in only a slight increase in the model's accuracy while carrying with it a very large burden not only in the creation of the model in MCNP but also by requiring unacceptably long computational times – the more complicated the geometry of the model, the longer MCNP takes to complete its task. Thus, using a simplified design, several different cases may be run in much less time. The hull (minus the keel), deck, and bulkheads of the boat were modeled in a simplified design, disregarding the curvatures of the various surfaces. Additionally, the interior contents of the boat were estimated and homogenized to create a uniform distribution of a single composite material.

Several other assumptions were used in this thesis. Since neutrons tend to have very long mean-free-paths in air, it was assumed that void suitably represents air so that neutrons do not interact in volumes of the model composed of void. Another simplification was the

use of pure water in the model. In reality, there would be various materials entrained in the water, such as organic matter, salts, and sediment, but the model disregards these materials.

The source in MCNP was simply an isotropic point source at a specified location. Most PNG systems emit neutrons isotropically from one end of a cylinder containing the deuterium and tritium used in creating the source neutrons. In reality, the source would be contained in a metal tube and associated electronics would be located nearby. However, due to the high energy of the neutrons and the position of the detector on the opposite side of the boat, the source equipment would not greatly alter the flow of neutrons. The source was also approximated as a delta function in time. In a typical PNG, the pulse time is approximately 10 μs, with about 10^6 neutrons emitted approximately uniformly over the time interval. In the model, however, all neutrons are born at time $t = 0$. Since the time scale of the problem was about 5 ms, and because most of the neutron information yielded in the first 1 ms was source driven, the time distribution of the source particles was comparatively negligible.

III.1.1. Materials specifications

The boat design was based on a schematic obtained from MacGregor Sailboats of Marina del Rey, CA [14]. The overall length was 8.23 m with 5.78 m of cabin space, the cabin width was 3.00 m, and the overall height was 2.33 m with 1.44 m of freeboard. The thickness of the hull, deck, and bulkheads were one-eighth-inch and comprised of E-Glass fibers, a general purpose fiberglass material. Side and top views of the boat are shown in Figure 10. The fiberglass composition was based on information from Michigan Tech University's Materials Engineering Department [17] and had a density of 2.5 g/cm^3. The composition of the fiberglass is listed in Table 3.

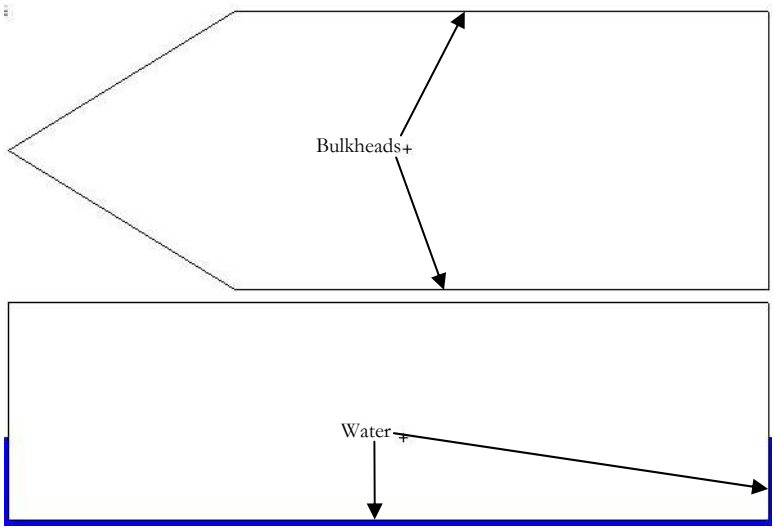

Figure 10. Top and Side Views of the Boat.

Table 3. Fiberglass Composition with MCNP ZAID.

Element/Isotope	% by mass	MCNP ZAID[3]
Si	25.2	14000.60c
^{16}O	49.0	8016.66c
^{17}O	0.0187	8017.66c
^{27}Al	7.41	13027.92c
Fe	0.350	26000.55c
^{10}B	0.649	5010.60c
^{11}B	2.61	5011.60c
C	1.81	12000.66c
Ca	12.9	20000.66c

For the sake of increasing the realism of the model, an approximation was made for the interior composition of the boat. The contents were approximated as two 70 kg people, 100 kg aluminum alloy 5052, 25 kg stainless steel alloy 316, 100 kg plastic, 20 kg of oil, and

[3] All materials are identified within MCNP by the ZAID, which is the numeric value formed by the equation $ZAID = Z * 1000 + A$, where Z is the atom number of the element, and A is the atomic mass of the isotope. In the case where the ZAID ends in 000, then MCNP automatically takes into account the relative abundances of the naturally occurring isotopes of a given element.

100 kg wood. Table 4 lists the isotopic composition of the interior materials along with the mass fraction and ZAID of each component.

Table 4. Interior Boat Material Composition with MCNP ZAID.

Element/Isotope	% by mass	MCNP ZAID	Element/Isotope	% by mass	MCNP ZAID
^{27}Al	20.06	13027.66c	C	32.25	6000.66c
Ca	0.2861	20000.66c	Cl	0.04095	17000.66c
^{50}Cr	0.01880	24050.66c	^{52}Cr	0.3626	24052.66c
^{53}Cr	0.04111	24053.66c	^{54}Cr	0.01023	24054.66c
^{63}Cu	0.002852	29063.66c	^{65}Cu	0.001271	29065.66c
^{54}Fe	0.2481	26054.66c	^{56}Fe	3.895	26056.66c
^{57}Fe	0.08996	26057.66c	^{58}Fe	0.01197	26058.66c
^{1}H	6.112	1001.66c	^{2}H	9.170e-4	1002.66c
K	0.05884	19000.66c	Mg	0.4854	12000.66c
^{55}Mn	0.1072	25055.66c	Mo	0.06559	42000.66c
^{14}N	0.7188	7014.66c	^{15}N	0.002641	7015.66c
^{23}Na	0.04325	11023.66c	^{58}Ni	0.2804	28058.66c
^{60}Ni	0.08026	28060.66c	^{61}Ni	0.003489	28061.66c
^{62}Ni	0.01112	28062.66c	^{64}Ni	0.002834	28064.66c
^{16}O	34.36	8016.66c	^{17}O	0.01309	8017.66c
^{31}P	0.2643	15031.66c	^{206}Pb	8.802e-6	82206.66c
^{207}Pb	8.071e-6	82207.66c	^{208}Pb	1.914e-5	82208.66c
^{85}Rb	1.063e-4	37085.66c	^{87}Rb	4.099e-5	37087.66c
S	0.06365	16000.66c	^{28}Si	0.05705	14028.66c
^{29}Si	0.002889	14029.66c	^{30}Si	0.001918	14030.66c
Zn	0.005085	30000.42c	Zr	2.045e-4	40000.66c

As mentioned previously, the detector of choice was a hydrogen gas filled proton recoil detector. Surrounding the outer edges of the detector was a one-eighth-inch thick layer of SS-304 with a density of 6.67 g/cm^3. Table 5 below displays the composition and MCNP material identifiers for the detector components.

Table 5. Detector Materials Composition and MCNP ZAID.

Element/Isotope	% by mass	MCNP ZAID
Proton Recoil Detector Fill Gas		
^{1}H	100	1001.66c
SS-304		
Fe	67.85	26000.55c
C	0.80	6000.66c
Si	1.00	14000.60c
Cr	18.00	24000.50c
Ni	9.80	28000.50c
^{55}Mn	1.80	25055.66c
^{31}P	0.45	15031.66c
S	0.30	16000.66c

As a method of variance reduction, the simulation incorporated the use of importance zones. Two zones of increasing importance were created around the detector, and as a neutron entered a zone with a higher importance, it was "split" into additional neutrons, each with an appropriate reduction in weight. Conversely, as a neutron crossed into a zone with lower importance, "Russian Roulette" was carried out so that a certain fraction of neutrons was eliminated in proportion to the adjacent cell importances. For example, if a neutron crossed from a cell with an importance of 4 into one with an importance of 8, then that neutron was split into 2 identical neutrons, each with its weight reduced by half. Conversely, if a neutron crossed from a cell with an importance of 8 into one with an importance of 4, its chances of being eliminated were one-half, but if it does survive elimination, then its weight was doubled. If used properly, such techniques allow for decreased variance in tallies without increasing the number of particle histories run. In this particular case, since only neutrons that can be detected were of interest, the importance zones increased the number of neutrons near, and in, the detector, thus decreasing the variance in the associated flux tallies without having to run additional particle histories.

Figure 11 shows the detector alongside the boat. Note the additional surfaces outlining the importance zones around the detector.

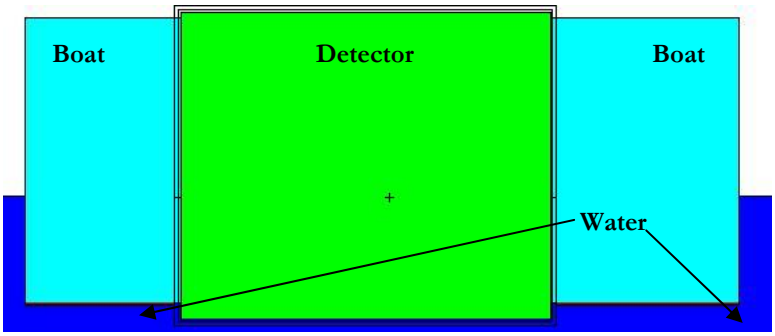

Figure 11. Side View of Boat with Detector.

III.1.2. Source and target specifications

The source inside MCNP was defined as a 14.0 MeV monoenergetic, isotropic point source with all neutrons born at time $t = 0$. The energy corresponds to those produced in the D-T reaction, which is typical of a PNG.

The target material, in this case SFM, was either 25 kg HEU at 95 percent ^{235}U, or 8 kg of weapons-grade plutonium at 94 percent ^{239}Pu. The target materials specifications are listed below in Table 6.

Table 6. SFM Material Specifications and ZAID.

Element/Isotope	% by mass	MCNP ZAID
WG Plutonium		
^{239}Pu	94.0	94239.66c
^{240}Pu	6.0	94240.66c
HEU		
^{235}U	95.0	92235.66c
^{238}U	5.0	92238.66c

III.2. Measurement parameters

MCNP uses various tally cards to record the behavior and quality of particles that exist within a simulation. This thesis used tallies to simulate the responses of the aforementioned types of detectors. The tally utilized was the F4:*n*, or cell flux tally. In MCNP [18], the cell flux tally is given in units of particle-pathlength per unit volume per source particle. The cell flux tally may be augmented by the addition of the flux multiplier card, where MCNP then calculates interaction probabilities of the particles traversing a cell and yields the flux of the resulting particles or interactions of interest. The cell flux tally may also be augmented with the edition of the E*n* card, whereby MCNP creates energy bins, and the resultant tallies are scored according to the energy of the particle being counted. Similarly, the T*n* card may be used to augment the cell flux tally whereby MCNP creates time bins, and the resultant tallies are scored according to the time at which the particle scored the tally since the current particle history began.

In the case of this thesis, the F4 tally and multiplier cards were used to estimate the total fission rate occurring in the spheres of SFM and the recoil-proton production rate in the detector. In the spheres of SFM, the F4:n, or neutron flux, tally was multiplied by the total fission cross section so that the results yielded the fission rate density. In the detector volume filled with hydrogen, the F4:n tally was multiplied by the elastic scattering cross section so that the results yielded the recoil-proton production rate, and hence the detectable neutron flux, in the detector. Since the minimum neutron energy required to create recoil protons and induce a charge in a typical proton recoil detector is about 100 eV, energy bins were used for the tally in the detector volume with a lower energy cutoff of 100

eV. Only those neutrons with energy greater than 100 eV were used in the analysis of results.

III.3. Simulation

Four general cases were simulated in MCNP:

- an active system with HEU present,
- an active system with plutonium present,
- an active system with no SFM present, and
- a passive system based on the spontaneous fission of plutonium.

Within each general case were nine runs with the detector and source, when used for active simulation, at evenly spaced positions along the side of the boat. The purpose of the spacing was to mimic the boat passing through a detector array. In each run, the source and detector assembly were at the same relative position along the boat such that the source was located directly across from the center of the detector on the opposite side. The nine source/detector positions were spaced 80 cm apart beginning at a distance of 20 cm from the back of the boat. Thus, the nine positions were 20, 100, 180, 260, 340, 420, 500, 580, and 660 cm.

The source used in the simulation was located 5 cm from the edge of the boat. This particular spacing was chosen to maximize the number of neutrons entering the boat and the probability of inducing fission. The purpose of locating the source opposite the detector was to aid in the discrimination of fission neutrons from source neutrons by minimizing the source neutrons detected in the detector. The source was also located 50 cm below the waterline, the same vertical position as the SFM on the interior (when present). In a

practical situation, the location of the SFM would not be known, but for the purposes of this simulation, the position was chosen to maximize the probability of inducing fissions.

The SFM sphere was located on the centerline of the boat, approximately 2.5 meters from the rear of the boat, and about 0.4 meters above the bottom of the hull. This placed the sphere about 50 cm below the waterline, equal to the vertical position of the source. Lastly, the detector formed a plane parallel to the sidewall of the boat at a distance of 5 cm from the sidewall of the boat. This position was chosen to maximize the detection of fission neutrons coming from the SFM. A view of the boat interior with detector and SFM sphere is shown in Figure 12.

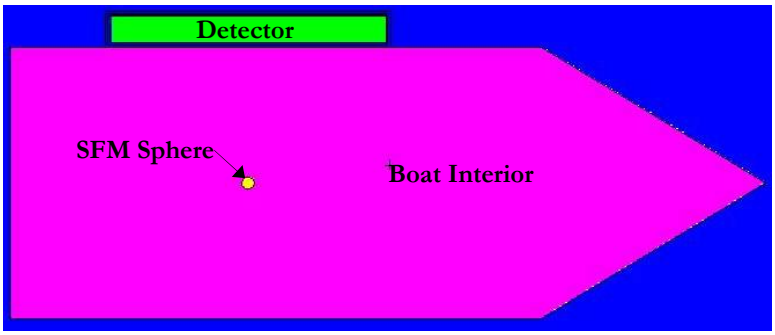

Figure 12. Boat with Detector and SFM Sphere.

To simulate the detection of die-away neutrons, a T*n* card was added to the cell flux tallies. The T*n* card modified the tally by discretizing the flux tally (or flux-multiplied tally) into time bins. This way, the time evolution of the flux in the cell of interest could be observed, and particular to this thesis, a determination of the presence of SFM could be made. In this thesis, the time bins were set at intervals of 0.35 ms from 0.1 to 5 ms (14 time steps), providing an ample time window to examine the die-away neutrons while comparing the time response in the neutron detectors to the fission reaction rate in the SFM sphere. In

a typical DDT application, the source is pulsed every 10 ms with 0.01 ms duration. Most of the useful information is recovered between 1 and 5 ms.

In the case of the passive system simulation, the MCNP input decks were modified such that the source particles were distributed uniformly and randomly within the plutonium sphere itself. The energy of a given source particle is random with a distribution determined by the Watt fission spectrum [18]:

$$f(E) = C\exp(-E/a)\sinh(bE)^{1/2} \tag{1}$$

with parameters *a* and *b* determined by the isotope undergoing spontaneous fission, and the constant *C* is a normalization factor such that $\int f(E)dE = 1$.

The history of a typical particle in an active simulation might go as follows. The neutron is created at time $t = 0$ seconds and is emitted isotropically from a point with an energy of 14 MeV. There are several options as to what happens next. The neutron could go straight into the detector and possibly scatter, causing a score to be tallied. It could go away from the system entirely until it is absorbed. Finally, the neutron could also thermalize and eventually make its way to the SFM sphere. In the sphere, the neutron might induce fission, causing about two other neutrons to be produced. On average, the fission neutron energy is about 2 MeV. Perhaps one of the fission neutrons could leave the sphere and arrive inside the detector without thermalizing where it scatters off a hydrogen nucleus producing a recoil proton, thus being recorded in the tally for the detector. Otherwise, if the fission neutrons are not detected, then they go elsewhere into the system where they are eventually absorbed. After four hundred million of these particle histories took place, the

time evolution of the neutron and fission fluxes took shape and came to be the resultant data from which the conclusions were drawn.

MCNP runs were executed for the nine detector/source positions for each of the four general cases. For each of the nine different positions, the input decks were modified to that detector and source location was moved an additional 80 cm from the rear of the boat (except in the case of the passive system, where only the detector was moved). Additionally, some modifications of the cell definitions were required to avoid geometry errors and non-physical overlapping of surfaces. Sample input decks of each of the general cases are listed in Appendix A.

CHAPTER IV

DISCUSSION OF RESULTS

In this Chapter the results of the MCNP simulations are presented, and the data is analyzed such that conclusions may be inferred. First, the method for statistical calculations is presented. Next, the criteria for the positive determination of the presence of fissile material are discussed. Following that is a presentation of the raw data for the various system configurations. Then, an analysis of background radiation in the system is carried out in order to determine the required source strength of the system. An estimation of the dose to passengers is then calculated. Finally, an analysis of the passive detection of spontaneous fission neutrons is presented.

IV.1. Formation of results and statistics

The flux values calculated by MCNP are given in dimensions of counts per source particle per unit area ($n \cdot src\text{-}part^{-1} \cdot cm^{-2}$). MCNP calculates the flux by summing the total track lengths of particles traversing a particular cell and dividing by the volume of that cell. In the specific case of this research, the actual cell volume was overridden and set to unity. Thus, the resulting flux estimates were actually the number of estimated reactions in the cell of interest ($rxns \cdot src\text{-}part^{-1}$). This results was translated into counts.

MCNP also outputs the standard deviation associated with each estimate, and the total standard deviation over several such estimates is given via the error propagation equation

$$\sigma^2_{F(x_1 \mathrm{K}\, x_N)} = \sum_{i=1}^{N} \sigma^2_{x_i} \left(\frac{\partial F}{\partial x_i} \right)^2 \qquad (2)$$

where $\sigma_{F(x_1 \mathrm{K}\, x_N)}$ is the estimated cumulative error associated with the parameters x_i each with error σ_{x_i}. When estimates are added together, such that

$$F\left(x_1 \ldots x_N\right) = x_1 + x_2 + \cdots + x_{N-1} + x_N\,, \tag{3}$$

then the cumulative error is given by

$$\sigma_F^2 = \sigma_1^2 + \sigma_2^2 + \cdots + \sigma_{N-1}^2 + \sigma_N^2\,. \tag{4}$$

The estimated error calculated by MCNP is based on Poisson counting statistics, where the standard deviation associated with an estimated flux is given by

$$\sigma_C = \sqrt{C} \tag{5}$$

where C is the number of counts. MCNP actually gives a fractional standard error value, where the tabulated value is the error divided by the counts. For example, in a simulation where $N = 10^9$ particles are run, if a bin registered $C = 10^4$ counts, then MCNP would yield an estimated flux of

$$\phi = \frac{C}{N} = \frac{10^4 \text{ neutrons}}{10^9 \text{ source particles}} = 10^{-5}\,\frac{\text{n}}{\text{src-part}}\,, \tag{6}$$

and the associated error would be calculated as

$$\sigma_C = \frac{\sqrt{C}}{N} = \frac{\sqrt{10^4}\ \text{n}}{10^9 \text{ src-part}} = 10^{-7}\,\frac{\text{n}}{\text{src-part}}\,, \tag{7}$$

and MCNP would output the fractional error

$$f_{err} = \frac{\sigma_C}{\phi} = \frac{\sqrt{C}}{C} = \frac{10^2}{10^4} = 0.01\,. \tag{8}$$

When examining the results returned by MCNP, the manual suggests that fractional errors of less than 0.10 suggest generally reliable tallies [18].

IV.2. Criteria for positive determination of the presence of fissile material

There are essentially two criteria for the positive determination of the presence of SFM in the system. The first describes the ability to discriminate between source neutrons and die-away neutrons. The second describes the practical ability to discriminate between die-away neutrons and background neutrons caused by cosmic rays.

Since the detection of die-away neutrons occurs at a time significantly longer than the time it takes source neutrons to vacate the system, it was generally valid to state that any fast neutrons detected after such time could only be attributed to the presence of SFM in the system. As such, the current system was modeled to simulate the detector response for a configuration with no SFM present. This data became the baseline to which the simulations with SFM present were compared. As is shown in the subsequent sections, there was a statistically significant difference between the system with and without the presence of SFM. In general, a statistically significant result was one in which the tallies with SFM present are greater than those with no SFM and have a fractional error less than 0.10. Essentially, if the tally for a particular detector position with SFM present was at least two standard deviations greater than the tally with no SFM present, then there was a 95 percent chance that a determination of the presence of SFM is possible for the given system configuration.

The mean neutron flux from cosmic rays is 0.00646 n/cm^2-s [19]. In general, the neutron flux in the system must be about twice as great as the background in order to discriminate between neutrons created in the system and those coming from background. With this information, a determination of the required source strength from a PNG can also be made.

IV.3. Presentation of results

The following section presents the results from MCNP for the cases with no SFM present in the system, then with the HEU sphere, and finally with the weapons-grade plutonium sphere. These results have had minimal post-processing and essentially represent the raw data on which further analysis was conducted to draw conclusions.

IV.3.1. No special fissile material system configuration

Before looking at the results with fissile material present in the system, it is useful to discuss the system with no such material present. Figure 13 below shows the scattering reactions in the detector with no fissile material present.

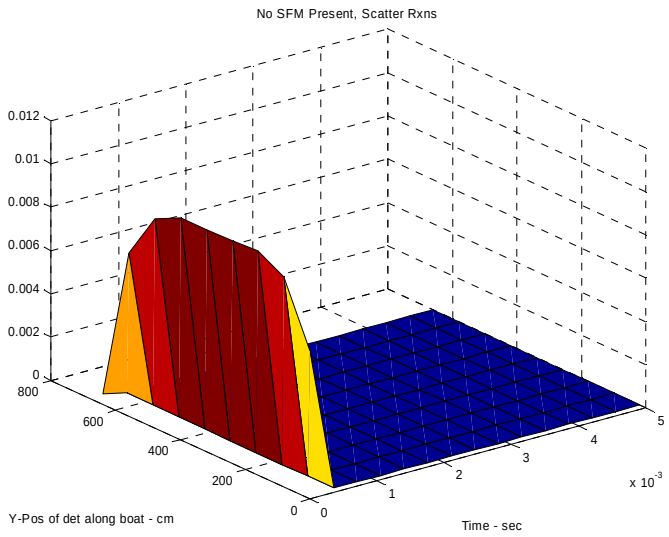

Figure 13. Scattering Reactions with No SFM.

The graph shows that the detector response grows as the source and detector position is farther from the fore and aft edges of the boat. The number of reactions holds nearly constant at 0.01 reactions per source particle throughout most of the interior of the boat.

Since the differential die-away technique depends on the source neutrons contributing to the detector response only in the first few moments after they are born, the first time bin of the tally could be neglected so that a baseline response could be formed to which the responses from the presence of SFM in the system could be compared. Figure 14 shows about a seven-order decrease in magnitude in the number of scattering reactions occurring after a time of 0.1 ms.

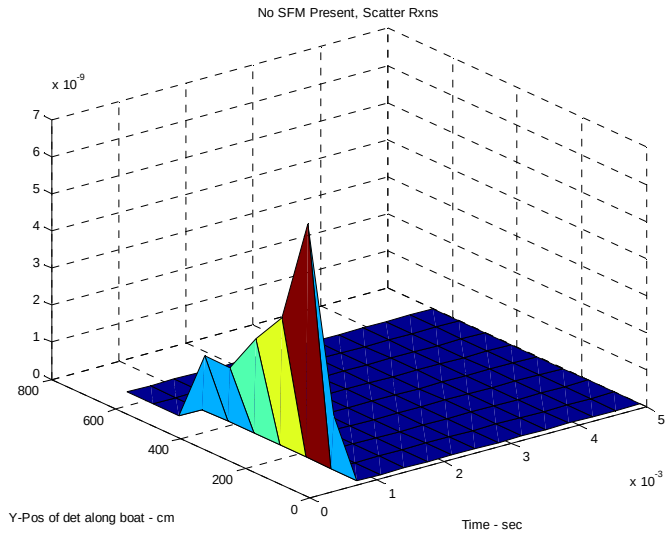

Figure 14. Scattering Reactions with No SFM at t>0.1 ms.

It should be noted here that the only time bin in Figure 14 with any non-zero values was at 0.45 ms. Thus, for detection purposes, there were no source neutrons in the system remaining after 0.45 ms.

IV.3.2 Highly enriched uranium system configuration

Presented now are the results for the system with the 25 kg sphere of HEU. Since the fission neutrons are of primary interest, the fission neutron tally inside the sphere is shown below in Figure 15. Note the figure represents the number of fissions occurring in

the sphere as the tally has been multiplied by the fission cross sections of the respective uranium isotopes used to create the sphere.

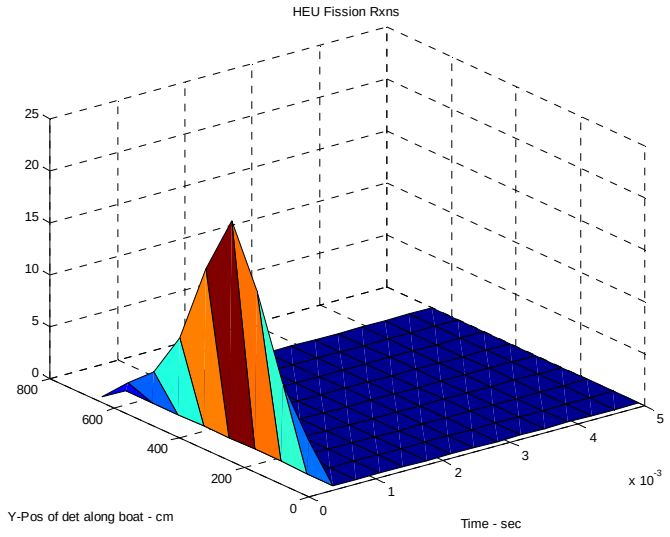

Figure 15. HEU Fission Reactions.

The majority of the fissions occurred within the first 0.1 ms after the source neutron was born. The temporal behavior of the fission reactions was more apparent after this time. Neglecting the first time bin of tally data shows more clearly both the spatial and temporal behavior of the fission reactions in the HEU sphere, as shown in Figure 16. To get a closer look at the temporal behavior, the fission rates can be summed across the nine detector positions. The exponential behavior observed in Figure 17 would be expected to drive the detector response, that is, the time-dependent behavior of the fission rate in the HEU sphere should be about the same as the production rate of recoil protons in the detectors. In the figure (and in all relevant subsequent figures), the solid line represents the estimated number of fission neutrons per source particle, and the dashed lines represent the estimated error bounds.

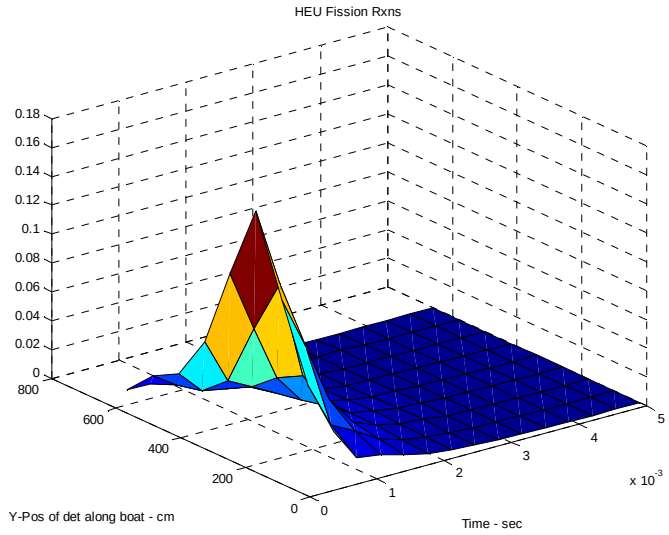

Figure 16. HEU Fission Reactions at t > 0.1 ms.

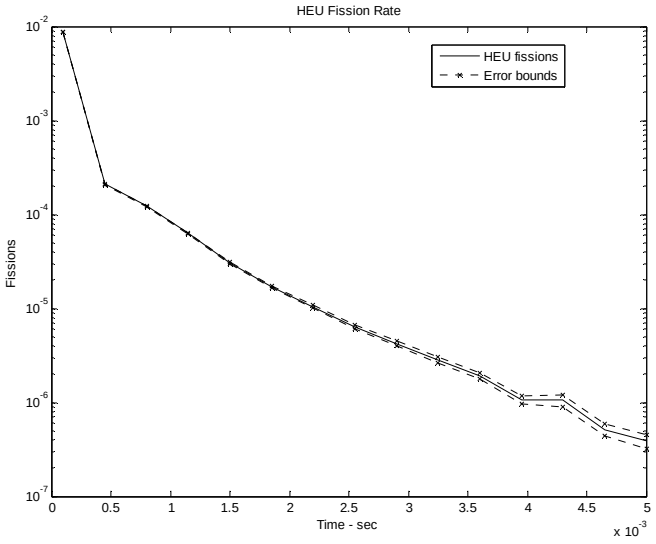

Figure 17. Integral Fission Reactions in HEU.

Switching focus now to the detector response for the sphere of HEU, Figure 18 shows the number of elastic scattering reactions occurring in the detector with respect to time and detector position.

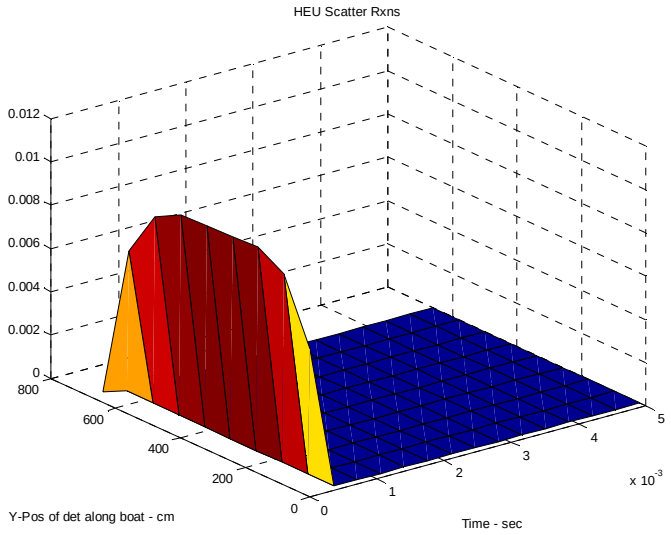

Figure 18. Scattering Reactions in Detector with HEU Sphere.

As can be seen from the figure, the response in the detector closely resembles the response in the case with no SFM present, again with a nearly constant value of 0.01 scattering reactions per source particle during the first 0.1 ms throughout the length of the boat. The first time-bin of the tally could be neglected again to see more detail of the detector response from the die-away neutrons, as shown in Figure 19 below.

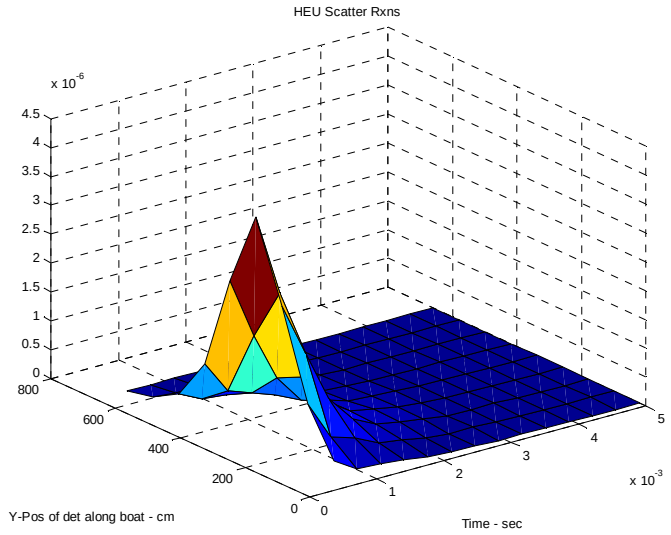

Figure 19. Scattering Reactions from HEU at t>0.1 ms.

Note that the magnitude of the response in this case was about 3 orders of magnitude greater than that of the case with no SFM present, and there were neutrons present after 0.45 ms, whereas there were none in the absence of SFM.

Figures 20 - 24 show the comparison of detector responses for the cases with and without HEU present for detector and source positions at 100, 180, 260, 340, and 420 cm from the rear of the boat. In each case, the sharply declining line was from the system with no SFM present, and the slowly attenuating line was from the presence of HEU. In each of these graphs, the only reactions tallied beyond 0.45 ms were from the HEU cases. These results alone suffice in showing a statistically significant difference between the system with and without HEU. The position with the greatest magnitude of response was at 260 cm, which was to be expected considering the SFM sphere was located at the same distance from the rear of the boat.

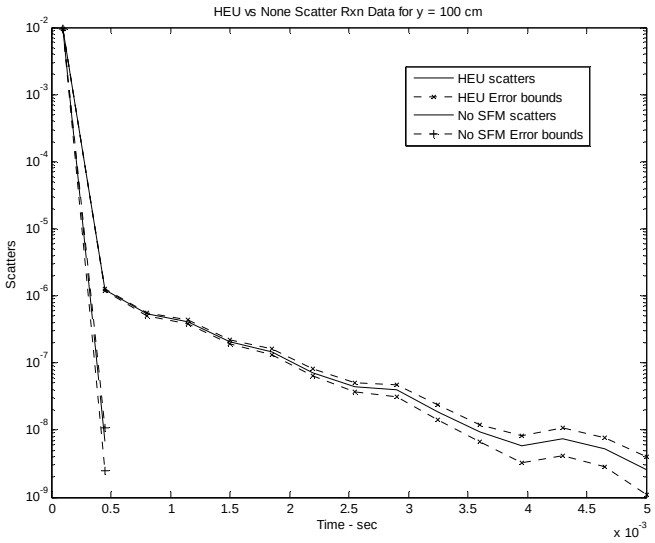

Figure 20. HEU vs. No SFM Reactions for Detector at 100 cm.

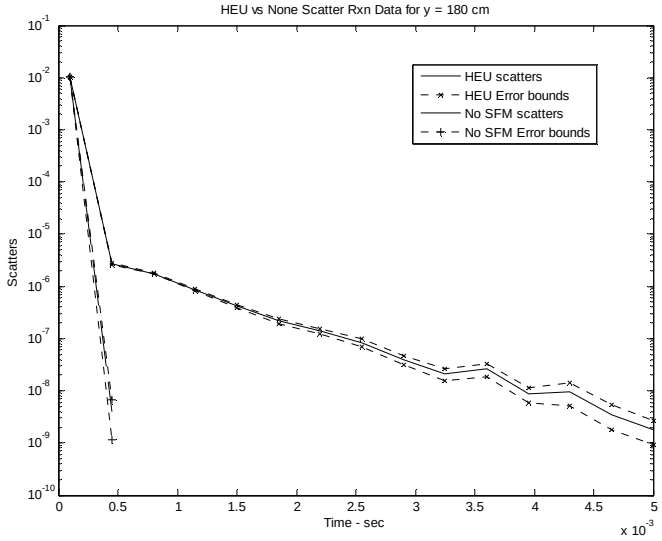

Figure 21. HEU vs. No SFM Reactions for Detector at 180 cm.

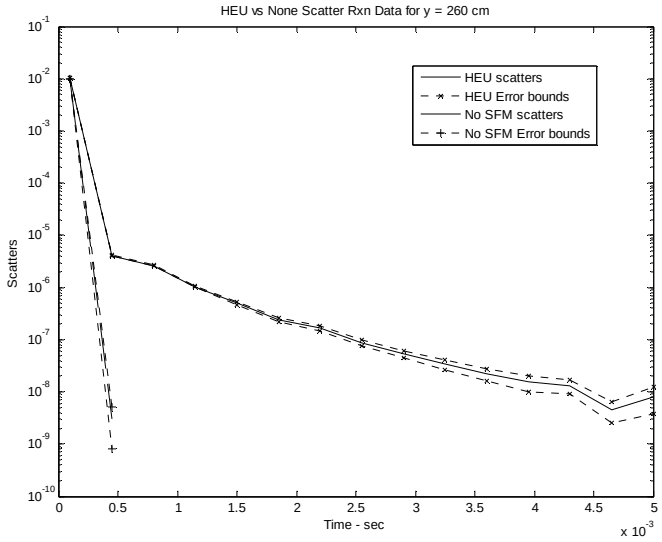

Figure 22. HEU vs. No SFM Reactions for Detector at 260 cm.

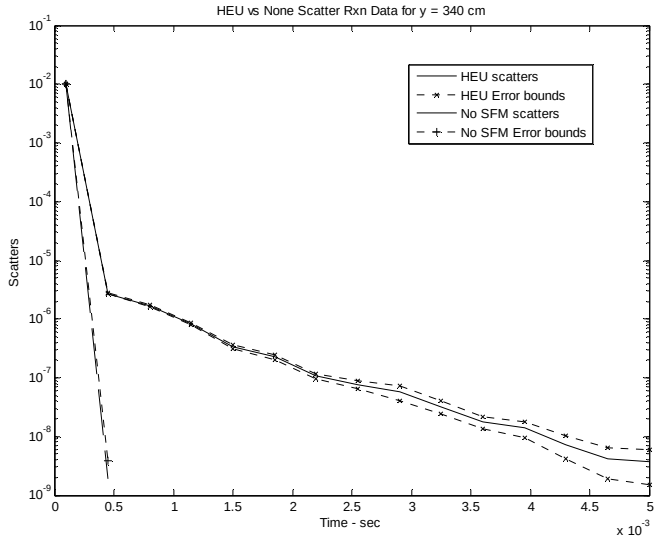

Figure 23. HEU vs. No SFM Reactions for Detector at 340 cm.

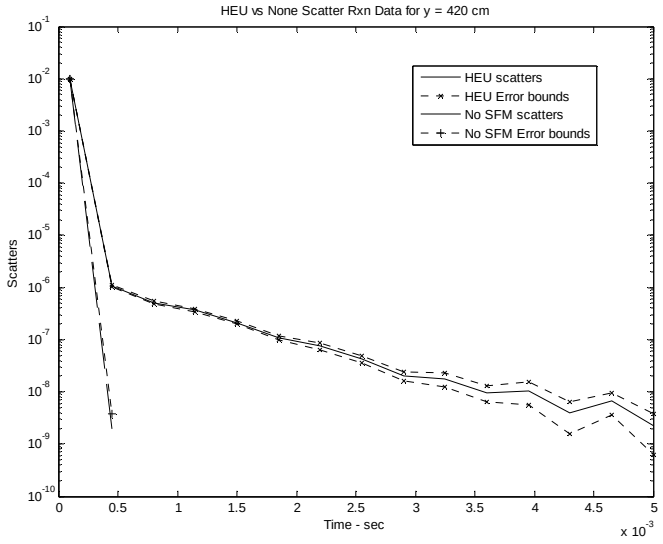

Figure 24. HEU vs. No SFM Reactions for Detector at 420 cm.

The remaining detector positions at 20, 500, 580, and 660 cm showed somewhat similar behavior, but due to fewer fissions and increased neutron attenuation, their associated detector responses became difficult to discriminate from the case with no SFM present.

In a practical situation, detector electronics would run continuously and acquire counts as a boat passed through the detector system. Thus, it was useful to sum the tallies from the nine detector positions and acquire an overall system response for the two configurations. Figure 25 shows the integral detector response for scattering reactions with HEU present compared to that with no SFM present. From the graph, the difference between the two system configurations is clear, and if a detector system showed such a response, then a positive determination of the presence of SFM could be made.

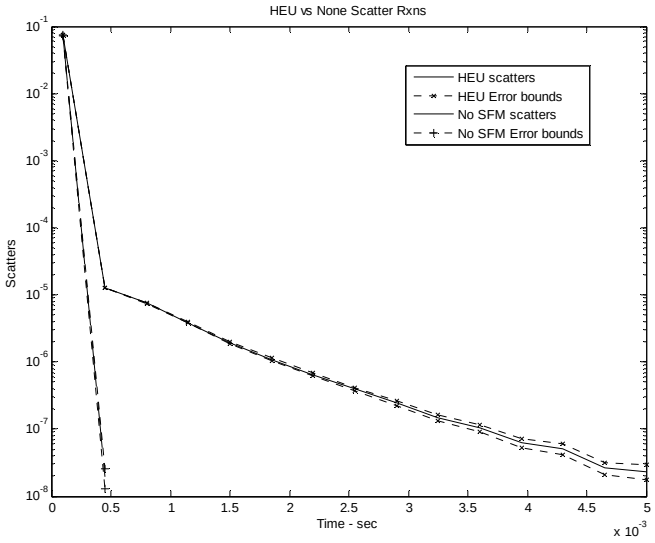

Figure 25. Integral Scattering Reactions for HEU and No SFM.

IV.3.3. Plutonium system configuration

Presented next are the results for the system with the 8 kg sphere of WG plutonium. Again, the fission neutrons were of primary interest, and the fission neutron tally inside the sphere is shown below in Figure 26. The figure again represents the number of fissions occurring in the sphere as the tally has been multiplied by the fission cross sections of the respective plutonium isotopes present in the sphere. The majority of the

fissions occurred within the first 0.1 ms after the source neutron was born. The temporal behavior of the fission reactions was more apparent after this time. Disregarding the first time bin of tally data shows more clearly both the spatial and temporal behavior of the fissions in the plutonium sphere, as shown in Figure 27.

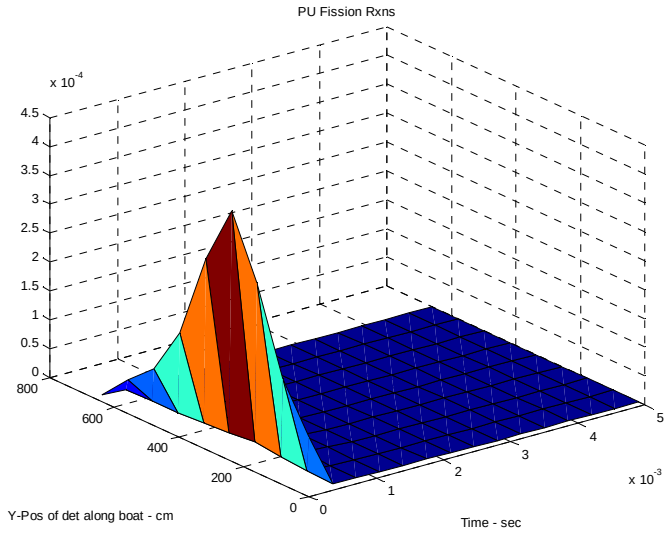

Figure 26. Plutonium Fission Reactions.

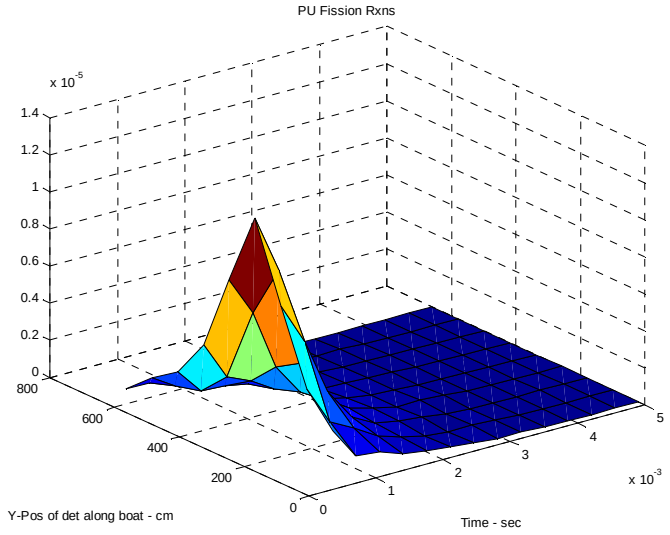

Figure 27. Plutonium Fission Reactions at t > 0.1 ms.

To get a closer look at the temporal behavior, the fission rates were summed across the nine detector positions. The exponential behavior observed in Figure 28 would be expected to drive the detector response similar to the HEU case.

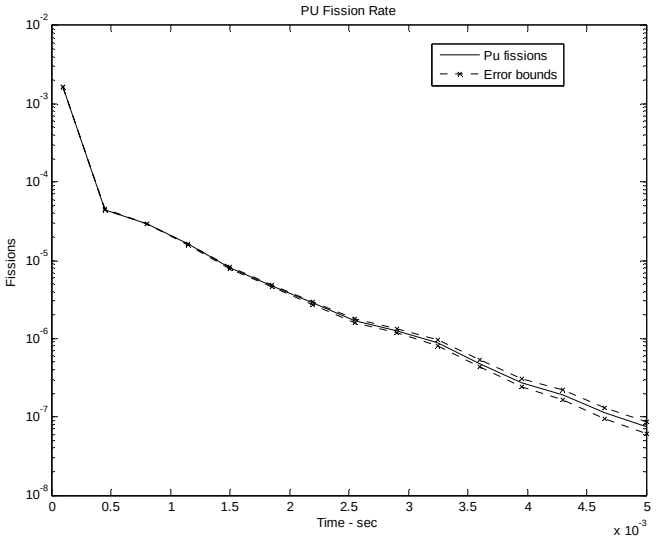

Figure 28. Integral Fissions in Plutonium.

Switching focus now to the detector response for the sphere of plutonium, Figure 29 shows the number of elastic scattering reactions occurring in the detector with respect to time and detector position. As can be seen from the figure, the response in the detector again closely resembled the response in the case with no SFM present, and was very similar to the response given by the HEU case. The first time-bin of the tally could be neglected again to see more detail of the detector response from the die-away neutrons, as shown in Figure 30 below. Note that the magnitude of the response in this case was about 2.5 orders of magnitude greater than that of the case with no SFM present, and there were neutrons present after 0.45 ms, whereas there were none in the absence of SFM.

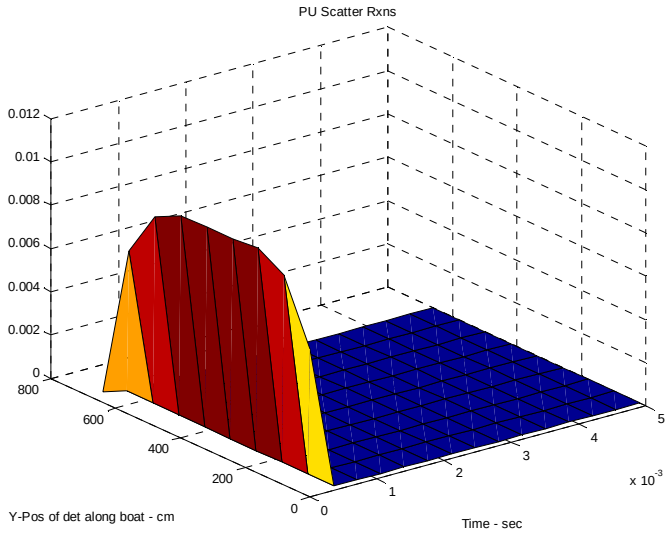

Figure 29. Scattering Reactions in Detector with Pu Sphere.

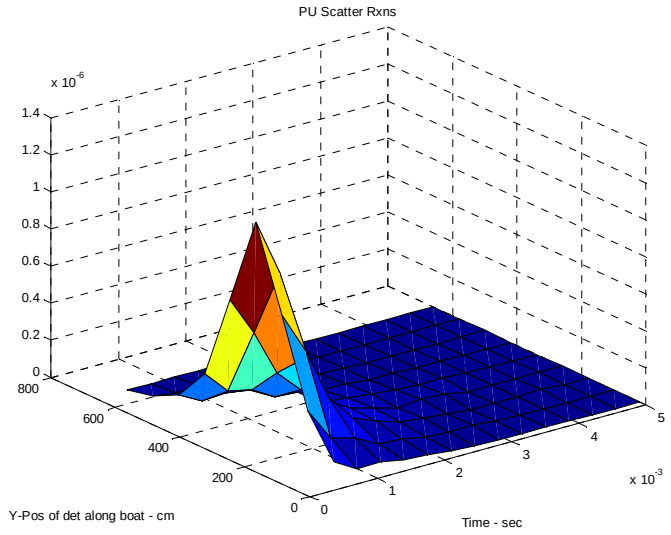

Figure 30. Scattering Reactions from Pu at t>0.1 ms.

The following figures, Figures 31 - 35, show the comparison of detector responses for the cases with and without SFM present for detector and source positions at 100, 180, 260, 340, and 420 cm. In each case, the sharply declining line was from the system with no SFM present, and the slowly attenuating line was from the presence of plutonium. In each

of these graphs, the only reactions tallied beyond 0.45 ms were from the plutonium cases. These results alone suffice in showing a statistically significant difference between the system with and without plutonium. Again, the position with the greatest magnitude of response was at 260 cm, which was to be expected considering the SFM sphere was located at the same position.

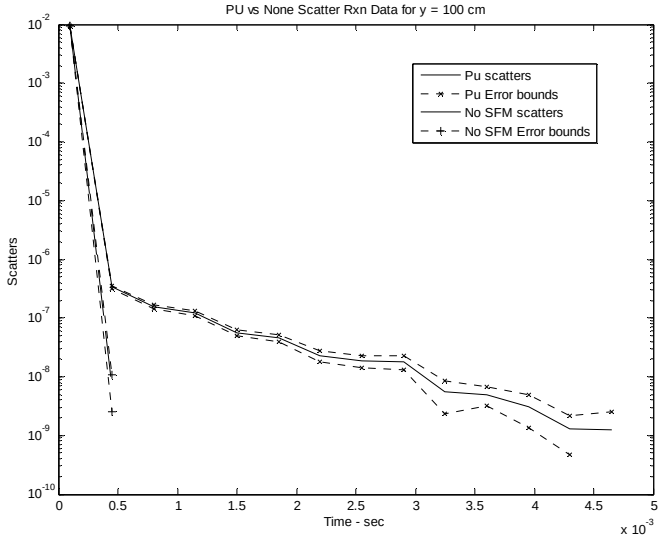

Figure 31. Plutonium vs. No SFM Reactions for Detector at 100 cm.

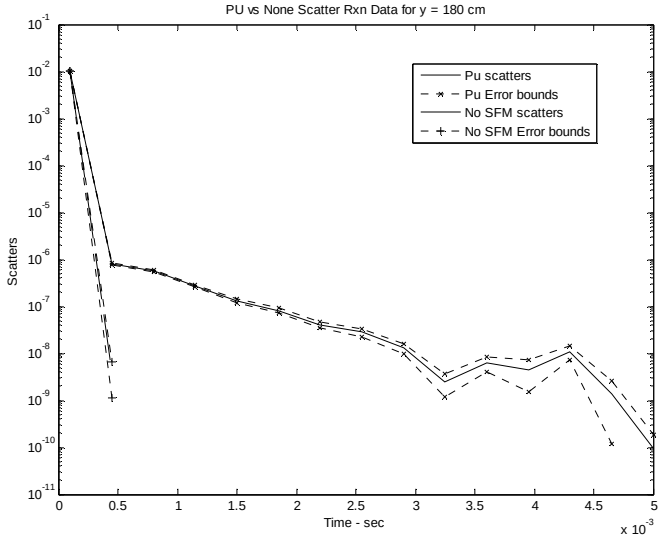

Figure 32. Plutonium vs. No SFM Reactions for Detector at 180 cm.

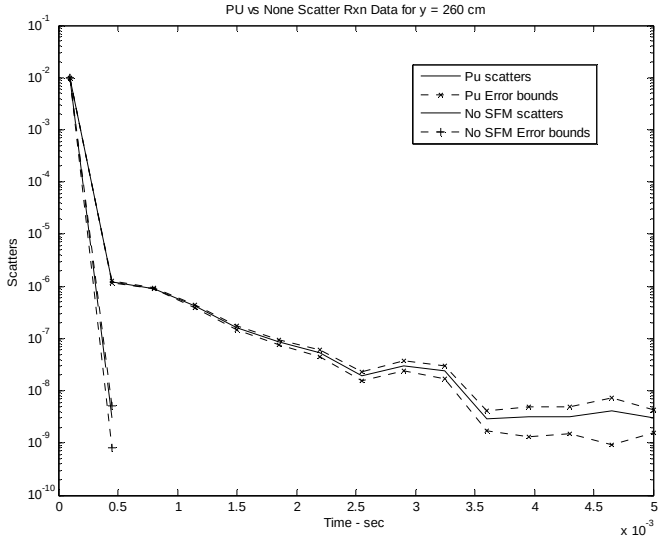

Figure 33. Plutonium vs. No SFM Reactions for Detector at 260 cm.

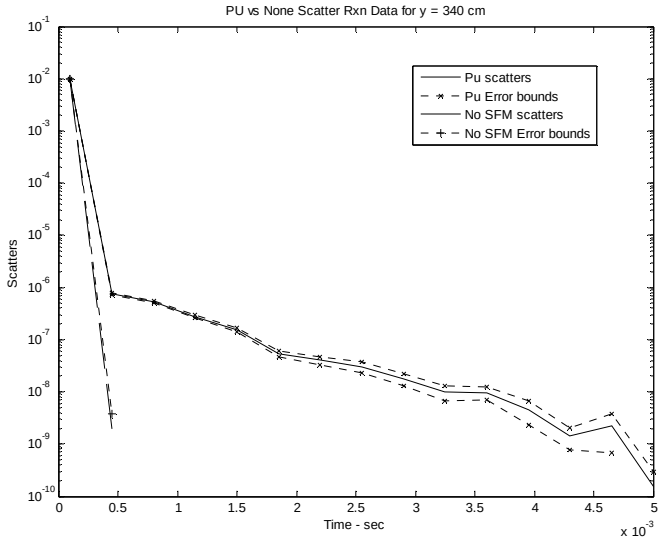

Figure 34. Plutonium vs. No SFM Reactions for Detector at 340 cm.

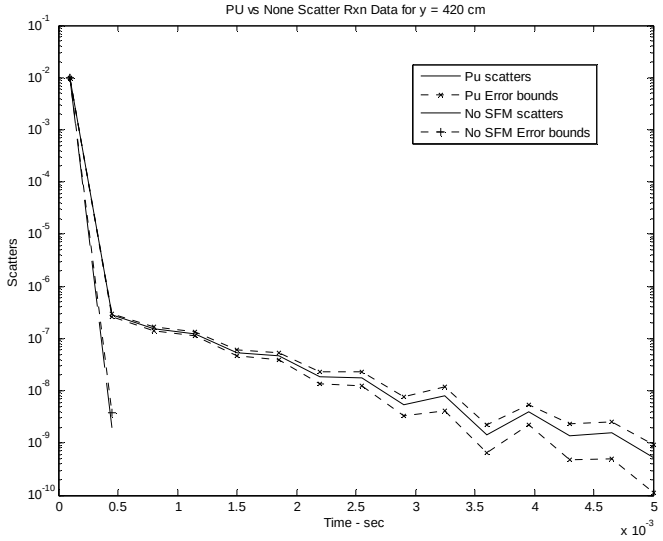

Figure 35. Plutonium vs. No SFM Reactions for Detector at 420 cm.

The remaining detector positions at 20, 500, 580, and 660 cm showed somewhat similar behavior, but due to fewer fissions and increased neutron attenuation, their associated detector responses became difficult to discriminate from the case with no SFM present.

As with the HEU case, the tallies could be summed across the nine detector positions to acquire an overall system response for the two configurations. Figure 36 shows the integral detector response for scattering reactions with plutonium present compared to that with no SFM present. From the graph, the difference between the two system configurations is clear, and if a detector system showed such a response, then a positive determination of the presence of SFM could be made.

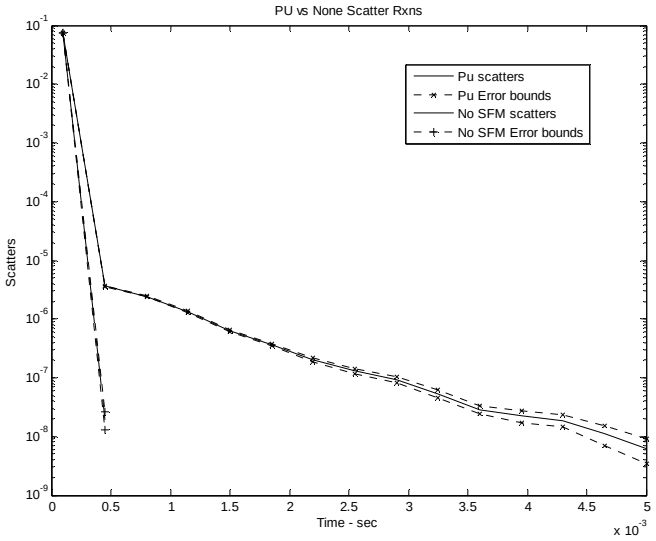

Figure 36. Integral Scattering Reactions for Plutonium and No SFM.

Overall, the magnitudes of the plutonium cases were less than those of the HEU cases. These results may seem surprising considering plutonium has an overall greater cross section for fission and has a greater average fission neutron yield than uranium does. However, the mass of ^{235}U used in these simulations was about three times greater than the ^{239}Pu mass in the simulations, and the volume of the HEU sphere was larger than the plutonium. The additional HEU mass and volume, therefore, had a greater effect than the nuclear properties of plutonium. This effect is demonstrated below in Figure 37. Table 7 shows the ratio of scattering reactions from HEU to plutonium for $t > 0.1$ ms. The average value was 3.02.

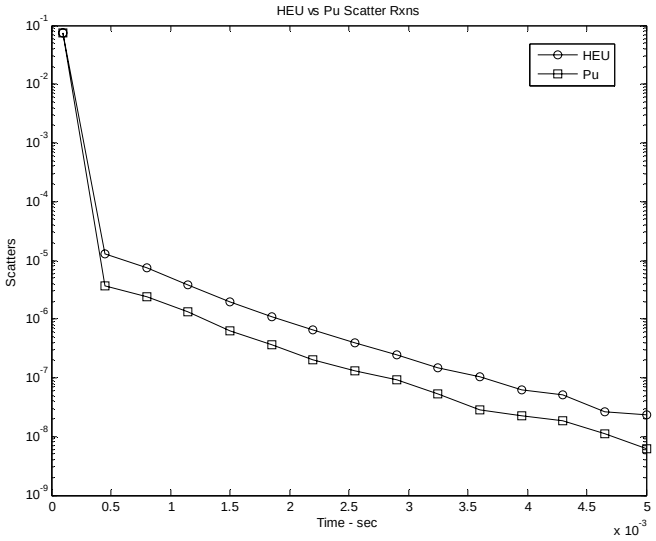

Figure 37. HEU vs. Pu Scatter Reactions.

Table 7. Scatter Reaction Ratio - HEU/Pu.

Time (ms)	Scatter Ratio (HEU/Pu)
0.45	3.50
0.80	3.10
1.15	2.91
1.50	3.06
1.85	2.98
2.20	3.25
2.55	3.03
2.90	2.61
3.25	2.71
3.60	3.55
3.95	2.83
4.30	2.70
4.65	2.37
5.00	3.75

IV.4. Analysis of background radiation

To satisfy the criteria for positive determination of the presence of SFM, knowledge of the natural background neutron radiation, and how it would be detected, was required.

As mentioned in Section *IV.2.*, the mean neutron flux at sea level is 0.00646 n/cm^2-s. From this, an estimate of the count rate in the detector could be determined using the following equation:

$$C'_{BG} = \bar{\phi}\bar{\sigma}NV \tag{9}$$

where

- C'_{BG} is the count rate due to background neutron flux,
- $\bar{\phi}$ is the mean background neutron flux (averaged over all energies),
- $\bar{\sigma}$ is the mean elastic scattering cross section (averaged over all energies),
- N is the atom density of detector material (^{1}H), and
- V is the volume of detector.

Detailed information of all the parameters would be necessary for an accurate calculation of the background count rate. However, a few conservative assumptions could be made here, yielding an over estimation that adds conservatism to the estimate.

The background neutron flux is energy-dependent with the majority of neutrons having energies less than about 100 keV, as seen in Figure 38 below. It was assumed in Section *I.5.1.3.* that the detector would not record counts for neutrons with an energy below 100 eV. It was assumed here that all background neutrons had an energy of at least 100 eV, thus adding additional conservatism to the overall analysis. Thus, $\bar{\phi}$ = 0.00646 n/cm^2-s.

As was shown seen in Figure 1 in Section *I.5.1.3.*, the elastic scattering cross section holds nearly constant at about 20.4 b from about 1 eV to 10 keV, then falls off as 1/E. The conservative assumption made was a mean scattering cross section of 20.4 b.

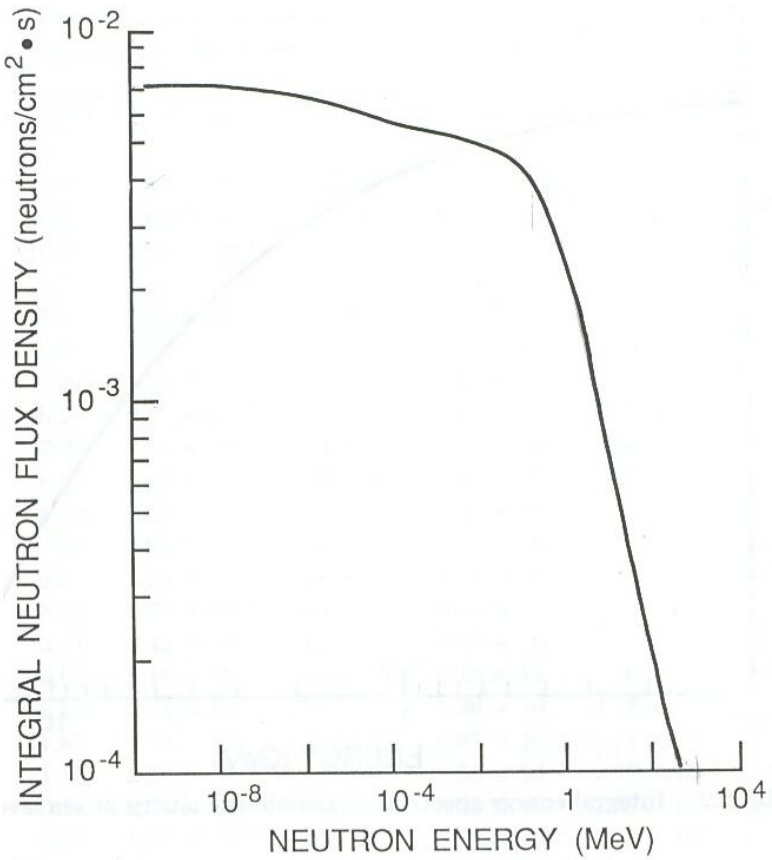

Figure 38. Background Neutron Spectrum [19].

The atom density was determined by the molar mass and density of hydrogen in the detector volume as such:

$$N = \frac{\rho N_A}{A} \tag{10}$$

where

- ρ is the mass density of hydrogen at 20 atmospheres (0.00178 g/cm^3),
- N_A is Avogadro's number (6.022 E+23 atoms/mole), and
- A is the molar mass of hydrogen (1.00794 g/mole).

Thus, the number density of hydrogen in the detector was N = 1.06 E+21 atoms/cm^3.

The volume term was calculated from the detector dimensions, which were 300 cm by 250 cm by 30 cm. The total detector volume was V = 2.25 E+6 cm^3.

The expected count rate due to background neutrons in the detector was thus

$$C'_{BG} = \left(0.00646\frac{1}{cm^2 s}\right)\left(20.4\,b\frac{10^{-24}cm^2}{b}\right)\left(1.06\times10^{21}\frac{1}{cm^3}\right)\left(2.25\times10^{6}\,cm^3\right) \quad (11)$$

$$C'_{BG} = 315 \text{ counts per second.} \quad (12)$$

The total number of background counts was then a function of Δt, the total time it takes the boat to traverse the detector system in seconds:

$$C_{BG} = 315\left(\Delta t\right) \text{ counts.} \quad (13)$$

IV.5. Estimation of required source strength

In this and the following sections, several curve fits based on the output from MCNP were calculated to approximate the fissions in the SFM spheres, the detector counts, and the dose. The results yielded by MCNP could have been used directly in a coarse approximation of these responses. However, using the curves was more useful in creating functional forms of these responses because they allowed for calculations that are smoother as functions of time and space.

The criterion that the number of induced counts in the detector was at least twice the background level was used to estimate the required source strength produced by the PNG. Doing so required an estimation of the total detector response as a function of both the die-away time and the time the boat takes traveling through the detector system. With

this function, a double integral over die-away time and time due to boat velocity yielded the total number of expected counts in the detector. Then, a comparison to twice the background was used to calculate the required source strength.

The detector response was a function consisting primarily of two components, a die-away component and a shape component. The die-away component represented the temporal dependence of the detector response after each pulse. The shape component represented the change in magnitude of the detector response as a function of source position. The general form of the function is

$$f(y,t) = AY(y)T(t) \tag{14}$$

where

- $Y(y)$ is the shape function in units of counts per centimeter,
- $T(t)$ is the die-away function in units of s^{-1}, and
- A is an appropriate dimensionless scaling constant.

The shape function came from the second time bin tally in the detector, since this was after the vast majority of source neutrons were no longer in the system, given by MCNP across the nine detector positions. This can be seen in Figure 39, which shows the comparison of the first two time bins of the system without SFM present. The difference between the first two time bins was about seven orders of magnitude. Thus, it was assumed that the shape of the data for the two SFM cases had little contribution from source neutrons beginning at 0.45 ms.

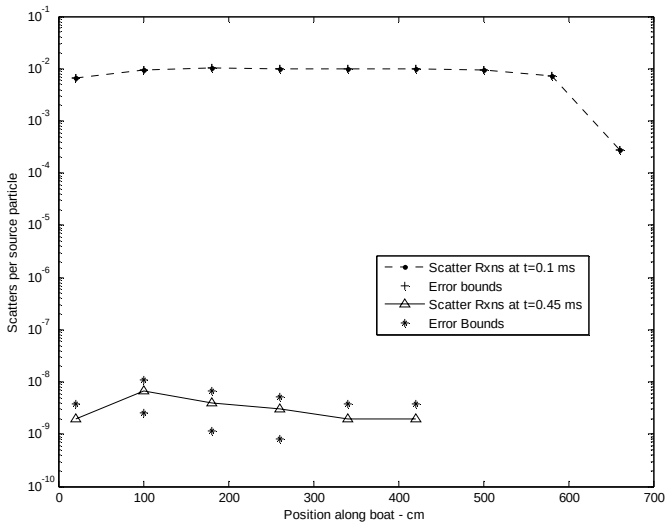

Figure 39. Scattering Reactions in Detector with No SFM, First Two Time Bins.

A shape function was fitted using the built-in Curve Fit Toolbox in MATLAB, using the general function

$$Y(y) = \frac{660\,a_1}{y\pi} e^{-b_1\left(\ln\left(\frac{y\pi}{660}\right)-c_1\right)^2} + m_1 e^{-n_1\left(\frac{y\pi}{660}-p_1\right)^2} \tag{15}$$

where the fit solved for the constants a_1, b_1, c_1, m_1, n_1, and p_1. The functional form chosen was the summation of lognormal and normal functions. The function was chose because it appeared to provide the best fit for the data. The die-away function came from the integral scattering reactions, similar to Figures 28 and 36, again beginning with the second time bin. The die-away function was

$$T(t) = a_2 e^{-b_2 t} + m_2 e^{-n_2 t}\,. \tag{16}$$

where the fit solves for the constants a, b, m, and n. The scaling constant, A, was calculated from the equation

$$A = \left(\int_{t_1}^{t_2} T(t)\, dt \right)^{-1} \tag{17}$$

where t_1 and t_2 were the lower and upper limits of the second time bin used in MCNP. The integral arose from the fact that the tally in the second time bin was a summation of all the scores that occurred between the end of the first time bin through the upper limit of the second. Thus, the scaling factor A served as a sort of normalization constant similar to what is calculated when deriving probability distributions.

The detector response function came from transforming the shape function into a function of time based on boat velocity, where $t_v = v\,y = 51.44 v_k y$. The factor 51.44 arose from the conversion of velocity, v, in centimeters per second to knots (nautical miles per hour), v_k. This conversion was necessary because the shape function was derived with position in terms of centimeters. Additionally, the detector response function was multiplied by the source strength to yield the total expected number of counts in any given time bin, as what might be expected using a multichannel scalar. The detector response was thus a function of boat velocity and source strength

$$DR(v_k, S) = S \int_{\frac{y_i}{51.44 v_k}}^{\frac{y_f}{51.44 v_k}} \int_{t_{lo}}^{t_{hi}} f\left(51.44 v_k t_v, t_d\right) dt_d\, dt_v \tag{18}$$

where

- S is the source strength (neutrons per pulse),
- y_i and y_f are the initial and final positions of the boat in the detector system (cm),
- t_{lo} and t_{hi} are the limits of the time bin (seconds), and

- v_k is the boat velocity (knots),

The estimation of counts due to background radiation was found by scaling the background count rate from Equation 10 by the bin width and multiplying by the total time the boat spends traveling through the detector system

$$C_{BG} = \frac{C'_{BG}\left(t_{hi} - t_{lo}\right)\left(y_f - y_i\right)}{51.44 v_k}. \tag{19}$$

IV.5.1. Required source strength for HEU

The constants for the shape function (Equation 13) were found using the MATLAB Curve Fit Toolbox using the data from the second time bin for the HEU case. The points used for the shape function fit are given in Table 8. The resulting constants for the shape function *Y(y)* are given in Table 9, and Figure 40 shows the interpolation points superimposed with the fitted shape function.

Table 8. HEU Shape Function Interpolation Points.

y (cm)	20	100	180	260	340
n/sp	4.4220e-7	1.2218e-6	2.7186e-6	4.0401e-6	2.7287e-6
$\sigma_{n/sp}$	2.8212e-8	5.0704e-8	7.7480e-8	9.7771e-8	7.9949e-8
y (cm)	420	500	580	660	
n/sp	1.0952e-6	3.5596e-7	1.1134e-7	4.3581e-9	
$\sigma_{n/sp}$	4.5452e-8	2.5842e-8	1.1813e-8	2.1769e-9	

Table 9. Shape Function Constants for HEU.

Constant	Value
a_1	3.336e-6
b_1	0.361
c_1	5.879
M_1	1.943e-6
n_1	1.975
p_1	0.9621

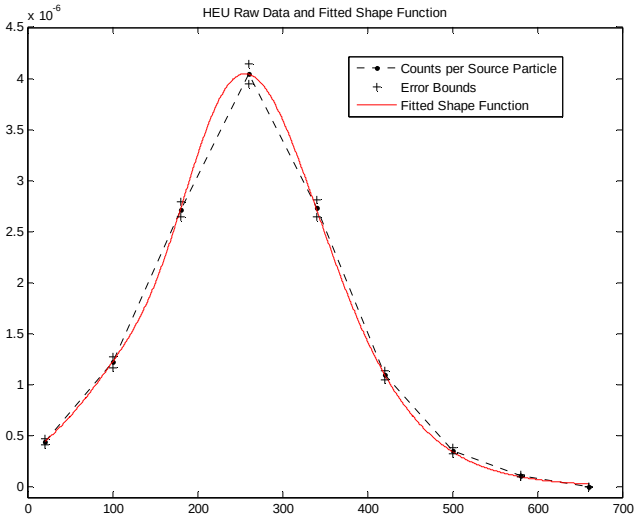

Figure 40. Fitted Shape Function for HEU.

The points used for the die-away function (Equation 14) are given below in Table 10. The resulting constants for the die-away function $T(t)$ are given in Table 11, and Figure 41 shows the interpolation points superimposed with the fitted die-away function. The scaling constant, A, was calculated to be 1.3808E+9.

Table 10. HEU Die-away Function Interpolation Points.

time (ms)	0.1	0.45	0.80	1.15	1.85	2.20	2.55
n/sp	1.2718e-5	7.5176e-6	3.8773e-6	1.9318e-6	1.0923e-6	6.5126e-7	3.9236e-7
$\sigma_{n/sp}$	1.6793e-7	1.1703e-7	8.0634e-8	5.497e-8	4.4757e-8	3.044e-8	2.4471e-8
time (ms)	2.90	3.25	3.60	3.95	4.30	4.65	5.00
n/sp	2.4284e-7	1.4779e-7	1.0316e-7	6.2857e-8	5.0804e-8	2.6377e-8	2.3561e-8
$\sigma_{n/sp}$	2.3025e-8	1.5155e-8	1.1811e-8	9.3919e-9	8.9074e-9	5.3401e-9	5.7166e-9

Table 11. Die-away Function Constants for HEU.

Constant	Value
a_2	3.102e-5
b_2	-2174
m_2	4.258e-6
n_2	-1040

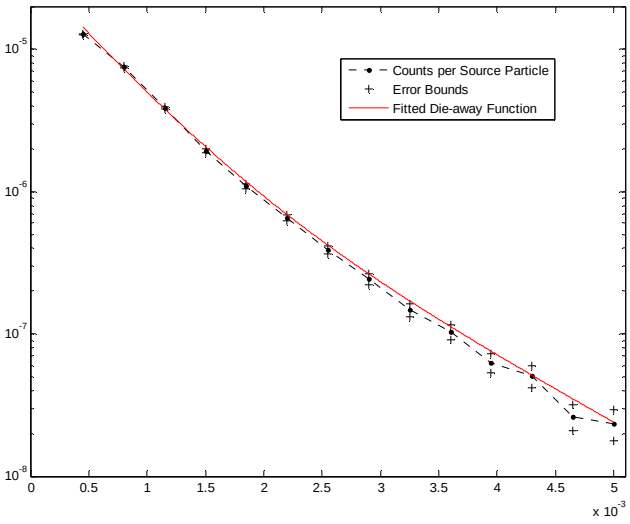

Figure 41. Fitted Die-away Curve for HEU.

Although the fitted die-away function seems to overestimate the data, especially at the later values, the function also slightly underestimates the data at earlier values. The errors tend to compensate each other, but the logarithmic scale seems to show greater disparity.

The required source strength, or neutrons per pulse, was then found by setting the detector response function (Equation 16) equal to twice the number of background counts (Equation 17) over the die-away time for boat positions 20 cm through 660 cm. Solving over the entire die-away time, rather than over the first time bin where the number of counts is greatest, provided a conservative estimate of the required source strength.

$$S \int_{\frac{20}{51.44 v_k}}^{\frac{660}{51.44 v_k}} \int_{0.0001}^{0.005} f\left(51.44 v_k t_v, t_d\right) dt_d dt_v = 2C_{BG} = 2\frac{C'_{BG}\left(t_{hi} - t_{lo}\right)\left(y_f - y_i\right)}{51.44 v_k} \qquad (20)$$

$$S\int_{\frac{20}{51.44v_k}}^{\frac{660}{51.44v_k}}\int_{0.0001}^{0.005} f\left(51.44v_k t_v, t_d\right) dt_d dt_v = 2\frac{315(0.005-0.0001)(660-20)}{51.44v_k} \tag{21}$$

$$(4.079E-5)\frac{S}{v_k} = 38.40\frac{1}{v_k} \tag{22}$$

$$S = 9.413E5 \text{ neutrons per pulse.} \tag{23}$$

Note the detector response function essentially collapses to a constant multiplied by source strength divided by boat velocity. Thus, the required source strength was about 940,000 neutrons per pulse, which is less than the typical operational level of a PNG at 1,000,000 neutrons per pulse. Table 12 shows the results and comparisons of detector response to HEU system counts (neutrons from the source and fission) and estimated background at a boat velocity of 5 knots and a pulse rate of 100 Hz with 10^6 neutrons per pulse.

Table 12. Comparison of Estimated System and Background Counts for HEU.

Interval	Estimated Counts		Ratio: Sys/Bac
	System	Background	
0.1 - 0.45 ms	390	27	14
0.1 - 5 ms	820	380	2.2

From the table, it is apparent the most of the counts due to source and fission neutrons occur soon after the pulse and are much greater than background, which should enable the detection of the HEU.

IV.5.2. Required source strength for plutonium

For the plutonium case, the constants for the shape function (Equation 13) were again found using the MATLAB Curve Fit toolbox and the second time bin data from

MCNP. The points used for the shape function fit are given in Table 13. The resulting constants for the shape function $Y(y)$ are given in Table 14, and Figure 42 below shows the interpolation points superimposed with the fitted shape function.

Table 13. Plutonium Shape Function Interpolation Points.

y (cm)	20	100	180	260	340
n/sp	1.2665e-7	3.345e-7	7.8891e-7	1.2273e-6	7.4323e-7
$\sigma_{n/sp}$	1.2715e-8	2.1976e-8	3.5895e-8	4.811e-8	3.3594e-8
y (cm)	420	500	580	660	
n/sp	2.7988e-7	1.0011e-7	3.3946e-8	1.3342e-9	
$\sigma_{n/sp}$	1.864e-8	1.3284e-8	5.8794e-9	1.3342e-9	

Table 14. Shape Function Constants for Plutonium.

Constant	Value
a_1	1.396e-6
b_1	0.3082
c_1	6.122
m_1	3.809e-7
n_1	3.028
p_1	0.6955

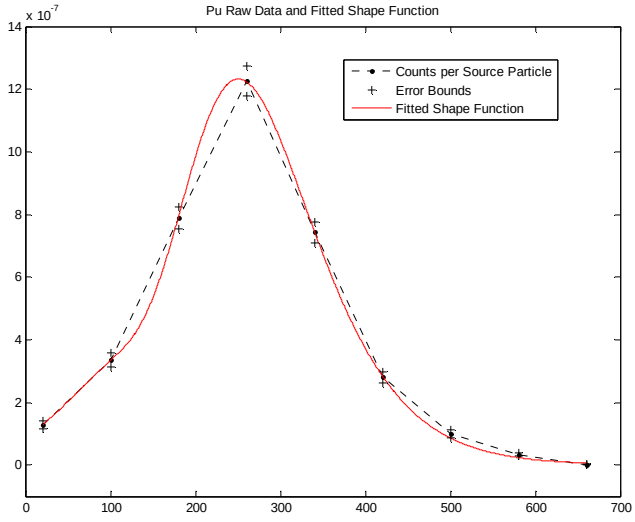

Figure 42. Fitted Shape Function for Plutonium.

The points used for the die-away function (Equation 14) are given below in Table 15. The resulting constants for the die-away function $T(t)$ are given in Table 16, and Figure 43 shows the interpolation points superimposed with the fitted die-away function. The scaling constant, A, was calculated to be 6.1299E+8.

Table 15. Plutonium Die-away Function Interpolation Points.

time (ms)	0.1	0.45	0.80	1.15	1.85	2.20	2.55
n/sp	3.6358e-6	2.4232e-6	1.3337e-6	6.3212e-7	3.6621e-7	2.0028e-7	1.2948e-7
$\sigma_{n/sp}$	7.7049e-8	5.6897e-8	4.0954e-8	2.8722e-8	2.0164e-8	1.5329e-8	1.2263e-8
time (ms)	2.90	3.25	3.60	3.95	4.30	4.65	5.00
n/sp	9.315e-8	5.439e-8	2.907e-8	2.2222e-8	1.8839e-8	1.1151e-8	6.2871e-9
$\sigma_{n/sp}$	1.0584e-8	9.3201e-9	4.4813e-9	5.0424e-9	4.229e-9	4.1182e-9	2.9078e-9

Table 16. Die-away Function Constants for Plutonium.

Constant	Value
a_2	-2.595e-6
b_2	-2915
m_2	8.999e-6
n2	-1597

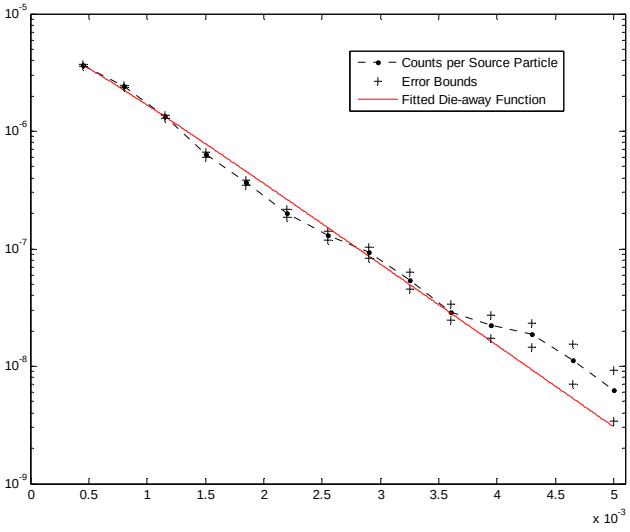

Figure 43. Fitted Die-away Curve for Plutonium.

The required source strength, in neutrons per pulse, was again found by setting the detector response function (Equation 16) equal to twice the number of background counts (Equation 17) over the die-away time for boat positions 20 cm through 660 cm.

$$S\int_{\frac{20}{51.44v_k}}^{\frac{660}{51.44v_k}}\int_{0.0001}^{0.005} f\left(51.44v_k t_v, t_d\right) dt_d dt_v = 2C_{BG} = 2\frac{C'_{BG}\left(t_{hi}-t_{lo}\right)\left(y_f - y_i\right)}{51.44v_k} \tag{24}$$

$$S\int_{\frac{20}{51.44v_k}}^{\frac{660}{51.44v_k}}\int_{0.0001}^{0.005} f\left(51.44v_k t_v, t_d\right) dt_d dt_v = 2\frac{315\left(0.005-0.0001\right)\left(660-20\right)}{51.44v_k} \tag{25}$$

$$\left(1.405E-5\right)\frac{S}{v_k} = 38.40\frac{1}{v_k} \tag{26}$$

$$S = 2.733E6 \text{ neutrons per pulse.} \tag{27}$$

Again, the detector response function essentially collapses to a constant multiplied by source strength divided by boat velocity. Thus, the required source strength was about 2,700,000 neutrons per pulse, which is greater than the typical operational level of a PNG at 10^6 neutrons per pulse. While this value was greater than what might be desired, it is worth noting that some commercial PNG's are able produce at this level and, as mentioned in the HEU case, the choice to solve over the entire die-away time was made as a conservative assumption. Additionally, there was a fair amount of conservatism in the estimate of the background neutron levels, so this result should not necessarily be interpreted as negative. Table 17 shows the results and comparisons of detector response to plutonium system counts (neutrons from the source and fission) and estimated background at a boat velocity of 5 knots and a pulse rate of 100 Hz with 10^6 neutrons per pulse.

Table 17. Comparison of Estimated System and Background Counts for Plutonium.

Interval	Estimated Counts		Ratio: Sys/Bac
	System	Background	
0.1 - 0.45 ms	110	27	4.0
0.1 - 5 ms	280	380	0.74

As can be seen in the table, although the response was weaker for plutonium than for HEU, the response due to plutonium in the system was still four times greater than background. This result shows that it could still be possible to detect plutonium in the given system configuration.

IV.6. Passive plutonium spontaneous fission measurements

As shown in Section *II.V.2.*, WG plutonium has a much higher spontaneous fission rate than HEU. Because of this, it was worthwhile to examine the possibility of detection plutonium passively via spontaneous fission (SF) neutrons. An estimation of the detector response to spontaneous fission neutron detection was calculated using the SF data of ^{240}Pu listed in Table 18. While other plutonium isotopes also spontaneously fission, Table 2 showed that each of their contributions are negligible compared to ^{240}Pu. Additionally, considering only ^{240}Pu adds conservatism to the estimated detector response. The parameters *a* and *b* of the Watt fission spectrum (Equation 1) for ^{240}Pu spontaneous fission are given in Table 18.

Table 18. Watt Fission Spectrum Parameters.

Isotope	*a* (MeV)	*b* (MeV^{-1})
^{240}Pu	0.799	4.903

The total counts in the detector due to SF was the estimated counts per SF neutron yielded by ^{240}Pu, SF_{240}, multiplied by the respective number of average SF neutrons from Table 2:

$$C_{SF} = 3.0E5\,SF_{240}\,. \tag{28}$$

As before, a shape function was calculated from the MCNP results for the SF results. The functional form in this case was the summation of two normal, or Gaussian, functions. The general shape function was

$$Y(y) = a_3 e^{-\left(\frac{y-b_3}{c_3}\right)^2} + m_3 e^{-\left(\frac{y-n_3}{p_3}\right)^2}\,. \tag{29}$$

Note the use of a scaling factor was not necessary in this case since the function directly estimates the overall response from the MCNP output and is already scaled according to the source strength of SF neutrons. The points used to fit the shape function are listed in Table 19.

Table 19. Interpolation Points for Spontaneous Fission Shape Function.

y (cm)	20	100	180	260	340
C_{SF}	11884	20303	27925	31046	28020
$\sigma_{C,SF}$	86.754	117.75	145.21	158.34	145.7
y (cm)	420	500	580	660	
C_{SF}	20722	12823	7440.7	4226.1	
$\sigma_{C,SF}$	122.26	91.041	67.711	49.868	

The constants for the shape function are given in Table 20, and a comparison of the interpolation points and the shape function is shown in Figure 44.

Table 20. Constants for Spontaneous Fission Shape Function.

Constant	Value
a_3	3.102E+4
b_3	259.3
c_3	244.3
m_3	2128
n_3	647.6
p_3	202.1

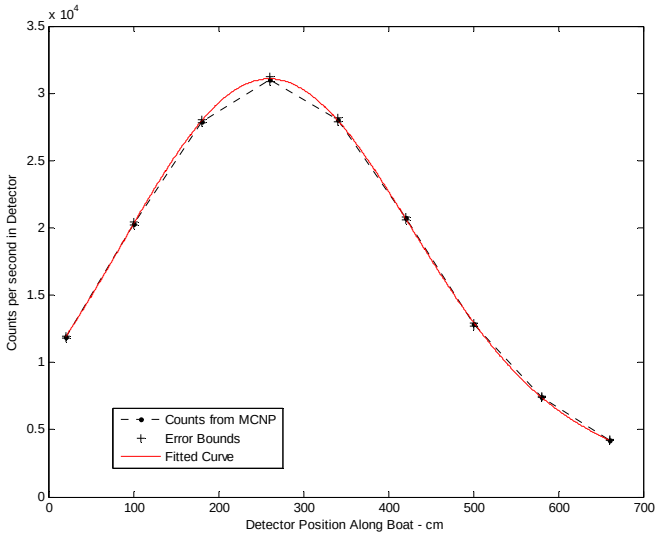

Figure 44. Shape Function for Spontaneous Fission Response.

The shape function was again transformed into a function of boat velocity, such that

$$DR(v_k) = \int_{\frac{20}{51.44 v_k}}^{\frac{660}{51.44 v_k}} Y(51.44 v_k t_v)\, dt_v \,. \tag{30}$$

The comparable background counts for this case was given by

$$C_{BG} = \frac{C'_{BG}(y_f - y_i)}{51.44 v_k} \,. \tag{31}$$

To see the relative magnitude of the detector response to spontaneous fission versus background, simply divide the two equations.

$$R_{DR/C_{BG}} = \frac{\int_{\frac{20}{51.44 v_k}}^{\frac{660}{51.44 v_k}} Y\left(51.44 v_k t_v\right) dt_v}{\frac{315(660-20)}{51.44 v_k}} \tag{32}$$

$$R_{DR/C_{BG}} = 62.4 . \tag{33}$$

Thus, the estimated number of counts in the detector from spontaneous fission should be sufficiently greater than background to allow for the detection of plutonium via passive neutron detection. The estimated total number of counts for a given pass with a boat velocity of 5 knots was about 49,000. This result was much greater than for either the HEU or the plutonium source-driven results, which lends to a much easier detection of plutonium, especially for a combined passive and active detector system.

IV.7. Estimated dose to passengers

A standard ICRU tissue-equivalent sphere was used to estimate the dose to a passenger onboard the boat. To provide a conservative estimate of the possible dose, the sphere was located directly adjacent to the SFM sphere, with the respective sphere centers in a line along the length of the boat, with the ICRU sphere towards the bow, and at an equivalent height on the boat interior, as seen in Figure 45. The composition of the ICRU tissue-equivalent sphere, with MCNP ZAID, is listed in Table 21.

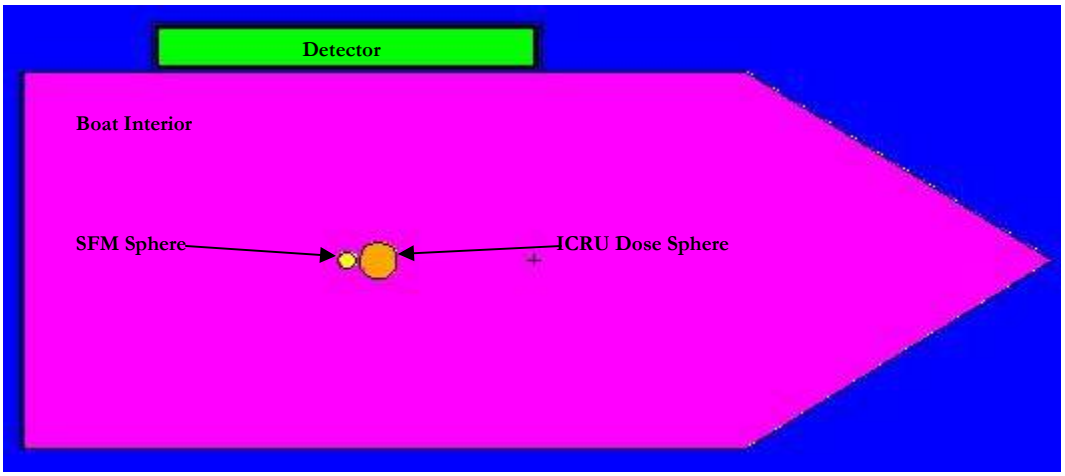

Figure 45. Boat with SFM Sphere and ICRU Dose Sphere.

Table 21. ICRU Sphere Composition.

Element/Isotope	% by mass	MCNP ZAID
^{1}H	10.098	1001.66c
^{2}H	0.001515	1002.66c
16O	76.171	8016.66c
17O	0.029014	8017.66c
14N	2.5905	7014.66c
15N	0.009516	7015.66c
C	11.1	6000.66c

MCNP also utilizes a set of flux-to-dose conversion factors that will change the flux tally to a dose tally based on the energy of the neutron being tallied. The set of factors used is listed below in Table 22. Where appropriate, MCNP logarithmically interpolates the conversion factors based on energy.

To find the total dose, a process similar to before was employed to estimate the shape of the dose response based on the total fissions induced in the sphere. This assumed that the shape of the fission curve was similar to the dose curve, which was appropriate since both were driven by the source in the problem. Where the response function differs was that there was no time-dependent factor because the total dose was desired.

Table 22. Flux-to-Dose Conversion Factors [20].

Energy (MeV)	Factor (10^{-12} Sv cm^2)	Energy (MeV)	Factor (10^{-12} Sv cm^2)
2.5E-8	8.0	1.5	362
1.0E-7	10.4	2.0	352
1.0E-6	11.2	3.0	380
1.0E-5	9.2	4.0	409
1.0E-4	7.1	5.0	378
1.0E-3	6.2	6.0	383
1.0E-2	8.6	7.0	403
2.0E-2	14.6	8.0	417
5.0E-2	35.0	10.0	446
1.0E-1	69.0	14.0	520
2.0E-1	126	17.0	610
5.0E-1	258	20.0	650
1.0	340		

The scaling factor in this case was determined by equating the value of the shape function at a given source position with the estimated dose given by MCNP at that position divided by the volume of the ICRU sphere. This was done because the volume of the sphere was set to unity in the MCNP input deck, resulting in the estimate being multiplied by the volume of the sphere. Because of these assumptions, only one MCNP calculation was done at the source-detector position that was inline with the HEU and plutonium spheres (the input decks are given in Appendix A). A similar transformation to dose as a function of boat velocity was done, so that the resulting dose response function is

$$H\left(v_k\right) = 1.0E5\, S\, A \int_{\frac{20}{51.44 v_k}}^{\frac{660}{51.44 v_k}} Y\left(51.44\, v_k t_v\right) dt_v \tag{34}$$

where

- 1.0E+5 comes from the conversion from Sv to mrem,

- $Y(y)$ is the shape function from Equation 13, but in units of Sieverts per second,
- A is a scaling factor, in units of seconds, and
- S is the source strength, in neutrons per second.

The scaling factor was determined by

$$A = \frac{\hat{H}(260\,cm)}{V_{sphere}} \frac{1}{Y(260\,cm)}$$

where

- $\hat{H}(260\,cm)$ is the estimated dose (Sv cm^3) given by MCNP,
- $V_{sphere} = \frac{4}{3}\pi(15\,cm)^3 = 1.13E5\,cm^3$, and
- $Y(260\,cm)$ is the shape function evaluated at 260 cm.

IV.7.1. Estimated dose with HEU

For the case with HEU present, MCNP estimated the dose at 260 cm to be 2.12494E-11 Sv cm^3. The constants for the shape function were calculated using the interpolation points given in Table 23. The shape function constants are listed in Table 24. The plot of the interpolation points with the fitted curve is shown below in Figure 46. The scaling constant was calculated to be 7.8761E-14 seconds. The estimated total dose for a boat velocity of 5 knots with a source strength of 10^8 n/s was 2.20 μrem (micro-rem).

Table 23. Interpolation Points for HEU Dose Shape Function.

y (cm)	20	100	180	260	340
n/sp	0.00053021	0.00098207	0.0018	0.0023929	0.0017854
$\sigma_{n/sp}$	4.0522e-6	5.4793e-6	7.4374e-6	8.7206e-6	7.3864e-6
y (cm)	420	500	580	660	
n/sp	0.00096152	0.00049402	0.00027268	9.39e-6	
$\sigma_{n/sp}$	5.4654e-6	3.9501e-6	2.8418e-6	5.477e-7	

Table 24. Shape Function Constants for HEU Dose.

Constant	Value
a_1	0.002661
b_1	0.4092
c_1	4.125
m_1	0.001034
n_1	1.989
p_1	0.6747

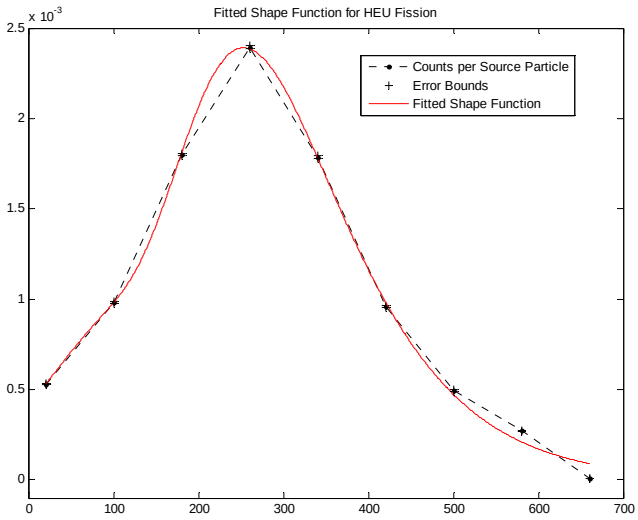

Figure 46. Fitted Shape Function for HEU Fission.

IV.7.2. Estimated dose with plutonium

For the case with plutonium present, MCNP estimated the dose at 260 cm to be 2.02920E-11 Sv cm^3. The constants for the shape function were calculated using the interpolation points given in Table 25. The constants for the shape function are listed in Table 26. The plot of the interpolation points with the fitted curve is shown below in Figure 47. The scaling constant was calculated to be 4.1414E-13 seconds. The estimated total dose for a boat velocity of 5 knots with a source strength of 10^8 n/s was 2.20 μrem, the same as in the HEU case (a discussion of this similarity is given in the following section).

Table 25. Interpolation Points for Plutonium Dose Shape Function.

y (cm)	20	100	180	260	340
n/sp	0.00010279	0.00018617	0.00034206	0.00045442	0.00034129
$\sigma_{n/sp}$	1.102e-6	1.4927e-6	2.0206e-6	2.3304e-6	2.0484e-6
y (cm)	420	500	580	660	
n/sp	0.00018347	9.4209e-5	5.2657e-5	2.1033e-6	
$\sigma_{n/sp}$	1.5225e-6	1.0692e-6	8.0562e-7	1.8216e-7	

Table 26. Shape Function Constants for Plutonium Dose.

Constant	Value
a	0.0005044
b	0.4102
c	4.094
m	0.0001954
n	1.922
p	0.6735

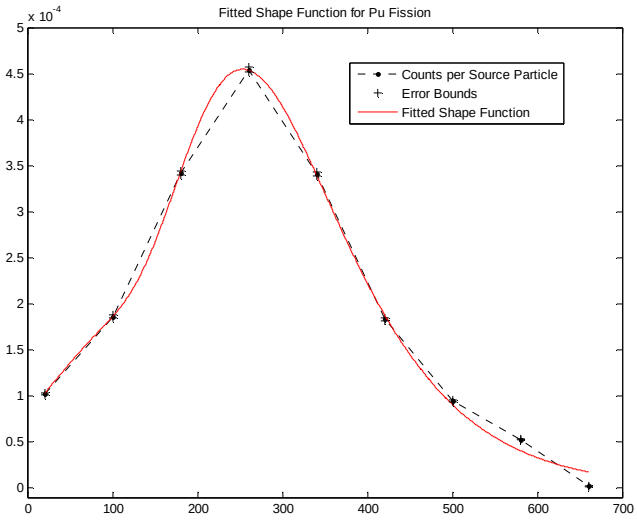

Figure 47. Fitted Shape Function for Plutonium Fission.

IV.8. Summary of results

It has been shown in this chapter than the active detection of SFM yields detector responses significantly greater than the naturally occurring background neutron

radioactivity. While the response of HEU to active interrogation is greater than plutonium, the response of plutonium to passive NDA is much greater than either HEU or plutonium in an active mode. In fact, a detector setup could feasibly be developed that ran part of the time in an active mode and part of the time in passive mode, which would enable for the determination of not only the presence of SFM, but also the determination of what kind of SFM – either HEU or plutonium.

Additionally, the estimation of dose to a passenger onboard the boat has shown that the radiological hazard to passengers is minimal. A detection system such as the one proposed in this thesis would require a license from the United States Nuclear Regulatory Commission, and as such would be subject to the United States Code of Federal Regulations (CFR). 10 CFR 20.1301 has set the dose limit to members of the general public at 100 mrem per year. At the calculated dose rate of 2.20 μrem per pass, a passenger would have to traverse the detector system more than 45,000 times before reaching the mandated limit. It is quite reasonable to assume, then, that this limit would not be reached in any reasonable manner.

CHAPTER V

CONCLUSIONS

This thesis has shown that it is feasible to use an active neutron system to detect a significant quantity of special fissile material onboard a small boat via the differential die-away technique. The system simulated the use of a pulsed neutron generator to induce fission in the fissile material and then detected the resulting neutrons using a proton-recoil detector. The use of a proton recoil detector differs from the standard practice of using ^{3}He detectors, but it has been shown the results are similar. The reason proton-recoil detectors were chosen was that they are non-responsive to thermal neutrons, and in this system, there would likely be a great deal of thermal neutrons because of the ubiquitous presence of water. There was a significant difference between the system with and without the presence of fissile material, and the estimated detector response for the system with fissile material present was shown to be sufficiently greater than the response due to background radiation only. Additionally, dose was estimated and found to be small enough that the system would not likely pose a significant radiological health risk to passengers on the boat.

Several considerations went into the design of the model. The selected watercraft was chosen to represent what would typically be found going in and out of a marina used by members of the general public. The detector gas was chosen to minimize the response to low-energy neutrons, thus effectively screening out the vast majority of the source-driven background radiation. Because of this property, the detection system is more practical because it would not have to rely on other materials to eliminate these background neutrons, such as cadmium, that could otherwise make the system heavier, bulky, and more

expensive to produce. Additionally, a cadmium cover would be prone to such hazards as the weather and collision with boats going through the detector system. The source type was chosen because of its practical availability and wide use in a variety of current applications, specifically to those using similar detection techniques. In general, simplicity of design is desirable when developing detector systems for practical field operations.

The criteria for a positive determination of the presence of special fissile material were detailed, and the system showed the ability to meet and surpass these criteria. The results with the highly enriched uranium present showed about a three times greater response than with the presence of weapons-grade plutonium. However, it was also shown that it could be possible to detect the presence of plutonium passively, that is, without having to induce fission, whereas this possibility would not exist for highly enriched uranium due to the very low level of spontaneous fission in highly enriched uranium. A comparison to background neutron radiation was made, and it was shown that despite an overestimation of background, the system still yielded a sufficiently greater response with the presence of fissile material.

The single greatest recommendation for future work is to build a physical experiment through which the estimates of the current research could be validated. A number of details would be required to accomplish such an endeavor. A more detailed analysis of the detector response to background radiation needs to be done. Also, the overall efficiency of the type of detector modeled in the current research would be required. It would be useful to determine the limits of the application of the current detection method. For example, the presence of shielding material around the fissile material would

likely cause a change in the detector response with a strong dependency on the type of shielding material, whether it was low-Z, high-Z, or a combination of the two.

Other capabilities of the system could also be examined. One capability of the system could be not only to determine the presence of fissile material, but also to identify the type of material. For example, if both passive and active detection techniques were employed, and if passive detectors showed a strong response with weak response from the active mode, then it might suggest the presence of plutonium specifically. Then, if there were a strong response in the active mode while at the same time showing a weak passive detector response, then it might suggest the presence of uranium. Another capability could be the ability to determine the location of the fissile material within the boat based on the change in magnitude of the count rate as the boat passed. Additionally, if several small detectors were placed along the vertical axis, then that could also yield information as to the position of the fissile material. Such capabilities would be useful to security personnel monitoring the detector system in that it would aid in the rapid interdiction of the boat and preempt activation of the device, if that were the intent of the passengers.

Overall, further development of both the theoretical and experimental facets of the detection system would be useful to the production and implementation of the detection system. Once implemented, there would be an additional layer of security to a country with open ports where people come and go freely and where there would otherwise be less stringent security currently in place.

REFERENCES

[1] IAEA Safeguards Glossary – 2001 ed. – Vienna: International Atomic Energy Agency, 2002.

[2] E.B. Norman, S.G. Prussin, R. Larimer, H. Shugart, E. Browne, A.R. Smith, R.J. McDonald, H. Nitsche, P. Gupta, M.I. Frank, T.B. Gosnell, Nuclear Instruments and Methods in Physics Research A 521 (2004) 608-610.

[3] C.S. Blessinger, B.D. Rooney, R.L. York, D.A. Close, H.E. Williams III, J.D. Weiting, L.L. Sprouse, Active Neutron Interrogation Package Monitor. Los Alamos National Laboratory Report LA-UR-02-5783, 2002.

[4] Ye.P. Bogolubov, S.A. Korotkov, L.A. Korytko, V.G. Morukov, V.I. Nazarov, Yu.G. Polkanov, T.O. Khasaev, Nuclear Instruments and Methods in Physics Research B 213 (2004) 439-444.

[5] G. Allison, Nuclear Terrorism: The Ultimate Preventable Catastrophe. New York, NY: Times Books, Henry Holt and Company, LLC, 2004.

[6] Public Broadcasting Station, Frontline: Loose Nukes: An Interview with Yuri Smirnov, http://www.pbs.org/wgbh/pages/frontline/shows/nukes/interviews/smirnov.html – information retrieved 11 October 2004.

[7] B.H. Armitage, P.M.J. Chard, S. Croft, K.P. Lambert, D.J. Lloyd, Nuclear Instrumentation and Methods in Physics Research A 354 (1995) 522-526.

[8] J.M. Veilleux, Active and Passive Mode Calibration of the Combined Thermal Epithermal Neutron (CTEN) System. Los Alamos National Laboratory Report LA-UR-02-3389, 3 June 2002.

[9] Nuclear Data Evaluation Lab, Korea Atomic Energy Research Institute, Table of Nuclides, 2000, http://atom.kaeri.re.kr/ – information retrieved between 2004 - 2006.

[10] C.E. Moss, C.A. Goulding, C.L. Hollas, W.L. Myers, Neutron Detectors for Active Interrogation of Highly Enriched Uranium, IEEE Transactions on Nuclear Science 51 (4), (August 2004) 1677-1681.

[11] J.T. Caldwell, W.E. Kunz, Experimental Evaluation of the Differential Die-Away Pulsed-Neutron Technique for the Fissile Assay of Hot Irradiated Fuel Waste, Los Alamos National Laboratory Report LA-UR-82-788, April 1982.

[12] R.A. Harlan, B.E. Wishard, R.D. Santpietro, B.P. Anderson, Performance Report for a Small Package Counter That Uses Active Neutron Interrogation, Rocky Flats Technical Document TD-93003, July 1993.

[13] A.-C. Raoux, A. Lyoussi, C. Passard, C. Denis, J. Loridon, J. Misraki, P. Chany. Nuclear Instruments and Methods in Physics Research B 207 (2003) 186-194.

[14] MacGregor Sailboats, MacGregor Sailboat Specifications http://www. macgregorsailboats.com/sailing-specifications.html – information retrieved 11 October 2004.

[15] D. Reilly, N. Ensslin, H. Smith, Jr., and S. Kreiner, Passive Nondestructive Assay of Nuclear Materials, NUREG/CR-5550, LA-UR-90-732, Washington, DC: U.S. Government Printing Office, March 1991.

[16] R.F. Mozley, The Politics and Technology of Nuclear Proliferation, Seattle, WA: University of Washington Press, 1998.

[17] Michigan Technological University, Glass Fibres Composites, http://www.mse.mtu.edu/~drjohn/my4150/class12/class12.html – information retrieved 11 October 2004.

[18] Los Alamos National Laboratory X-5 Monte Carlo Team, MCNP – A General Monte Carlo N-Particle Transport Code, Version 5, Vols. I – III, Los Alamos National Laboratory Report LA-UR-03-1987, April 2003.

[19] National Council on Radiation Protection, Exposure of the Population in the United States and Canada from Natural Background Radiation, Bethesda, MD: NCRP Report No. 94, 1988.

[20] J.K. Shultis, R.E. Faw, Radiation Shielding, Upper Saddle River, NJ: Prentice Hall PTR, 1996.

APPENDIX A

MCNP INPUT DECKS

The following inputs decks are samples of what was used in the research. For the sake of brevity, only one input deck is given for each particular case. The remaining input decks vary only in the positioning of detector-source positions in the description of the surfaces cards and necessary modifications to cell definitions.

The following input deck is for the active mode, no SFM present case, at a source-detector position of 260 cm from the rear of the boat.

```
Boat for Transporting Nuclear Weapons
c
c    67891123456789212345678931234567894123456789512345678961234567897123456789 8
c
c     -- Cell Cards --
c
1     1  -2.50 +3 -4 -5 +7 +1 -15          imp:n=1  $keel not under V
2     1  -2.50 +3 -4 -11 -13 +15           imp:n=1  $keel under V
3     1  -2.50 +1 -2 -5 +7 +4 -10          imp:n=1  $stern bulkhead
4     1  -2.50 -5 +6 +2 -15 +4 -10          imp:n=1  $starboard bulkhead
5     1  -2.50 +7 -8 +2 -15 +4 -10          imp:n=1  $port bulkhead
6     1  -2.50 +15 +4 -10(-11 +12 -13:+6 -12)
                                           imp:n=1  $bow stbd qtr blkhd
7     1  -2.50 +15 +4 -10(-13 +14 -12 +7:+15 -14 -8)
                                           imp:n=1  $bow port qtr blkhd
8     1  -2.50 -9 +10 -5 +7 +1 -11 -13     imp:n=1  $weather deck
9     6  -0.007885 -6 +8 +2 -12 -14 +4 -10
                                           imp:n=1  $boat interior
10    2  -1.00 +18(-16(+15(+11:-11 +13):-15( +1( +5:+50  -7:-53):
                      +58 +53 -50): +1 -61 +53 -50: -1:
                      -13 +15  -7):
                    -3( +1  +7  -5 -13 -11: +5 -11 +15):
                   -54(+61 +53 -58 -50))
                                           imp:n=1  $water
11    0        -19(+16(+15(+11:-11 +13):-15( +1( +5:+50  -7:-53):
                      +58 +53 -50): +1 -61 +53 -50: -1:
                      -13 +15  -7):
                    +9( +1  +7  -5 -13 -11: +5 -11 +15):
                   +57(+61 +53 -58 -50))
                                           imp:n=1  $sky
c
c
c     - H Detector -
c
30    5  -6.67    +41 -38 +33 -30 (+34 -35:+36 -37) :
                  +35 -36 +33 -30 (+41 -40:+39 -38) :
                  +35 -36 +40 -39 (+33 -32:+31 -30)   imp:n=8  $ SS-304 shell
31    4  -0.00178 +32 -31 +35 -36 +40 -39    vol=1.0  imp:n=16 $ 20-atm H gas
c
```

```
c     - Importance Zones -
c
40    0           +60 -59 +52 -51          +37 -56 :
                  +16 -37 +52 -51 (+60 -41:+38 -59):          $ imp=4 zone
                  +16 -37 +41 -38 (+52 -33:+30 -51)   imp:n=4  $ above waterline
41    2  -1.00    +60 -59 +52 -51 (+55 -34        ):
                  +34 -16 +52 -51 (+60 -41:+38 -59):          $ imp=4 zone
                  +34 -16 +41 -38 (+52 -33:+30 -51)   imp:n=4  $ below waterline
42    0           +61 -58 +53 -50          +56 -57 :
                  +16 -56 +53 -50 (+61 -60:+59 -58):          $ imp=2 zone
                  +16 -56 +60 -59 (+53 -52:+51 -50)   imp:n=2  $ above waterline
43    2  -1.00    +61 -58 +53 -50  +54 -55         :
                  +55 -16 +53 -50 (+61 -60:+59 -58):          $ imp=2 zone
                  +55 -16 +60 -59 (+53 -52:+51 -50)   imp:n=2  $ below waterline
998   0    -18                            imp:n=0
999   0    +19                            imp:n=0

c
c     -- Surface Cards --
c
1     py    0.0                       $outer stern plane
2     py    0.3175                    $inside stern plane
3     pz  -89.0                       $outer keel
4     pz  -88.6825                    $inner keel
5     px  150.0                       $outer starboard bulkhead
6     px  149.6825                    $inner starboard bulkhead
7     px -150.0                       $outer port bulkhead
8     px -149.6825                    $inner port bulkhead
9     pz  144.6                       $outer deck
10    pz  144.2566                    $inner deck
11    p     1.631333 1.0 0.0 823      $outer bow starboard quarter
12    p     1.632672 1.0 0.0 822.6825 $inner bow starboard quarter
13    p    -1.631333 1.0 0.0 823      $outer bow port quarter
14    p    -1.632672 1.0 0.0 822.6825 $inner bow port quarter
15    py  578.3                       $beginning of forecastle
16    pz    0.0                       $waterline
c
18    pz -5000.0
19    pz  5000.0
c 20    px   165.0        $source plane
c
30    px  -154.6825     $outer SS surface facing boat
31    px  -155.0        $outer H surface facing boat
32    px  -185.0        $outer H surface away from boat
33    px  -185.3175     $outer SS surface away from boat
34    pz  -100.3175     $outer SS surface at bottom
35    pz  -100.0        $outer H surface at bottom
36    pz   150.0        $outer H surface at top
37    pz   150.3175     $outer SS surface at top
38    py   410.3175     $outer SS surface forward
39    py   410.0        $outer H surface forward
40    py   110.0        $outer H surface rear
41    py   109.6825     $outer SS surface rear
c
50    px  -150.0001     $outer imp=2 zone facing boat
51    px  -153.0        $outer imp=4 zone facing boat
52    px  -187.0        $outer imp=4 zone
53    px  -190.0        $outer imp=2 zone
54    pz  -105.0        $outer imp=2 zone at bottom
55    pz  -102.0        $outer imp=4 zone at bottom
56    pz   152.0        $outer imp=4 zone at top
57    pz   155.0        $outer imp=2 zone at top
58    py   415.0        $outer imp=2 zone forward
59    py   412.0        $outer imp=4 zone forward
60    py   108.0        $outer imp=4 zone rear
61    py   105.0        $outer imp=2 zone rear
c
```

```
c
c     -- Data Cards --
c
c   sdef  sur=20 pos=165.0 260.0 -50.0 vec=1 0 0.0001 dir=-1 rad=d1 erg=14.0 par=1
c   si1   0 0.5
c   sp1   -21 1
c
sdef  pos=155.0 260.0 -50.0 erg=14.0 par=1
c
c   sdef pos=160.0 660.0 -50.0 erg=14.0 vec=-1 0 0 dir=d1 par=1
c   sb1  -31 0.5
mode n
c
cut:n  500000
totnu
nps   400000000
prdmp 0 500000 -1 5 0
m1    14000.60c  -0.631037
       8016.66c  -1.226159
       8017.66c  -0.000467
      13027.66c  -0.185238
      26000.55c  -0.008743
       5010.66c  -0.016223
       5011.66c  -0.065301
      12000.66c  -0.045228
      20000.66c  -0.321611    $ Fiberglass
m2     1001.66c   2.0
       8016.66c   1.0         $ Water
mt2    lwtr.60t               $ S(alpha,beta) for Water
c
c
m4     1001.66c   1.0         $ H gas
m5    26000.55c  -0.6785
       6000.66c  -0.0080
      14000.60c  -0.0100
      24000.50c  -0.1800
      28000.50c  -0.0980
      25055.66c  -0.0180
      15031.66c  -0.0045
      16000.66c  -0.0030      $ Stainless Steel 304
m6    13027.66c  -2.00619e-1
       6000.66c  -3.22547e-1
      20000.66c  -2.86071e-3
      17000.66c  -4.09456e-4
      24050.66c  -1.88012e-4
      24052.66c  -3.62563e-3
      24053.66c  -4.11118e-4
      24054.66c  -1.02336e-4
      29063.66c  -2.85237e-5
      29065.66c  -1.27134e-5
      26054.66c  -2.48137e-3
      26056.66c  -3.89523e-2
      26057.66c  -8.99578e-4
      26058.66c  -1.19717e-4
       1001.66c  -6.11210e-2
       1002.66c  -9.16952e-6
      19000.66c  -5.88412e-4
      12000.66c  -4.85391e-3
      25055.66c  -1.07216e-3
      42000.66c  -6.55891e-4
       7014.66c  -7.18835e-3
       7015.66c  -2.64060e-5
      11023.66c  -4.32547e-4
      28058.66c  -2.80372e-3
      28060.66c  -8.02640e-4
      28061.66c  -3.48934e-5
```

```
      28062.66c  -1.11230e-4
      28064.66c  -2.83432e-5
       8016.66c  -3.43649e-1
       8017.66c  -1.30898e-4
      15031.66c  -2.64326e-3
      82206.66c  -8.80160e-8
      82207.66c  -8.07117e-8
      82208.66c  -1.91371e-7
      37085.66c  -1.06261e-6
      37087.66c  -4.09863e-7
      16000.66c  -6.36451e-4
      14028.66c  -5.70495e-4
      14029.66c  -2.88866e-5
      14030.66c  -1.91753e-5
      30000.42c  -5.08488e-5
      40000.66c  -2.04522e-6  $ Composite boat interior
c
c
f314:n  31                    $ Elastic scatter Rxns in H
fm314   -1 4 2
e314   100.0e-6 100.0
t0     10000 13I 500000
```

The following input deck is for the active mode with HEU, at a source-detector position of 260 cm from the rear of the boat.

```
Boat for Transporting Nuclear Weapons
c
c    678911234567892123456789312345678941234567895123456789612345678971234567898
c
c     -- Cell Cards --
c
1     1  -2.50 +3 -4 -5 +7 +1 -15          imp:n=1  $keel not under V
2     1  -2.50 +3 -4 -11 -13 +15           imp:n=1  $keel under V
3     1  -2.50 +1 -2 -5 +7 +4 -10          imp:n=1  $stern bulkhead
4     1  -2.50 -5 +6 +2 -15 +4 -10         imp:n=1  $starboard bulkhead
5     1  -2.50 +7 -8 +2 -15 +4 -10         imp:n=1  $port bulkhead
6     1  -2.50 +15 +4 -10(-11 +12 -13:+6 -12)
                                          imp:n=1  $bow stbd qtr blkhd
7     1  -2.50 +15 +4 -10(-13 +14 -12 +7:+15 -14 -8)
                                          imp:n=1  $bow port qtr blkhd
8     1  -2.50 -9 +10 -5 +7 +1 -11 -13     imp:n=1  $weather deck
9     6  -0.007885 -6 +8 +2 -12 -14 +4 -10 +17
                                          imp:n=1  $boat interior
10    2  -1.00 +18(-16(+15(+11:-11 +13):-15( +1( +5:+50  -7:-53):
                       +58 +53 -50): +1 -61 +53 -50: -1:
                       -13 +15  -7):
                    -3( +1  +7  -5 -13 -11: +5 -11 +15):
                   -54(+61 +53 -58 -50))
                                          imp:n=1  $water
11    0        -19(+16(+15(+11:-11 +13):-15( +1( +5:+50  -7:-53):
                       +58 +53 -50): +1 -61 +53 -50: -1:
                       -13 +15  -7):
                    +9( +1  +7  -5 -13 -11: +5 -11 +15):
                   +57(+61 +53 -58 -50))
                                          imp:n=1  $sky
12    3  -18.9 -17               vol=1.0  imp:n=1  $HEU Sphere
c
c     - H Detector -
c
30    5  -6.67    +41 -38 +33 -30 (+34 -35:+36 -37) :
```

```
                +35 -36 +33 -30 (+41 -40:+39 -38) :
                +35 -36 +40 -39 (+33 -32:+31 -30)   imp:n=8  $ SS-304 shell
31    4  -0.00178 +32 -31 +35 -36 +40 -39    vol=1.0  imp:n=16 $ 20-atm H gas
c
c     - Importance Zones -
c
40    0          +60 -59 +52 -51          +37 -56 :
                +16 -37 +52 -51 (+60 -41:+38 -59):          $ imp=4 zone
                +16 -37 +41 -38 (+52 -33:+30 -51)   imp:n=4  $ above waterline
41    2  -1.00    +60 -59 +52 -51 (+55 -34        ):
                +34 -16 +52 -51 (+60 -41:+38 -59):          $ imp=4 zone
                +34 -16 +41 -38 (+52 -33:+30 -51)   imp:n=4  $ below waterline
42    0          +61 -58 +53 -50          +56 -57 :
                +16 -56 +53 -50 (+61 -60:+59 -58):          $ imp=2 zone
                +16 -56 +60 -59 (+53 -52:+51 -50)   imp:n=2  $ above waterline
43    2  -1.00    +61 -58 +53 -50  +54 -55         :
                +55 -16 +53 -50 (+61 -60:+59 -58):          $ imp=2 zone
                +55 -16 +60 -59 (+53 -52:+51 -50)   imp:n=2  $ below waterline
998   0    -18                              imp:n=0
999   0    +19                              imp:n=0

c
c     -- Surface Cards --
c
1     py    0.0                         $outer stern plane
2     py    0.3175                      $inside stern plane
3     pz  -89.0                         $outer keel
4     pz  -88.6825                      $inner keel
5     px  150.0                         $outer starboard bulkhead
6     px  149.6825                      $inner starboard bulkhead
7     px -150.0                         $outer port bulkhead
8     px -149.6825                      $inner port bulkhead
9     pz  144.6                         $outer deck
10    pz  144.2566                      $inner deck
11    p     1.631333 1.0 0.0 823        $outer bow starboard quarter
12    p     1.632672 1.0 0.0 822.6825   $inner bow starboard quarter
13    p    -1.631333 1.0 0.0 823        $outer bow port quarter
14    p    -1.632672 1.0 0.0 822.6825   $inner bow port quarter
15    py  578.3                         $beginning of forecastle
16    pz    0.0                         $waterline
17    s     0.0 260.0 -50.0 6.80973     $25-kg HEU sphere
18    pz -5000.0
19    pz  5000.0
c 20    px   165.0        $source plane
c
30    px  -154.6825     $outer SS surface facing boat
31    px  -155.0        $outer H surface facing boat
32    px  -185.0        $outer H surface away from boat
33    px  -185.3175     $outer SS surface away from boat
34    pz  -100.3175     $outer SS surface at bottom
35    pz  -100.0        $outer H surface at bottom
36    pz   150.0        $outer H surface at top
37    pz   150.3175     $outer SS surface at top
38    py   410.3175     $outer SS surface forward
39    py   410.0        $outer H surface forward
40    py   110.0        $outer H surface rear
41    py   109.6825     $outer SS surface rear
c
50    px  -150.0001     $outer imp=2 zone facing boat
51    px  -153.0        $outer imp=4 zone facing boat
52    px  -187.0        $outer imp=4 zone
53    px  -190.0        $outer imp=2 zone
54    pz  -105.0        $outer imp=2 zone at bottom
55    pz  -102.0        $outer imp=4 zone at bottom
56    pz   152.0        $outer imp=4 zone at top
57    pz   155.0        $outer imp=2 zone at top
58    py   415.0        $outer imp=2 zone forward
```

```
59    py   412.0        $outer imp=4 zone forward
60    py   108.0        $outer imp=4 zone rear
61    py   105.0        $outer imp=2 zone rear
c

c
c     -- Data Cards --
c
c   sdef  sur=20 pos=165.0 260.0 -50.0 vec=1 0 0.0001 dir=-1 rad=d1 erg=14.0 par=1
c   si1   0 0.5
c   sp1   -21 1
c
sdef  pos=155.0 260.0 -50.0 erg=14.0 par=1
c
c   sdef pos=160.0 660.0 -50.0 erg=14.0 vec=-1 0 0 dir=d1 par=1
c   sb1  -31 0.5
mode n
phys:n 150.0 0 1
cut:n  500000
totnu
nps   400000000
prdmp 0 100000 -1 5 0
m1    14000.60c  -0.631037
       8016.66c  -1.226159
       8017.66c  -0.000467
      13027.66c  -0.185238
      26000.55c  -0.008743
       5010.66c  -0.016223
       5011.66c  -0.065301
      12000.66c  -0.045228
      20000.66c  -0.321611    $ Fiberglass
m2     1001.66c   2.0
       8016.66c   1.0         $ Water
mt2    lwtr.60t               $ S(alpha,beta) for Water
m3    92235.66c   0.95
      92238.66c   0.05        $ HEU
m4     1001.66c   1.0         $ H gas
m5    26000.55c  -0.6785
       6000.66c  -0.0080
      14000.60c  -0.0100
      24000.50c  -0.1800
      28000.50c  -0.0980
      25055.66c  -0.0180
      15031.66c  -0.0045
      16000.66c  -0.0030      $ Stainless Steel 304
m6    13027.66c  -2.00619e-1
       6000.66c  -3.22547e-1
      20000.66c  -2.86071e-3
      17000.66c  -4.09456e-4
      24050.66c  -1.88012e-4
      24052.66c  -3.62563e-3
      24053.66c  -4.11118e-4
      24054.66c  -1.02336e-4
      29063.66c  -2.85237e-5
      29065.66c  -1.27134e-5
      26054.66c  -2.48137e-3
      26056.66c  -3.89523e-2
      26057.66c  -8.99578e-4
      26058.66c  -1.19717e-4
       1001.66c  -6.11210e-2
       1002.66c  -9.16952e-6
      19000.66c  -5.88412e-4
      12000.66c  -4.85391e-3
      25055.66c  -1.07216e-3
      42000.66c  -6.55891e-4
       7014.66c  -7.18835e-3
       7015.66c  -2.64060e-5
```

```
      11023.66c  -4.32547e-4
      28058.66c  -2.80372e-3
      28060.66c  -8.02640e-4
      28061.66c  -3.48934e-5
      28062.66c  -1.11230e-4
      28064.66c  -2.83432e-5
       8016.66c  -3.43649e-1
       8017.66c  -1.30898e-4
      15031.66c  -2.64326e-3
      82206.66c  -8.80160e-8
      82207.66c  -8.07117e-8
      82208.66c  -1.91371e-7
      37085.66c  -1.06261e-6
      37087.66c  -4.09863e-7
      16000.66c  -6.36451e-4
      14028.66c  -5.70495e-4
      14029.66c  -2.88866e-5
      14030.66c  -1.91753e-5
      30000.42c  -5.08488e-5
      40000.66c  -2.04522e-6  $ Composite boat interior
f124:n  12                    $ Flux in HEU sphere
fm124   -1 3 -6               $ Fission rates in fissions/cc/source particle
f314:n  31                    $ Elastic scatter Rxns in H
fm314   -1 4 2
e314   100.0e-6 100.0
t0     10000 13I 500000
```

The following input deck is for the active mode with plutonium, at a source-detector position of 260 cm from the rear of the boat.

```
Boat for Transporting Nuclear Weapons
c
c    678911234567892123456789312345678941234567895123456789612345678971234567898
c
c     -- Cell Cards --
c
1     1  -2.50 +3 -4 -5 +7 +1 -15          imp:n=1  $keel not under V
2     1  -2.50 +3 -4 -11 -13 +15           imp:n=1  $keel under V
3     1  -2.50 +1 -2 -5 +7 +4 -10          imp:n=1  $stern bulkhead
4     1  -2.50 -5 +6 +2 -15 +4 -10         imp:n=1  $starboard bulkhead
5     1  -2.50 +7 -8 +2 -15 +4 -10         imp:n=1  $port bulkhead
6     1  -2.50 +15 +4 -10(-11 +12 -13:+6 -12)
                                          imp:n=1  $bow stbd qtr blkhd
7     1  -2.50 +15 +4 -10(-13 +14 -12 +7:+15 -14 -8)
                                          imp:n=1  $bow port qtr blkhd
8     1  -2.50 -9 +10 -5 +7 +1 -11 -13     imp:n=1  $weather deck
9     6  -0.007885 -6 +8 +2 -12 -14 +4 -10 +17
                                          imp:n=1  $boat interior
10    2  -1.00 +18(-16(+15(+11:-11 +13):-15( +1( +5:+50  -7:-53):
                      +58 +53 -50): +1 -61 +53 -50: -1:
                      -13 +15  -7):
                   -3( +1  +7  -5 -13 -11: +5 -11 +15):
                  -54(+61 +53 -58 -50))
                                          imp:n=1  $water
11    0        -19(+16(+15(+11:-11 +13):-15( +1( +5:+50  -7:-53):
                      +58 +53 -50): +1 -61 +53 -50: -1:
                      -13 +15  -7):
                    +9( +1  +7  -5 -13 -11: +5 -11 +15):
                  +57(+61 +53 -58 -50))
                                          imp:n=1  $sky
12    3  -15.6 -17               vol=1.0  imp:n=1  $Pu Sphere
```

```
c
c     - H Detector -
c
30    5  -6.67    +41 -38 +33 -30 (+34 -35:+36 -37) :
                 +35 -36 +33 -30 (+41 -40:+39 -38) :
                 +35 -36 +40 -39 (+33 -32:+31 -30)   imp:n=8  $ SS-304 shell
31    4  -0.00178 +32 -31 +35 -36 +40 -39    vol=1.0  imp:n=16 $ 20-atm H gas
c
c     - Importance Zones -
c
40    0           +60 -59 +52 -51          +37 -56 :
                 +16 -37 +52 -51 (+60 -41:+38 -59):          $ imp=4 zone
                 +16 -37 +41 -38 (+52 -33:+30 -51)   imp:n=4  $ above waterline
41    2  -1.00    +60 -59 +52 -51 (+55 -34        ):
                 +34 -16 +52 -51 (+60 -41:+38 -59):          $ imp=4 zone
                 +34 -16 +41 -38 (+52 -33:+30 -51)   imp:n=4  $ below waterline
42    0           +61 -58 +53 -50          +56 -57 :
                 +16 -56 +53 -50 (+61 -60:+59 -58):          $ imp=2 zone
                 +16 -56 +60 -59 (+53 -52:+51 -50)   imp:n=2  $ above waterline
43    2  -1.00    +61 -58 +53 -50  +54 -55         :
                 +55 -16 +53 -50 (+61 -60:+59 -58):          $ imp=2 zone
                 +55 -16 +60 -59 (+53 -52:+51 -50)   imp:n=2  $ below waterline
998   0    -18                              imp:n=0
999   0    +19                              imp:n=0

c
c     -- Surface Cards --
c
1     py    0.0                        $outer stern plane
2     py    0.3175                     $inside stern plane
3     pz  -89.0                        $outer keel
4     pz  -88.6825                     $inner keel
5     px  150.0                        $outer starboard bulkhead
6     px  149.6825                     $inner starboard bulkhead
7     px -150.0                        $outer port bulkhead
8     px -149.6825                     $inner port bulkhead
9     pz  144.6                        $outer deck
10    pz  144.2566                     $inner deck
11    p     1.631333 1.0 0.0 823       $outer bow starboard quarter
12    p     1.632672 1.0 0.0 822.6825  $inner bow starboard quarter
13    p    -1.631333 1.0 0.0 823       $outer bow port quarter
14    p    -1.632672 1.0 0.0 822.6825  $inner bow port quarter
15    py  578.3                        $beginning of forecastle
16    pz    0.0                        $waterline
17    s     0.0 260.0 -50.0 4.2454     $5-kg Pu sphere
18    pz -5000.0
19    pz  5000.0
c 20    px   165.0        $source plane
c
30    px  -154.6825     $outer SS surface facing boat
31    px  -155.0        $outer H surface facing boat
32    px  -185.0        $outer H surface away from boat
33    px  -185.3175     $outer SS surface away from boat
34    pz  -100.3175     $outer SS surface at bottom
35    pz  -100.0        $outer H surface at bottom
36    pz   150.0        $outer H surface at top
37    pz   150.3175     $outer SS surface at top
38    py   410.3175     $outer SS surface forward
39    py   410.0        $outer H surface forward
40    py   110.0        $outer H surface rear
41    py   109.6825     $outer SS surface rear
c
50    px  -150.0001     $outer imp=2 zone facing boat
51    px  -153.0        $outer imp=4 zone facing boat
52    px  -187.0        $outer imp=4 zone
53    px  -190.0        $outer imp=2 zone
54    pz  -105.0        $outer imp=2 zone at bottom
```

```
55    pz  -102.0        $outer imp=4 zone at bottom
56    pz   152.0        $outer imp=4 zone at top
57    pz   155.0        $outer imp=2 zone at top
58    py   415.0        $outer imp=2 zone forward
59    py   412.0        $outer imp=4 zone forward
60    py   108.0        $outer imp=4 zone rear
61    py   105.0        $outer imp=2 zone rear
c

c
c     -- Data Cards --
c
c   sdef  sur=20 pos=165.0 260.0 -50.0 vec=1 0 0.0001 dir=-1 rad=d1 erg=14.0 par=1
c   si1   0 0.5
c   sp1   -21 1
c
sdef  pos=155.0 260.0 -50.0 erg=14.0 par=1
c
c   sdef pos=160.0 660.0 -50.0 erg=14.0 vec=-1 0 0 dir=d1 par=1
c   sb1  -31 0.5
mode n
phys:n 150.0 0 1
cut:n  500000
totnu
nps   400000000
prdmp 0 250000 -1 5 0
m1    14000.60c  -0.631037
       8016.66c  -1.226159
       8017.66c  -0.000467
      13027.66c  -0.185238
      26000.55c  -0.008743
       5010.66c  -0.016223
       5011.66c  -0.065301
      12000.66c  -0.045228
      20000.66c  -0.321611    $ Fiberglass
m2     1001.66c   2.0
       8016.66c   1.0         $ Water
mt2    lwtr.60t               $ S(alpha,beta) for Water
m3    94239.66c   0.94
      94240.66c   0.06        $ WG plutonium
m4     1001.66c   1.0         $ H gas
m5    26000.55c  -0.6785
       6000.66c  -0.0080
      14000.60c  -0.0100
      24000.50c  -0.1800
      28000.50c  -0.0980
      25055.66c  -0.0180
      15031.66c  -0.0045
      16000.66c  -0.0030      $ Stainless Steel 304
m6    13027.66c  -2.00619e-1
       6000.66c  -3.22547e-1
      20000.66c  -2.86071e-3
      17000.66c  -4.09456e-4
      24050.66c  -1.88012e-4
      24052.66c  -3.62563e-3
      24053.66c  -4.11118e-4
      24054.66c  -1.02336e-4
      29063.66c  -2.85237e-5
      29065.66c  -1.27134e-5
      26054.66c  -2.48137e-3
      26056.66c  -3.89523e-2
      26057.66c  -8.99578e-4
      26058.66c  -1.19717e-4
       1001.66c  -6.11210e-2
       1002.66c  -9.16952e-6
      19000.66c  -5.88412e-4
      12000.66c  -4.85391e-3
```

```
      25055.66c  -1.07216e-3
      42000.66c  -6.55891e-4
       7014.66c  -7.18835e-3
       7015.66c  -2.64060e-5
      11023.66c  -4.32547e-4
      28058.66c  -2.80372e-3
      28060.66c  -8.02640e-4
      28061.66c  -3.48934e-5
      28062.66c  -1.11230e-4
      28064.66c  -2.83432e-5
       8016.66c  -3.43649e-1
       8017.66c  -1.30898e-4
      15031.66c  -2.64326e-3
      82206.66c  -8.80160e-8
      82207.66c  -8.07117e-8
      82208.66c  -1.91371e-7
      37085.66c  -1.06261e-6
      37087.66c  -4.09863e-7
      16000.66c  -6.36451e-4
      14028.66c  -5.70495e-4
      14029.66c  -2.88866e-5
      14030.66c  -1.91753e-5
      30000.42c  -5.08488e-5
      40000.66c  -2.04522e-6  $ Composite boat interior
f124:n  12                    $ Flux in PU sphere
fm124   -1 3 -6               $ Fission rates in fissions/cc/source particle
f314:n  31                    $ Elastic scatter Rxns in H
fm314   -1 4 2
e314   100.0e-6 100.0
t0     10000 13I 500000
```

The following input deck is for the passive mode spontaneous fission with ^{240}Pu, at a source-detector position of 260 cm from the rear of the boat.

```
Boat for Transporting Nuclear Weapons
c
c    67891123456789212345678931234567894123456789512345678961234567897123456789 8
c
c     -- Cell Cards --
c
1     1  -2.50 +3 -4 -5 +7 +1 -15          imp:n=1  $keel not under V
2     1  -2.50 +3 -4 -11 -13 +15           imp:n=1  $keel under V
3     1  -2.50 +1 -2 -5 +7 +4 -10          imp:n=1  $stern bulkhead
4     1  -2.50 -5 +6 +2 -15 +4 -10          imp:n=1  $starboard bulkhead
5     1  -2.50 +7 -8 +2 -15 +4 -10          imp:n=1  $port bulkhead
6     1  -2.50 +15 +4 -10(-11 +12 -13:+6 -12)
                                           imp:n=1  $bow stbd qtr blkhd
7     1  -2.50 +15 +4 -10(-13 +14 -12 +7:+15 -14 -8)
                                           imp:n=1  $bow port qtr blkhd
8     1  -2.50 -9 +10 -5 +7 +1 -11 -13     imp:n=1  $weather deck
9     6  -0.007885 -6 +8 +2 -12 -14 +4 -10 +17
                                           imp:n=1  $boat interior
10    2  -1.00 +18(-16(+15(+11:-11 +13):-15( +1( +5:+50  -7:-53):
                      +58 +53 -50): +1 -61 +53 -50: -1:
                      -13 +15  -7):
                    -3( +1  +7  -5 -13 -11: +5 -11 +15):
                   -54(+61 +53 -58 -50))
                                           imp:n=1  $water
11    0        -19(+16(+15(+11:-11 +13):-15( +1( +5:+50  -7:-53):
                      +58 +53 -50): +1 -61 +53 -50: -1:
                      -13 +15  -7):
```

```
                  +9( +1  +7  -5 -13 -11: +5 -11 +15):
                 +57(+61 +53 -58 -50))
                                          imp:n=1  $sky
12    3  -15.6 -17               vol=1.0  imp:n=1  $Pu Sphere
c
c     - H Detector -
c
30    5  -6.67    +41 -38 +33 -30 (+34 -35:+36 -37) :
                 +35 -36 +33 -30 (+41 -40:+39 -38) :
                 +35 -36 +40 -39 (+33 -32:+31 -30)   imp:n=8  $ SS-304 shell
31    4  -0.00178 +32 -31 +35 -36 +40 -39    vol=1.0  imp:n=16 $ 20-atm H gas
c
c     - Importance Zones -
c
40    0           +60 -59 +52 -51          +37 -56 :
                  +16 -37 +52 -51 (+60 -41:+38 -59):          $ imp=4 zone
                  +16 -37 +41 -38 (+52 -33:+30 -51)   imp:n=4  $ above waterline
41    2  -1.00    +60 -59 +52 -51 (+55 -34        ):
                  +34 -16 +52 -51 (+60 -41:+38 -59):          $ imp=4 zone
                  +34 -16 +41 -38 (+52 -33:+30 -51)   imp:n=4  $ below waterline
42    0           +61 -58 +53 -50          +56 -57 :
                  +16 -56 +53 -50 (+61 -60:+59 -58):          $ imp=2 zone
                  +16 -56 +60 -59 (+53 -52:+51 -50)   imp:n=2  $ above waterline
43    2  -1.00    +61 -58 +53 -50  +54 -55         :
                  +55 -16 +53 -50 (+61 -60:+59 -58):          $ imp=2 zone
                  +55 -16 +60 -59 (+53 -52:+51 -50)   imp:n=2  $ below waterline
998   0    -18                              imp:n=0
999   0    +19                              imp:n=0

c
c     -- Surface Cards --
c
1     py    0.0                       $outer stern plane
2     py    0.3175                    $inside stern plane
3     pz  -89.0                       $outer keel
4     pz  -88.6825                    $inner keel
5     px  150.0                       $outer starboard bulkhead
6     px  149.6825                    $inner starboard bulkhead
7     px -150.0                       $outer port bulkhead
8     px -149.6825                    $inner port bulkhead
9     pz  144.6                       $outer deck
10    pz  144.2566                    $inner deck
11    p     1.631333 1.0 0.0 823      $outer bow starboard quarter
12    p     1.632672 1.0 0.0 822.6825 $inner bow starboard quarter
13    p    -1.631333 1.0 0.0 823      $outer bow port quarter
14    p    -1.632672 1.0 0.0 822.6825 $inner bow port quarter
15    py  578.3                       $beginning of forecastle
16    pz    0.0                       $waterline
17    s     0.0 260.0 -50.0 4.2454    $5-kg Pu sphere
18    pz -5000.0
19    pz  5000.0
c 20    px   165.0        $source plane
c
30    px  -154.6825     $outer SS surface facing boat
31    px  -155.0        $outer H surface facing boat
32    px  -185.0        $outer H surface away from boat
33    px  -185.3175     $outer SS surface away from boat
34    pz  -100.3175     $outer SS surface at bottom
35    pz  -100.0        $outer H surface at bottom
36    pz   150.0        $outer H surface at top
37    pz   150.3175     $outer SS surface at top
38    py   410.3175     $outer SS surface forward
39    py   410.0        $outer H surface forward
40    py   110.0        $outer H surface rear
41    py   109.6825     $outer SS surface rear
c
50    px  -150.0001     $outer imp=2 zone facing boat
```

```
51    px  -153.0        $outer imp=4 zone facing boat
52    px  -187.0        $outer imp=4 zone
53    px  -190.0        $outer imp=2 zone
54    pz  -105.0        $outer imp=2 zone at bottom
55    pz  -102.0        $outer imp=4 zone at bottom
56    pz   152.0        $outer imp=4 zone at top
57    pz   155.0        $outer imp=2 zone at top
58    py   415.0        $outer imp=2 zone forward
59    py   412.0        $outer imp=4 zone forward
60    py   108.0        $outer imp=4 zone rear
61    py   105.0        $outer imp=2 zone rear
c

c
c     -- Data Cards --
c
sdef  pos=0.0 260.0 -50.0 erg=d1 cel=12 rad=d2 par=1
sp1   -3 0.799    4.903
si2   0 4.2454
mode n
phys:n 150.0 0 1
totnu
nps   40000
prdmp 0 8000 -1 5 0
m1    14000.60c  -0.631037
       8016.66c  -1.226159
       8017.66c  -0.000467
      13027.66c  -0.185238
      26000.55c  -0.008743
       5010.66c  -0.016223
       5011.66c  -0.065301
      12000.66c  -0.045228
      20000.66c  -0.321611    $ Fiberglass
m2     1001.66c   2.0
       8016.66c   1.0         $ Water
mt2    lwtr.60t               $ S(alpha,beta) for Water
m3    94238.66c   -0.012
      94239.66c  -93.8
      94240.66c   -6.0
      94241.66c   -0.35
      94242.66c   -0.022      $ WG plutonium
m4     1001.66c   1.0         $ H gas
m5    26000.55c  -0.6785
       6000.66c  -0.0080
      14000.60c  -0.0100
      24000.50c  -0.1800
      28000.50c  -0.0980
      25055.66c  -0.0180
      15031.66c  -0.0045
      16000.66c  -0.0030      $ Stainless Steel 304
m6    13027.66c  -2.00619e-1
       6000.66c  -3.22547e-1
      20000.66c  -2.86071e-3
      17000.66c  -4.09456e-4
      24050.66c  -1.88012e-4
      24052.66c  -3.62563e-3
      24053.66c  -4.11118e-4
      24054.66c  -1.02336e-4
      29063.66c  -2.85237e-5
      29065.66c  -1.27134e-5
      26054.66c  -2.48137e-3
      26056.66c  -3.89523e-2
      26057.66c  -8.99578e-4
      26058.66c  -1.19717e-4
       1001.66c  -6.11210e-2
       1002.66c  -9.16952e-6
      19000.66c  -5.88412e-4
```

```
      12000.66c  -4.85391e-3
      25055.66c  -1.07216e-3
      42000.66c  -6.55891e-4
       7014.66c  -7.18835e-3
       7015.66c  -2.64060e-5
      11023.66c  -4.32547e-4
      28058.66c  -2.80372e-3
      28060.66c  -8.02640e-4
      28061.66c  -3.48934e-5
      28062.66c  -1.11230e-4
      28064.66c  -2.83432e-5
       8016.66c  -3.43649e-1
       8017.66c  -1.30898e-4
      15031.66c  -2.64326e-3
      82206.66c  -8.80160e-8
      82207.66c  -8.07117e-8
      82208.66c  -1.91371e-7
      37085.66c  -1.06261e-6
      37087.66c  -4.09863e-7
      16000.66c  -6.36451e-4
      14028.66c  -5.70495e-4
      14029.66c  -2.88866e-5
      14030.66c  -1.91753e-5
      30000.42c  -5.08488e-5
      40000.66c  -2.04522e-6  $ Composite boat interior
f124:n  12                    $ Flux in PU sphere
fm124   -1 3 -6               $ Fission rates in fissions/cc/source particle
f314:n  31                    $ Elastic scatter Rxns in H
fm314   -1 4 2
e314   100.0e-6 100.0
```

The following input deck is for the dose calculation with HEU present, at a source-detector position of 260 cm from the rear of the boat.

```
Boat for Transporting Nuclear Weapons
c
c    67891123456789212345678931234567894123456789512345678961234567897123456789 8
c
c     -- Cell Cards --
c
1     1  -2.50 +3 -4 -5 +7 +1 -15          imp:n=1  $keel not under V
2     1  -2.50 +3 -4 -11 -13 +15           imp:n=1  $keel under V
3     1  -2.50 +1 -2 -5 +7 +4 -10          imp:n=1  $stern bulkhead
4     1  -2.50 -5 +6 +2 -15 +4 -10         imp:n=1  $starboard bulkhead
5     1  -2.50 +7 -8 +2 -15 +4 -10         imp:n=1  $port bulkhead
6     1  -2.50 +15 +4 -10(-11 +12 -13:+6 -12)
                                           imp:n=1  $bow stbd qtr blkhd
7     1  -2.50 +15 +4 -10(-13 +14 -12 +7:+15 -14 -8)
                                           imp:n=1  $bow port qtr blkhd
8     1  -2.50 -9 +10 -5 +7 +1 -11 -13     imp:n=1  $weather deck
9     6  -0.007885 -6 +8 +2 -12 -14 +4 -10 +17 +21
                                           imp:n=1  $boat interior
10    2  -1.00 +18(-16(+15(+11:-11 +13):-15( +1( +5:+50  -7:-53):
                      +58 +53 -50): +1 -61 +53 -50: -1:
                      -13 +15  -7):
                    -3( +1  +7  -5 -13 -11: +5 -11 +15):
                   -54(+61 +53 -58 -50))
                                           imp:n=1  $water
11    0        -19(+16(+15(+11:-11 +13):-15( +1( +5:+50  -7:-53):
                      +58 +53 -50): +1 -61 +53 -50: -1:
                      -13 +15  -7):
```

```
                  +9( +1  +7  -5 -13 -11: +5 -11 +15):
                 +57(+61 +53 -58 -50))
                                          imp:n=1  $sky
12    3  -18.9 -17               vol=1.0  imp:n=1  $HEU Sphere
13    7  -1.0  -21               vol=1.0  imp:n=1  $ICRU Sphere
c
c     - H Detector -
c
30    5  -6.67    +41 -38 +33 -30 (+34 -35:+36 -37) :
                 +35 -36 +33 -30 (+41 -40:+39 -38) :
                 +35 -36 +40 -39 (+33 -32:+31 -30)   imp:n=8  $ SS-304 shell
31    4  -0.00178 +32 -31 +35 -36 +40 -39    vol=1.0  imp:n=16 $ 20-atm H gas
c
c     - Importance Zones -
c
40    0           +60 -59 +52 -51          +37 -56 :
                  +16 -37 +52 -51 (+60 -41:+38 -59):          $ imp=4 zone
                  +16 -37 +41 -38 (+52 -33:+30 -51)   imp:n=4  $ above waterline
41    2  -1.00    +60 -59 +52 -51 (+55 -34        ):
                  +34 -16 +52 -51 (+60 -41:+38 -59):          $ imp=4 zone
                  +34 -16 +41 -38 (+52 -33:+30 -51)   imp:n=4  $ below waterline
42    0           +61 -58 +53 -50          +56 -57 :
                  +16 -56 +53 -50 (+61 -60:+59 -58):          $ imp=2 zone
                  +16 -56 +60 -59 (+53 -52:+51 -50)   imp:n=2  $ above waterline
43    2  -1.00    +61 -58 +53 -50  +54 -55         :
                  +55 -16 +53 -50 (+61 -60:+59 -58):          $ imp=2 zone
                  +55 -16 +60 -59 (+53 -52:+51 -50)   imp:n=2  $ below waterline
998   0    -18                              imp:n=0
999   0    +19                              imp:n=0

c
c     -- Surface Cards --
c
1     py    0.0                       $outer stern plane
2     py    0.3175                    $inside stern plane
3     pz  -89.0                       $outer keel
4     pz  -88.6825                    $inner keel
5     px  150.0                       $outer starboard bulkhead
6     px  149.6825                    $inner starboard bulkhead
7     px -150.0                       $outer port bulkhead
8     px -149.6825                    $inner port bulkhead
9     pz  144.6                       $outer deck
10    pz  144.2566                    $inner deck
11    p     1.631333 1.0 0.0 823      $outer bow starboard quarter
12    p     1.632672 1.0 0.0 822.6825 $inner bow starboard quarter
13    p    -1.631333 1.0 0.0 823      $outer bow port quarter
14    p    -1.632672 1.0 0.0 822.6825 $inner bow port quarter
15    py  578.3                       $beginning of forecastle
16    pz    0.0                       $waterline
17    s     0.0 260.0 -50.0 6.80973   $25-kg HEU sphere
18    pz -5000.0
19    pz  5000.0
c 20    px   165.0        $source plane
21    s     0.0 285.0 -50.0 15.0      $30-cm diameter ICRU Sphere
c
30    px  -154.6825     $outer SS surface facing boat
31    px  -155.0        $outer H surface facing boat
32    px  -185.0        $outer H surface away from boat
33    px  -185.3175     $outer SS surface away from boat
34    pz  -100.3175     $outer SS surface at bottom
35    pz  -100.0        $outer H surface at bottom
36    pz   150.0        $outer H surface at top
37    pz   150.3175     $outer SS surface at top
38    py   410.3175     $outer SS surface forward
39    py   410.0        $outer H surface forward
40    py   110.0        $outer H surface rear
41    py   109.6825     $outer SS surface rear
```

```
c
50    px  -150.0001     $outer imp=2 zone facing boat
51    px  -153.0        $outer imp=4 zone facing boat
52    px  -187.0        $outer imp=4 zone
53    px  -190.0        $outer imp=2 zone
54    pz  -105.0        $outer imp=2 zone at bottom
55    pz  -102.0        $outer imp=4 zone at bottom
56    pz   152.0        $outer imp=4 zone at top
57    pz   155.0        $outer imp=2 zone at top
58    py   415.0        $outer imp=2 zone forward
59    py   412.0        $outer imp=4 zone forward
60    py   108.0        $outer imp=4 zone rear
61    py   105.0        $outer imp=2 zone rear
c

c
c     -- Data Cards --
c
c   sdef  sur=20 pos=165.0 260.0 -50.0 vec=1 0 0.0001 dir=-1 rad=d1 erg=14.0 par=1
c   si1   0 0.5
c   sp1   -21 1
c
sdef  pos=155.0 260.0 -50.0 erg=14.0 par=1
c
c   sdef pos=160.0 660.0 -50.0 erg=14.0 vec=-1 0 0 dir=d1 par=1
c   sb1  -31 0.5
mode n
phys:n 150.0 0 1
cut:n  500000
totnu
nps   400000000
prdmp 0 100000 -1 5 0
m1    14000.60c  -0.631037
       8016.66c  -1.226159
       8017.66c  -0.000467
      13027.66c  -0.185238
      26000.55c  -0.008743
       5010.66c  -0.016223
       5011.66c  -0.065301
      12000.66c  -0.045228
      20000.66c  -0.321611    $ Fiberglass
m2     1001.66c   2.0
       8016.66c   1.0         $ Water
mt2    lwtr.60t               $ S(alpha,beta) for Water
m3    92235.66c   0.95
      92238.66c   0.05        $ HEU
m4     1001.66c   1.0         $ H gas
m5    26000.55c  -0.6785
       6000.66c  -0.0080
      14000.60c  -0.0100
      24000.50c  -0.1800
      28000.50c  -0.0980
      25055.66c  -0.0180
      15031.66c  -0.0045
      16000.66c  -0.0030      $ Stainless Steel 304
m6    13027.66c  -2.00619e-1
       6000.66c  -3.22547e-1
      20000.66c  -2.86071e-3
      17000.66c  -4.09456e-4
      24050.66c  -1.88012e-4
      24052.66c  -3.62563e-3
      24053.66c  -4.11118e-4
      24054.66c  -1.02336e-4
      29063.66c  -2.85237e-5
      29065.66c  -1.27134e-5
      26054.66c  -2.48137e-3
      26056.66c  -3.89523e-2
```

```
      26057.66c  -8.99578e-4
      26058.66c  -1.19717e-4
       1001.66c  -6.11210e-2
       1002.66c  -9.16952e-6
      19000.66c  -5.88412e-4
      12000.66c  -4.85391e-3
      25055.66c  -1.07216e-3
      42000.66c  -6.55891e-4
       7014.66c  -7.18835e-3
       7015.66c  -2.64060e-5
      11023.66c  -4.32547e-4
      28058.66c  -2.80372e-3
      28060.66c  -8.02640e-4
      28061.66c  -3.48934e-5
      28062.66c  -1.11230e-4
      28064.66c  -2.83432e-5
       8016.66c  -3.43649e-1
       8017.66c  -1.30898e-4
      15031.66c  -2.64326e-3
      82206.66c  -8.80160e-8
      82207.66c  -8.07117e-8
      82208.66c  -1.91371e-7
      37085.66c  -1.06261e-6
      37087.66c  -4.09863e-7
      16000.66c  -6.36451e-4
      14028.66c  -5.70495e-4
      14029.66c  -2.88866e-5
      14030.66c  -1.91753e-5
      30000.42c  -5.08488e-5
      40000.66c  -2.04522e-6  $ Composite boat interior
m7     1001.66c  -0.10098
       1002.66c  -0.00001515
       8016.66c  -0.76171
       8017.66c  -0.00029014
       7014.66c  -0.025905
       7015.66c  -0.00009516
       6000.66c  -0.111       $ ICRU tissue equivalent
c
c
f134:n  13                    $ Dose tally in ICRU sphere
de134 2.5E-8   1.0E-7   1.0E-6   1.0E-5   1.0E-4   1.0E-3   1.0E-2
      2.0E-2   5.0E-2   1.0E-1   2.0E-1   5.0E-1   1.0      1.5
      2.0      3.0      4.0      5.0      6.0      7.0      8.0
      10.0     14.0     17.0     20.0
df134 8.0E-12  1.04E-11 1.12E-11 9.2E-12  7.1E-12  6.2E-12  8.6E-12
      1.46E-11 3.50E-11 6.90E-11 1.26E-10 2.58E-10 3.4E-10  3.62E-10
      3.52E-10 3.8E-10  4.09E-10 3.78E-10 3.83E-10 4.03E-10 4.17E-10
      4.46E-10 5.20E-10 6.10E-10 6.50E-10
```

The following input deck is for the dose calculation with plutonium present, at a source-detector position of 260 cm from the rear of the boat.

```
Boat for Transporting Nuclear Weapons
c
c    67891123456789212345678931234567894123456789512345678961234567897123456789 8
c
c     -- Cell Cards --
c
1     1  -2.50 +3 -4 -5 +7 +1 -15          imp:n=1  $keel not under V
2     1  -2.50 +3 -4 -11 -13 +15           imp:n=1  $keel under V
3     1  -2.50 +1 -2 -5 +7 +4 -10          imp:n=1  $stern bulkhead
```

```
4     1  -2.50 -5 +6 +2 -15 +4 -10         imp:n=1  $starboard bulkhead
5     1  -2.50 +7 -8 +2 -15 +4 -10         imp:n=1  $port bulkhead
6     1  -2.50 +15 +4 -10(-11 +12 -13:+6 -12)
                                           imp:n=1  $bow stbd qtr blkhd
7     1  -2.50 +15 +4 -10(-13 +14 -12 +7:+15 -14 -8)
                                           imp:n=1  $bow port qtr blkhd
8     1  -2.50 -9 +10 -5 +7 +1 -11 -13     imp:n=1  $weather deck
9     6  -0.007885 -6 +8 +2 -12 -14 +4 -10 +17 +21
                                           imp:n=1  $boat interior
10    2  -1.00 +18(-16(+15(+11:-11 +13):-15( +1( +5:+50  -7:-53):
                     +58 +53 -50): +1 -61 +53 -50: -1:
                     -13 +15  -7):
                  -3( +1  +7  -5 -13 -11: +5 -11 +15):
                 -54(+61 +53 -58 -50))
                                           imp:n=1  $water
11    0        -19(+16(+15(+11:-11 +13):-15( +1( +5:+50  -7:-53):
                     +58 +53 -50): +1 -61 +53 -50: -1:
                     -13 +15  -7):
                   +9( +1  +7  -5 -13 -11: +5 -11 +15):
                  +57(+61 +53 -58 -50))
                                           imp:n=1  $sky
12    3  -15.6 -17               vol=1.0  imp:n=1  $Pu Sphere
13    7  -1.0  -21               vol=1.0  imp:n=1  $ICRU Sphere
c
c     - H Detector -
c
30    5  -6.67    +41 -38 +33 -30 (+34 -35:+36 -37) :
                 +35 -36 +33 -30 (+41 -40:+39 -38) :
                 +35 -36 +40 -39 (+33 -32:+31 -30)   imp:n=8  $ SS-304 shell
31    4  -0.00178 +32 -31 +35 -36 +40 -39    vol=1.0  imp:n=16 $ 20-atm H gas
c
c     - Importance Zones -
c
40    0           +60 -59 +52 -51          +37 -56 :
                  +16 -37 +52 -51 (+60 -41:+38 -59):          $ imp=4 zone
                  +16 -37 +41 -38 (+52 -33:+30 -51)   imp:n=4  $ above waterline
41    2  -1.00    +60 -59 +52 -51 (+55 -34        ):
                  +34 -16 +52 -51 (+60 -41:+38 -59):          $ imp=4 zone
                  +34 -16 +41 -38 (+52 -33:+30 -51)   imp:n=4  $ below waterline
42    0           +61 -58 +53 -50          +56 -57 :
                  +16 -56 +53 -50 (+61 -60:+59 -58):          $ imp=2 zone
                  +16 -56 +60 -59 (+53 -52:+51 -50)   imp:n=2  $ above waterline
43    2  -1.00    +61 -58 +53 -50  +54 -55         :
                  +55 -16 +53 -50 (+61 -60:+59 -58):          $ imp=2 zone
                  +55 -16 +60 -59 (+53 -52:+51 -50)   imp:n=2  $ below waterline
998   0    -18                           imp:n=0
999   0    +19                           imp:n=0

c
c     -- Surface Cards --
c
1     py    0.0                      $outer stern plane
2     py    0.3175                   $inside stern plane
3     pz  -89.0                      $outer keel
4     pz  -88.6825                   $inner keel
5     px  150.0                      $outer starboard bulkhead
6     px  149.6825                   $inner starboard bulkhead
7     px -150.0                      $outer port bulkhead
8     px -149.6825                   $inner port bulkhead
9     pz  144.6                      $outer deck
10    pz  144.2566                   $inner deck
11    p     1.631333 1.0 0.0 823     $outer bow starboard quarter
12    p     1.632672 1.0 0.0 822.6825  $inner bow starboard quarter
13    p    -1.631333 1.0 0.0 823     $outer bow port quarter
14    p    -1.632672 1.0 0.0 822.6825  $inner bow port quarter
15    py  578.3                      $beginning of forecastle
16    pz    0.0                      $waterline
```

```
17    s     0.0 260.0 -50.0 4.2454     $5-kg Pu sphere
18    pz -5000.0
19    pz  5000.0
c 20    px   165.0        $source plane
21    s     0.0 285.0 -50.0 15.0       $30-cm diameter ICRU Sphere
c
30    px  -154.6825     $outer SS surface facing boat
31    px  -155.0        $outer H surface facing boat
32    px  -185.0        $outer H surface away from boat
33    px  -185.3175     $outer SS surface away from boat
34    pz  -100.3175     $outer SS surface at bottom
35    pz  -100.0        $outer H surface at bottom
36    pz   150.0        $outer H surface at top
37    pz   150.3175     $outer SS surface at top
38    py   410.3175     $outer SS surface forward
39    py   410.0        $outer H surface forward
40    py   110.0        $outer H surface rear
41    py   109.6825     $outer SS surface rear
c
50    px  -150.0001     $outer imp=2 zone facing boat
51    px  -153.0        $outer imp=4 zone facing boat
52    px  -187.0        $outer imp=4 zone
53    px  -190.0        $outer imp=2 zone
54    pz  -105.0        $outer imp=2 zone at bottom
55    pz  -102.0        $outer imp=4 zone at bottom
56    pz   152.0        $outer imp=4 zone at top
57    pz   155.0        $outer imp=2 zone at top
58    py   415.0        $outer imp=2 zone forward
59    py   412.0        $outer imp=4 zone forward
60    py   108.0        $outer imp=4 zone rear
61    py   105.0        $outer imp=2 zone rear
c

c
c     -- Data Cards --
c
c   sdef  sur=20 pos=165.0 260.0 -50.0 vec=1 0 0.0001 dir=-1 rad=d1 erg=14.0 par=1
c   si1   0 0.5
c   sp1   -21 1
c
sdef  pos=155.0 260.0 -50.0 erg=14.0 par=1
c
c   sdef pos=160.0 660.0 -50.0 erg=14.0 vec=-1 0 0 dir=d1 par=1
c   sb1  -31 0.5
mode n
phys:n 150.0 0 1
cut:n  500000
totnu
nps   400000000
prdmp 0 250000 -1 5 0
m1    14000.60c  -0.631037
       8016.66c  -1.226159
       8017.66c  -0.000467
      13027.66c  -0.185238
      26000.55c  -0.008743
       5010.66c  -0.016223
       5011.66c  -0.065301
      12000.66c  -0.045228
      20000.66c  -0.321611    $ Fiberglass
m2     1001.66c   2.0
       8016.66c   1.0         $ Water
mt2    lwtr.60t               $ S(alpha,beta) for Water
m3    94239.66c   0.94
      94240.66c   0.06        $ WG plutonium
m4     1001.66c   1.0         $ H gas
m5    26000.55c  -0.6785
       6000.66c  -0.0080
```

```
      14000.60c  -0.0100
      24000.50c  -0.1800
      28000.50c  -0.0980
      25055.66c  -0.0180
      15031.66c  -0.0045
      16000.66c  -0.0030      $ Stainless Steel 304
m6    13027.66c  -2.00619e-1
       6000.66c  -3.22547e-1
      20000.66c  -2.86071e-3
      17000.66c  -4.09456e-4
      24050.66c  -1.88012e-4
      24052.66c  -3.62563e-3
      24053.66c  -4.11118e-4
      24054.66c  -1.02336e-4
      29063.66c  -2.85237e-5
      29065.66c  -1.27134e-5
      26054.66c  -2.48137e-3
      26056.66c  -3.89523e-2
      26057.66c  -8.99578e-4
      26058.66c  -1.19717e-4
       1001.66c  -6.11210e-2
       1002.66c  -9.16952e-6
      19000.66c  -5.88412e-4
      12000.66c  -4.85391e-3
      25055.66c  -1.07216e-3
      42000.66c  -6.55891e-4
       7014.66c  -7.18835e-3
       7015.66c  -2.64060e-5
      11023.66c  -4.32547e-4
      28058.66c  -2.80372e-3
      28060.66c  -8.02640e-4
      28061.66c  -3.48934e-5
      28062.66c  -1.11230e-4
      28064.66c  -2.83432e-5
       8016.66c  -3.43649e-1
       8017.66c  -1.30898e-4
      15031.66c  -2.64326e-3
      82206.66c  -8.80160e-8
      82207.66c  -8.07117e-8
      82208.66c  -1.91371e-7
      37085.66c  -1.06261e-6
      37087.66c  -4.09863e-7
      16000.66c  -6.36451e-4
      14028.66c  -5.70495e-4
      14029.66c  -2.88866e-5
      14030.66c  -1.91753e-5
      30000.42c  -5.08488e-5
      40000.66c  -2.04522e-6  $ Composite boat interior
m7     1001.66c  -0.10098
       1002.66c  -0.00001515
       8016.66c  -0.76171
       8017.66c  -0.00029014
       7014.66c  -0.025905
       7015.66c  -0.00009516
       6000.66c  -0.111       $ ICRU tissue equivalent
c
c
f134:n  13                     $ Dose tally in ICRU sphere
de134 2.5E-8   1.0E-7   1.0E-6   1.0E-5   1.0E-4   1.0E-3   1.0E-2
      2.0E-2   5.0E-2   1.0E-1   2.0E-1   5.0E-1   1.0      1.5
      2.0      3.0      4.0      5.0      6.0      7.0      8.0
      10.0     14.0     17.0     20.0
df134 8.0E-12  1.04E-11 1.12E-11 9.2E-12  7.1E-12  6.2E-12  8.6E-12
      1.46E-11 3.50E-11 6.90E-11 1.26E-10 2.58E-10 3.4E-10  3.62E-10
      3.52E-10 3.8E-10  4.09E-10 3.78E-10 3.83E-10 4.03E-10 4.17E-10
      4.46E-10 5.20E-10 6.10E-10 6.50E-10
```

APPENDIX B

TABULATED MCNP RESULTS

The following data are the raw results from MCNP. These are the data used in all calculations and fitted functions presented in Chapter IV.

The following data are the estimated number of scattering reactions in the detector per source particle for the active mode, no SFM present case.

Pos (cm) time (ms)	20	100	180	260	340	420	500	580	660
0.1	6.63E-03	9.50E-03	1.02E-02	1.01E-02	1.00E-02	1.00E-02	9.44E-03	7.30E-03	0.00027412
0.45	1.93E-09	6.76E-09	3.92E-09	3.02E-09	1.93E-09	1.93E-09	0.00E+00	0.00E+00	0.00E+00
0.8	0.00E+00	0.00E+00	0.00E+00	0.00E+00	0.00E+00	0.00E+00	0.00E+00	0.00E+00	0.00E+00
1.15	0.00E+00	0.00E+00	0.00E+00	0.00E+00	0.00E+00	0.00E+00	0.00E+00	0.00E+00	0.00E+00
1.5	0.00E+00	0.00E+00	0.00E+00	0.00E+00	0.00E+00	0.00E+00	0.00E+00	0.00E+00	0.00E+00
1.85	0.00E+00	0.00E+00	0.00E+00	0.00E+00	0.00E+00	0.00E+00	0.00E+00	0.00E+00	0.00E+00
2.2	0.00E+00	0.00E+00	0.00E+00	0.00E+00	0.00E+00	0.00E+00	0.00E+00	0.00E+00	0.00E+00
2.55	0.00E+00	0.00E+00	0.00E+00	0.00E+00	0.00E+00	0.00E+00	0.00E+00	0.00E+00	0.00E+00
2.9	0.00E+00	0.00E+00	0.00E+00	0.00E+00	0.00E+00	0.00E+00	0.00E+00	0.00E+00	0.00E+00
3.25	0.00E+00	0.00E+00	0.00E+00	0.00E+00	0.00E+00	0.00E+00	0.00E+00	0.00E+00	0.00E+00
3.6	0.00E+00	0.00E+00	0.00E+00	0.00E+00	0.00E+00	0.00E+00	0.00E+00	0.00E+00	0.00E+00
3.95	0.00E+00	0.00E+00	0.00E+00	0.00E+00	0.00E+00	0.00E+00	0.00E+00	0.00E+00	0.00E+00
4.3	0.00E+00	0.00E+00	0.00E+00	0.00E+00	0.00E+00	0.00E+00	0.00E+00	0.00E+00	0.00E+00
4.65	0.00E+00	0.00E+00	0.00E+00	0.00E+00	0.00E+00	0.00E+00	0.00E+00	0.00E+00	0.00E+00
5	0.00E+00	0.00E+00	0.00E+00	0.00E+00	0.00E+00	0.00E+00	0.00E+00	0.00E+00	0.00E+00

The following data are the estimated standard deviations of the number of scattering reactions in the detector per source particle for the active mode, no SFM present case.

Pos(cm) time(ms)	20	100	180	260	340	420	500	580	660
0.1	2.65E-06	3.80E-06	3.05E-06	4.03E-06	4.01E-06	4.02E-06	3.78E-06	2.92E-06	5.48E-07
0.45	1.93E-09	4.25E-09	2.77E-09	2.22E-09	1.93E-09	1.93E-09	0.00E+00	0.00E+00	0.00E+00
0.8	0.00E+00	0.00E+00	0.00E+00	0.00E+00	0.00E+00	0.00E+00	0.00E+00	0.00E+00	0.00E+00
1.15	0.00E+00	0.00E+00	0.00E+00	0.00E+00	0.00E+00	0.00E+00	0.00E+00	0.00E+00	0.00E+00
1.5	0.00E+00	0.00E+00	0.00E+00	0.00E+00	0.00E+00	0.00E+00	0.00E+00	0.00E+00	0.00E+00
1.85	0.00E+00	0.00E+00	0.00E+00	0.00E+00	0.00E+00	0.00E+00	0.00E+00	0.00E+00	0.00E+00
2.2	0.00E+00	0.00E+00	0.00E+00	0.00E+00	0.00E+00	0.00E+00	0.00E+00	0.00E+00	0.00E+00
2.55	0.00E+00	0.00E+00	0.00E+00	0.00E+00	0.00E+00	0.00E+00	0.00E+00	0.00E+00	0.00E+00
2.9	0.00E+00	0.00E+00	0.00E+00	0.00E+00	0.00E+00	0.00E+00	0.00E+00	0.00E+00	0.00E+00
3.25	0.00E+00	0.00E+00	0.00E+00	0.00E+00	0.00E+00	0.00E+00	0.00E+00	0.00E+00	0.00E+00
3.6	0.00E+00	0.00E+00	0.00E+00	0.00E+00	0.00E+00	0.00E+00	0.00E+00	0.00E+00	0.00E+00
3.95	0.00E+00	0.00E+00	0.00E+00	0.00E+00	0.00E+00	0.00E+00	0.00E+00	0.00E+00	0.00E+00
4.3	0.00E+00	0.00E+00	0.00E+00	0.00E+00	0.00E+00	0.00E+00	0.00E+00	0.00E+00	0.00E+00
4.65	0.00E+00	0.00E+00	0.00E+00	0.00E+00	0.00E+00	0.00E+00	0.00E+00	0.00E+00	0.00E+00
5	0.00E+00	0.00E+00	0.00E+00	0.00E+00	0.00E+00	0.00E+00	0.00E+00	0.00E+00	0.00E+00

The following data are the estimated number of fissions per source particle for the HEU sphere in the active mode runs.

Pos(cm) time(ms)	20	100	180	260	340	420	500	580	660
0.1	0.0004995	0.000933	0.001709	0.002267	0.001697	0.000916	0.00047	0.000256	8.70E-06
0.45	1.32E-05	2.17E-05	3.93E-05	5.82E-05	4.00E-05	2.05E-05	1.00E-05	6.56E-06	2.64E-07
0.8	5.43E-06	1.04E-05	2.64E-05	3.88E-05	2.50E-05	9.45E-06	4.17E-06	2.71E-06	1.01E-07
1.15	4.58E-06	7.34E-06	1.24E-05	1.50E-05	1.17E-05	6.55E-06	3.21E-06	2.09E-06	8.63E-08
1.5	2.91E-06	3.87E-06	5.18E-06	6.25E-06	4.86E-06	3.49E-06	2.15E-06	1.51E-06	5.02E-08
1.85	1.68E-06	2.15E-06	2.82E-06	2.95E-06	2.89E-06	1.84E-06	1.65E-06	1.05E-06	7.51E-08
2.2	1.04E-06	1.32E-06	1.67E-06	1.89E-06	1.55E-06	1.33E-06	1.02E-06	6.48E-07	2.97E-08
2.55	7.27E-07	7.81E-07	1.24E-06	1.07E-06	9.27E-07	7.07E-07	5.43E-07	3.91E-07	8.39E-09
2.9	4.16E-07	4.59E-07	5.43E-07	6.97E-07	7.25E-07	5.36E-07	3.89E-07	4.24E-07	3.28E-08
3.25	2.41E-07	2.95E-07	3.35E-07	4.62E-07	4.69E-07	4.03E-07	2.56E-07	3.73E-07	2.97E-08
3.6	2.15E-07	2.01E-07	3.30E-07	2.85E-07	2.87E-07	2.03E-07	2.23E-07	1.68E-07	3.88E-09
3.95	7.68E-08	1.55E-07	1.42E-07	1.44E-07	1.82E-07	1.69E-07	9.27E-08	9.33E-08	4.74E-09
4.3	9.27E-08	1.13E-07	1.58E-07	1.24E-07	1.11E-07	1.30E-07	2.33E-07	9.09E-08	9.26E-10
4.65	7.23E-08	1.15E-07	3.57E-08	7.24E-08	5.90E-08	8.04E-08	2.81E-08	4.78E-08	0
5	4.28E-08	3.54E-08	7.15E-08	8.73E-08	4.62E-08	3.10E-08	3.38E-08	3.93E-08	0

The following data are the standard deviations of the number of fissions per source particle for the HEU sphere in the active mode runs.

Pos(cm) time(ms)	20	100	180	260	340	420	500	580	660
0.1	4.00E-06	5.41E-06	7.35E-06	8.61E-06	7.30E-06	5.40E-06	3.90E-06	2.80E-06	5.39E-07
0.45	4.94E-07	6.14E-07	7.79E-07	9.90E-07	8.43E-07	5.96E-07	4.42E-07	3.43E-07	8.07E-08
0.8	2.69E-07	3.75E-07	5.93E-07	7.34E-07	5.83E-07	3.30E-07	2.36E-07	1.99E-07	2.75E-08
1.15	2.29E-07	3.33E-07	4.18E-07	4.07E-07	3.70E-07	3.01E-07	2.05E-07	1.70E-07	3.65E-08
1.5	1.88E-07	2.25E-07	2.38E-07	2.64E-07	2.31E-07	2.05E-07	1.54E-07	1.55E-07	1.56E-08
1.85	1.31E-07	1.64E-07	1.97E-07	2.11E-07	1.83E-07	1.16E-07	1.69E-07	1.12E-07	2.01E-08
2.2	1.01E-07	9.77E-08	1.16E-07	1.48E-07	1.27E-07	1.36E-07	1.14E-07	7.38E-08	9.74E-09
2.55	1.05E-07	7.65E-08	1.63E-07	1.01E-07	9.05E-08	6.85E-08	6.19E-08	6.78E-08	3.74E-09
2.9	6.16E-08	5.04E-08	6.77E-08	8.90E-08	1.62E-07	6.64E-08	5.47E-08	9.54E-08	1.24E-08
3.25	4.28E-08	3.80E-08	5.63E-08	6.66E-08	7.19E-08	9.71E-08	5.00E-08	1.21E-07	1.54E-08
3.6	4.81E-08	2.86E-08	7.92E-08	4.73E-08	4.78E-08	5.02E-08	7.61E-08	3.14E-08	3.28E-09
3.95	1.76E-08	3.40E-08	3.01E-08	2.84E-08	4.49E-08	6.12E-08	2.01E-08	2.92E-08	4.74E-09
4.3	2.93E-08	3.73E-08	5.73E-08	3.27E-08	3.44E-08	4.68E-08	1.11E-07	3.33E-08	9.26E-10
4.65	2.85E-08	5.11E-08	8.97E-09	1.91E-08	1.81E-08	2.84E-08	8.62E-09	2.01E-08	0
5	2.04E-08	1.48E-08	2.76E-08	4.49E-08	1.53E-08	1.15E-08	1.52E-08	1.10E-08	0

The following data are the estimated number of scattering reactions in the detector per source particle for the active mode with HEU present.

Pos(cm) time(ms)	20	100	180	260	340	420	500	580	660
0.1	6.64E-03	9.55E-03	1.03E-02	1.02E-02	1.01E-02	1.01E-02	9.46E-03	7.31E-03	0.00027423
0.45	4.42E-07	1.22E-06	2.72E-06	4.04E-06	2.73E-06	1.10E-06	3.56E-07	1.11E-07	4.36E-09
0.8	1.92E-07	5.33E-07	1.77E-06	2.62E-06	1.67E-06	5.16E-07	1.58E-07	5.66E-08	1.46E-09
1.15	1.60E-07	4.11E-07	8.72E-07	1.05E-06	8.37E-07	3.71E-07	1.28E-07	4.78E-08	2.00E-09
1.5	1.23E-07	2.09E-07	4.20E-07	5.02E-07	3.39E-07	2.13E-07	9.40E-08	3.01E-08	3.44E-10
1.85	6.18E-08	1.46E-07	2.18E-07	2.37E-07	2.24E-07	1.09E-07	6.78E-08	2.46E-08	2.86E-09
2.2	3.54E-08	7.24E-08	1.40E-07	1.67E-07	1.06E-07	7.55E-08	3.52E-08	1.89E-08	0
2.55	2.57E-08	4.45E-08	8.37E-08	8.63E-08	7.63E-08	4.28E-08	2.20E-08	1.12E-08	0
2.9	1.45E-08	3.93E-08	3.92E-08	5.26E-08	5.79E-08	2.03E-08	1.13E-08	7.61E-09	0
3.25	1.30E-08	1.90E-08	2.13E-08	3.43E-08	3.20E-08	1.77E-08	5.50E-09	4.58E-09	3.88E-10
3.6	7.41E-09	9.45E-09	2.60E-08	2.20E-08	1.75E-08	9.69E-09	8.13E-09	2.93E-09	0
3.95	5.40E-09	5.80E-09	8.69E-09	1.53E-08	1.38E-08	1.06E-08	2.76E-09	4.34E-10	0
4.3	4.07E-09	7.49E-09	9.68E-09	1.32E-08	7.18E-09	4.03E-09	4.42E-09	7.12E-10	0
4.65	1.03E-09	5.22E-09	3.54E-09	4.46E-09	4.21E-09	6.62E-09	3.27E-10	9.69E-10	0
5	2.14E-09	2.54E-09	1.79E-09	8.17E-09	3.71E-09	2.21E-09	4.06E-10	2.60E-09	0

The following data are the estimated standard deviations of the number of scattering reactions in the detector per source particle for the active mode with HEU present.

Pos(cm) time(ms)	20	100	180	260	340	420	500	580	660
0.1	2.66E-06	3.82E-06	4.11E-06	4.06E-06	4.05E-06	4.04E-06	3.78E-06	2.92E-06	5.48E-07
0.45	2.82E-08	5.07E-08	7.75E-08	9.78E-08	7.99E-08	4.55E-08	2.58E-08	1.18E-08	2.18E-09
0.8	1.56E-08	2.89E-08	5.82E-08	7.15E-08	5.57E-08	2.67E-08	1.50E-08	8.68E-09	7.72E-10
1.15	1.44E-08	2.68E-08	3.99E-08	4.11E-08	3.84E-08	2.38E-08	1.44E-08	6.95E-09	1.70E-09
1.5	1.26E-08	1.64E-08	2.62E-08	2.94E-08	2.46E-08	1.63E-08	1.14E-08	6.43E-09	2.03E-10
1.85	9.61E-09	1.55E-08	2.24E-08	2.20E-08	2.05E-08	1.11E-08	1.07E-08	5.22E-09	1.62E-09
2.2	6.35E-09	8.55E-09	1.40E-08	1.74E-08	1.13E-08	1.12E-08	6.71E-09	4.12E-09	0
2.55	4.98E-09	6.80E-09	1.41E-08	1.12E-08	1.13E-08	6.87E-09	4.06E-09	3.26E-09	0
2.9	4.72E-09	7.70E-09	7.28E-09	8.47E-09	1.65E-08	4.32E-09	4.50E-09	3.42E-09	0
3.25	3.58E-09	4.88E-09	5.57E-09	7.70E-09	7.99E-09	5.21E-09	2.08E-09	2.72E-09	3.88E-10
3.6	3.09E-09	2.74E-09	7.39E-09	5.79E-09	3.90E-09	3.23E-09	2.47E-09	1.61E-09	0
3.95	1.84E-09	2.57E-09	2.81E-09	5.09E-09	4.25E-09	4.98E-09	1.15E-09	4.34E-10	0
4.3	1.93E-09	3.31E-09	4.54E-09	3.97E-09	2.95E-09	2.47E-09	3.60E-09	7.07E-10	0
4.65	9.34E-10	2.37E-09	1.76E-09	1.91E-09	2.32E-09	3.05E-09	2.33E-10	7.45E-10	0
5	1.60E-09	1.44E-09	8.78E-10	4.30E-09	2.18E-09	1.59E-09	3.57E-10	1.19E-09	0

The following data are the estimated number of fissions per source particle for the plutonium sphere in the active mode runs.

Pos(cm) time(ms)	20	100	180	260	340	420	500	580	660
0.1	9.56E-05	1.75E-04	3.21E-04	4.25E-04	3.20E-04	1.73E-04	8.84E-05	4.89E-05	1.96E-06
0.45	2.91E-06	4.55E-06	8.37E-06	1.25E-05	8.49E-06	4.34E-06	2.27E-06	1.27E-06	4.63E-08
0.8	1.23E-06	2.43E-06	6.10E-06	9.35E-06	6.39E-06	2.28E-06	8.89E-07	5.41E-07	3.12E-08
1.15	1.11E-06	1.73E-06	3.07E-06	3.97E-06	3.10E-06	1.74E-06	8.36E-07	5.82E-07	1.58E-08
1.5	6.80E-07	9.75E-07	1.37E-06	1.64E-06	1.44E-06	9.50E-07	5.86E-07	4.39E-07	1.36E-08
1.85	4.71E-07	5.90E-07	7.21E-07	8.51E-07	7.08E-07	5.50E-07	4.73E-07	3.10E-07	1.59E-08
2.2	3.38E-07	3.21E-07	4.64E-07	5.17E-07	4.18E-07	2.71E-07	2.43E-07	2.49E-07	1.51E-08
2.55	1.97E-07	1.89E-07	3.31E-07	2.38E-07	2.51E-07	2.38E-07	1.78E-07	7.25E-08	3.47E-09
2.9	8.94E-08	1.97E-07	1.56E-07	2.44E-07	1.80E-07	1.86E-07	1.14E-07	9.29E-08	3.71E-09
3.25	1.00E-07	1.30E-07	7.46E-08	1.69E-07	1.12E-07	1.27E-07	7.24E-08	1.08E-07	0
3.6	5.80E-08	7.23E-08	7.18E-08	4.62E-08	6.87E-08	6.54E-08	5.35E-08	4.74E-08	0
3.95	1.61E-08	3.94E-08	3.50E-08	3.53E-08	4.32E-08	4.35E-08	3.65E-08	2.80E-08	0
4.3	2.95E-09	2.38E-08	7.35E-08	1.74E-08	3.05E-08	1.02E-08	2.34E-08	1.14E-08	0
4.65	7.78E-09	1.40E-08	2.05E-08	1.82E-08	1.16E-08	2.30E-08	1.29E-08	4.41E-09	0
5	4.20E-09	4.25E-09	1.32E-08	1.82E-08	6.78E-09	1.08E-08	4.94E-09	1.18E-08	0

The following data are the standard deviations of the number of fissions per source particle for the plutonium sphere in the active mode runs.

Pos(cm) time(ms)	20	100	180	260	340	420	500	580	660
0.1	1.08E-06	1.47E-06	1.99E-06	2.29E-06	2.02E-06	1.50E-06	1.05E-06	7.92E-07	1.81E-07
0.45	1.54E-07	1.88E-07	2.38E-07	2.86E-07	2.33E-07	1.72E-07	1.28E-07	8.07E-08	1.33E-08
0.8	8.52E-08	1.15E-07	1.75E-07	2.13E-07	2.04E-07	1.02E-07	7.02E-08	5.01E-08	1.15E-08
1.15	7.39E-08	9.40E-08	1.24E-07	1.46E-07	1.26E-07	1.01E-07	6.80E-08	6.59E-08	7.78E-09
1.5	5.67E-08	7.69E-08	8.05E-08	9.19E-08	9.97E-08	6.62E-08	6.03E-08	5.37E-08	5.32E-09
1.85	5.71E-08	4.98E-08	5.49E-08	6.83E-08	5.56E-08	4.90E-08	5.78E-08	4.53E-08	7.57E-09
2.2	4.61E-08	3.33E-08	4.22E-08	5.07E-08	4.87E-08	3.03E-08	2.62E-08	4.04E-08	6.55E-09
2.55	3.65E-08	2.56E-08	4.00E-08	2.77E-08	3.12E-08	3.93E-08	3.34E-08	1.39E-08	2.30E-09
2.9	1.84E-08	3.69E-08	2.61E-08	3.75E-08	2.94E-08	3.50E-08	2.17E-08	2.32E-08	2.56E-09
3.25	2.88E-08	2.30E-08	1.82E-08	3.77E-08	2.69E-08	3.11E-08	1.62E-08	2.72E-08	0
3.6	1.53E-08	1.77E-08	1.98E-08	1.19E-08	1.52E-08	2.01E-08	1.39E-08	1.37E-08	0
3.95	5.44E-09	1.05E-08	1.07E-08	8.41E-09	1.44E-08	1.30E-08	1.15E-08	1.28E-08	0
4.3	2.02E-09	8.77E-09	2.24E-08	6.03E-09	9.23E-09	4.32E-09	9.03E-09	5.40E-09	0
4.65	3.60E-09	5.95E-09	7.28E-09	7.35E-09	4.80E-09	8.45E-09	6.76E-09	2.34E-09	0
5	2.43E-09	2.10E-09	6.92E-09	6.85E-09	2.93E-09	6.48E-09	2.07E-09	5.65E-09	0

The following data are the estimated number of scattering reactions in the detector per source particle for the active mode with plutonium present.

Pos(cm) time(ms)	20	100	180	260	340	420	500	580	660
0.1	6.63E-03	9.51E-03	1.02E-02	1.01E-02	1.01E-02	1.01E-02	9.45E-03	7.30E-03	0.00027415
0.45	1.27E-07	3.35E-07	7.89E-07	1.23E-06	7.43E-07	2.80E-07	1.00E-07	3.39E-08	1.33E-09
0.8	5.31E-08	1.58E-07	5.63E-07	9.18E-07	5.30E-07	1.53E-07	3.69E-08	1.19E-08	0
1.15	5.46E-08	1.23E-07	2.71E-07	4.18E-07	2.79E-07	1.25E-07	4.45E-08	1.85E-08	0
1.5	3.18E-08	5.68E-08	1.30E-07	1.60E-07	1.55E-07	5.39E-08	2.74E-08	1.78E-08	0
1.85	2.46E-08	4.60E-08	8.19E-08	8.58E-08	5.40E-08	4.61E-08	2.11E-08	5.83E-09	8.00E-10
2.2	1.03E-08	2.24E-08	4.05E-08	5.32E-08	4.04E-08	1.86E-08	7.32E-09	6.19E-09	1.30E-09
2.55	7.56E-09	1.87E-08	2.80E-08	1.92E-08	3.01E-08	1.78E-08	6.03E-09	1.92E-09	0
2.9	1.12E-09	1.81E-08	1.30E-08	3.08E-08	1.78E-08	5.47E-09	6.83E-09	1.25E-10	0
3.25	3.40E-09	5.52E-09	2.42E-09	2.37E-08	1.01E-08	7.99E-09	5.16E-10	7.73E-10	0
3.6	2.98E-09	4.95E-09	6.28E-09	2.92E-09	9.67E-09	1.43E-09	7.55E-10	8.22E-11	0
3.95	3.35E-10	3.13E-09	4.41E-09	3.19E-09	4.48E-09	3.90E-09	1.11E-09	1.66E-09	0
4.3	0.00E+00	1.30E-09	1.09E-08	3.19E-09	1.41E-09	1.40E-09	5.94E-10	0.00E+00	0
4.65	0.00E+00	1.25E-09	1.34E-09	4.12E-09	2.23E-09	1.54E-09	6.75E-10	0.00E+00	0
5	0	0	9.23E-11	2.99E-09	1.50E-10	5.23E-10	2.53E-09	0	0

The following data are the estimated standard deviations of the number of scattering reactions in the detector per source particle for the active mode with plutonium present.

Pos(cm) time(ms)	20	100	180	260	340	420	500	580	660
0.1	2.65E-06	3.80E-06	3.06E-06	4.03E-06	4.03E-06	4.02E-06	3.78E-06	2.92E-06	5.48E-07
0.45	1.27E-08	2.20E-08	3.59E-08	4.81E-08	3.36E-08	1.86E-08	1.33E-08	5.88E-09	1.33E-09
0.8	7.28E-09	1.34E-08	2.83E-08	3.42E-08	2.84E-08	1.30E-08	6.26E-09	3.97E-09	0
1.15	7.54E-09	1.21E-08	1.69E-08	2.58E-08	1.78E-08	1.17E-08	6.68E-09	4.66E-09	0
1.5	5.64E-09	7.13E-09	1.28E-08	1.37E-08	1.68E-08	6.63E-09	6.13E-09	5.08E-09	0
1.85	5.39E-09	6.62E-09	9.32E-09	1.02E-08	7.00E-09	7.38E-09	5.93E-09	1.95E-09	8.00E-10
2.2	2.56E-09	4.75E-09	6.39E-09	8.83E-09	6.88E-09	4.83E-09	2.47E-09	2.94E-09	1.30E-09
2.55	2.68E-09	4.41E-09	5.48E-09	3.59E-09	6.77E-09	5.54E-09	1.78E-09	9.76E-10	0
2.9	7.89E-10	5.09E-09	3.24E-09	6.18E-09	4.59E-09	2.08E-09	3.37E-09	1.25E-10	0
3.25	1.63E-09	3.17E-09	1.23E-09	6.82E-09	3.25E-09	3.90E-09	3.56E-10	4.54E-10	0
3.6	1.41E-09	1.75E-09	2.27E-09	1.23E-09	2.74E-09	7.85E-10	5.03E-10	6.05E-11	0
3.95	2.43E-10	1.75E-09	2.87E-09	1.85E-09	2.14E-09	1.62E-09	8.34E-10	1.66E-09	0
4.3	0.00E+00	8.25E-10	3.59E-09	1.71E-09	6.24E-10	9.15E-10	3.66E-10	0.00E+00	0
4.65	0	1.25E-09	1.23E-09	3.18E-09	1.55E-09	1.03E-09	5.35E-10	0	0
5	0	0	9.23E-11	1.39E-09	1.50E-10	4.11E-10	2.51E-09	0	0

The following data are the estimated number of scattering reactions in the detector per source particle with fractional error for the passive mode with ^{240}Pu.

Pos (cm)	Rxns/sp	Frac. error
20	0.039614	0.0073
100	0.067675	0.0058
180	0.093082	0.0052
260	0.10349	0.0051
340	0.0934	0.0052
420	0.069074	0.0059
500	0.042742	0.0071
580	0.024802	0.0091
660	0.014087	0.0118

APPENDIX C

MATLAB SCRIPTS

The following scripts were written for the data processing and presentation using MATLAB and the output data from MCNP.

The script for the initial data processing and plotting was as follows.

```
%   DATPROC.M   MATLAB script for formatting and plotting data.
%   Written for use in MS thesis research.
%
%   Trey Johansen
%   Graduate Student
%   Nuclear Engineering
%   Texas A&M University
%
%   Last revision:  2006 March 27
%
%   5678911234567892123456789312345678941234567895123456789612345678971234 5

clear all

format short g, format compact, opengl neverselect
warning off MATLAB:divideByZero

load no1.dat, load no2.dat, load no3.dat, load no4.dat, load no5.dat
load no6.dat, load no7.dat, load no8.dat, load no9.dat
load pu1.dat, load pu2.dat, load pu3.dat, load pu4.dat, load pu5.dat
load pu6.dat, load pu7.dat, load pu8.dat, load pu9.dat
load  u1.dat, load  u2.dat, load  u3.dat, load  u4.dat, load  u5.dat
load  u6.dat, load  u7.dat, load  u8.dat, load  u9.dat

ndet = 1;  % Total number of detectors in string
nduw = 0;  % Number of underwater detectors
nair = 0;  % Number of detectors in air
nlin = 1;  % Number of detectors at waterline

mintim = 10000; % input('What is the start time for tally information?\n');  % Start time
maxtim = 500000;% input('What is the time range of the problem?\n');  % Stop time
ntt = 15; % input('How many time steps?\n');  % Number of time steps in problem
tt = 1e-8.*linspace(mintim,maxtim,ntt); % Time bins
tscale = zeros(size(tt));
tscale(1) = tt(1);
for i = 2:ntt
    tscale(i) = tt(i) - tt(i-1);
end
ypos = [20:80:660];   % y-pos of "sample" points

datlen = (ntt + 1).*2; % Number of data pieces for each type of tally.
                       % The tallies include a sum-bin at the end of each
                       % set of time bins, hence the "ntt + 1".  Also included
                       % in each bin is the relative error, hence "*2"

%  The order of output data from MCTAL files goes in order from lowest z-pos
%  to highest z-pos.  So it covers the 4 uw dets, then one at wtrln, then 5
%  in air.  MCTAL gives 4 tally bins per line with respective uncertainties,
```

```
%  thus 8 entries per line.  In the case where the number of tallies is not
%  integrally divisible by 4, the final line ends with a series of zero-entries.
%  Thus, the data needs to be properly formatted, as is done below.

%  Creating matrix with fission data for PU then HEU samples:

nlinefiss = ceil((ntt + 1).*2./8);
%  This is the number of data lines for fission data

temp = zeros(9,nlinefiss,2);

for i = 1:nlinefiss
    temp(:,(i-1)*8+1:i*8,1) = [pu1(i,:); pu2(i,:); pu3(i,:); pu4(i,:); pu5(i,:);
pu6(i,:); pu7(i,:); pu8(i,:); pu9(i,:)];
    temp(:,(i-1)*8+1:i*8,2) = [ u1(i,:);  u2(i,:);  u3(i,:);  u4(i,:);  u5(i,:);
u6(i,:);  u7(i,:);  u8(i,:);  u9(i,:)];
end

%  Errors in MCTAL file are given relative to tally data, thus actual error
%  value is the relative error multiplied by tally value.
for i = 1:9
    puflux(i,:) = temp(i,1:2:datlen-3,1);%./tscale;
    pustd(i,:)  = temp(i,1:2:datlen-3,1).*temp(i,2:2:datlen-2,1);%./tscale;
     uflux(i,:) = temp(i,1:2:datlen-3,2);%./tscale;
     ustd(i,:)  = temp(i,1:2:datlen-3,2).*temp(i,2:2:datlen-2,2);%./tscale;
end

clear temp

c = 1; % This is my figure number counter

figure(c), clf reset, c = c + 1;
surf(tt,ypos,sum(puflux,3))
% colormap gray
title('PU Fission Rxns')
xlabel('Time - sec')
ylabel('Y-Pos of det along boat - cm')

figure(c), clf reset, c = c + 1;
surf(tt(:,2:ntt),ypos,sum(puflux(:,2:ntt),3))
% colormap gray
title('PU Fission Rxns')
xlabel('Time - sec')
ylabel('Y-Pos of det along boat - cm')

figure(c), clf reset, c = c + 1;
semilogy(tt,sum(puflux,1),'k-',tt,sum(puflux,1)+sqrt(sum(pustd.^2,1)),'kx:'); hold on
legend('Pu fissions','Error bounds',0)
semilogy(tt,sum(puflux,1)-sqrt(sum(pustd.^2,1)),'kx:');
title('PU Fission Rate')
xlabel('Time - sec')
ylabel('Fissions')

figure(c), clf reset, c = c + 1;
semilogy(tt(:,2:ntt),sum(puflux(:,2:ntt),1),'k-
',tt(:,2:ntt),sum(puflux(:,2:ntt),1)+sqrt(sum(pustd(:,2:ntt).^2,1)),'kx:'); hold on
legend('Pu fissions','Error bounds',0)
semilogy(tt(:,2:ntt),sum(puflux(:,2:ntt),1)-sqrt(sum(pustd(:,2:ntt).^2,1)),'kx:');
title('PU Fission Rate')
xlabel('Time - sec')
ylabel('Fissions')

figure(c), clf reset, c = c + 1;
surf(tt,ypos,sum(uflux,3))
% colormap gray
title('HEU Fission Rxns')
xlabel('Time - sec')
```

```
ylabel('Y-Pos of det along boat - cm')

figure(c), clf reset, c = c + 1;
surf(tt(:,2:ntt),ypos,sum(uflux(:,2:ntt),3))
% colormap gray
title('HEU Fission Rxns')
xlabel('Time - sec')
ylabel('Y-Pos of det along boat - cm')

figure(c), clf reset, c = c + 1;
semilogy(tt,sum( uflux,1),'k-',tt,sum( uflux,1)+sqrt(sum( ustd.^2,1)),'kx:'); hold on
legend('HEU fissions','Error bounds',0)
semilogy(tt,sum( uflux,1)-sqrt(sum( ustd.^2,1)),'kx:');
title('HEU Fission Rate')
xlabel('Time - sec')
ylabel('Fissions')

figure(c), clf reset, c = c + 1;
semilogy(tt(:,2:ntt),sum( uflux(:,2:ntt),1),'k-',tt(:,2:ntt),sum(
uflux(:,2:ntt),1)+sqrt(sum( ustd(:,2:ntt).^2,1)),'kx:'); hold on
semilogy(tt(:,2:ntt),sum( uflux(:,2:ntt),1)-sqrt(sum( ustd(:,2:ntt).^2,1)),'kx:');
legend('HEU fissions','Error bounds',0)
title('HEU Fission Rate')
xlabel('Time - sec')
ylabel('Fissions')

nlinedets = ceil(nduw.*(ntt + 1).*2./8) + ceil(nlin.*(ntt + 1).*2./8) + ceil(nair.*(ntt +
1).*2./8);
%  This is the number of lines for tally data for neutrons
nlineuw = ceil(nduw.*(ntt + 1).*2./8);
nlinlin = ceil(nlin.*(ntt + 1).*2./8);
nlinair = ceil(nair.*(ntt + 1).*2./8);

temp = zeros(9,nlinedets,3);

for i = 1:nlinedets
    temp(:,(i-1)*8+1:i*8,1) = [no1(i,:);           no2(i,:);           no3(i,:);
no4(i,:);           no5(i,:);           no6(i,:);           no7(i,:);           no8(i,:);
no9(i,:)];
    temp(:,(i-1)*8+1:i*8,2) = [pu1(i+nlinefiss,:); pu2(i+nlinefiss,:);
pu3(i+nlinefiss,:); pu4(i+nlinefiss,:); pu5(i+nlinefiss,:); pu6(i+nlinefiss,:);
pu7(i+nlinefiss,:); pu8(i+nlinefiss,:); pu9(i+nlinefiss,:)];
    temp(:,(i-1)*8+1:i*8,3) = [u1(i+nlinefiss,:);  u2(i+nlinefiss,:);  u3(i+nlinefiss,:);
u4(i+nlinefiss,:);  u5(i+nlinefiss,:);  u6(i+nlinefiss,:);  u7(i+nlinefiss,:);
u8(i+nlinefiss,:);  u9(i+nlinefiss,:)];
end

%  Clear laoded files to free memory.
clear no1 no2 no3 no4 no5 no6 no7 no8 no9 pu1 pu2 pu3 pu4 pu5 pu6 pu7 pu8 pu9 u1 u2 u3 u4
u5 u6 u7 u8 u9

%  The current 'temp' file includes lots of extra zero-entries, so I'll
%  consolidate now to make the next steps easier.
temp1 = zeros(9,ndet.*(ntt + 1).*2,3);

temp1(:,1:nduw.*(ntt+1).*2,:) = temp(:,1:nduw.*(ntt+1).*2,:);
temp1(:,nduw.*(ntt+1).*2+1:(nduw+nlin).*(ntt+1).*2,:) =
temp(:,8.*nlineuw+1:8.*nlineuw+nlin.*(ntt+1).*2,:);
temp1(:,(nduw+nlin).*(ntt+1).*2+1:ndet.*(ntt+1).*2,:) =
temp(:,8.*(nlineuw+nlinlin)+1:8.*(nlineuw+nlinlin)+nair.*(ntt+1).*2,:);

%  Break up into groups of NO SFM, PU, and HEU
nondat = temp1(:,1:ndet.*(ntt+1).*2,1);
pundat = temp1(:,1:ndet.*(ntt+1).*2,2);
undat  = temp1(:,1:ndet.*(ntt+1).*2,3);

clear temp temp1
```

```
%  Create flux and error matrices
nonfluxdat = nondat(:,1:2:ndet.*(ntt+1).*2-1);
nonstddat  = nondat(:,1:2:ndet.*(ntt+1).*2-1).*nondat(:,2:2:ndet.*(ntt+1).*2);
punfluxdat = pundat(:,1:2:ndet.*(ntt+1).*2-1);
punstddat  = pundat(:,1:2:ndet.*(ntt+1).*2-1).*pundat(:,2:2:ndet.*(ntt+1).*2);
unfluxdat  = undat(:,1:2:ndet.*(ntt+1).*2-1);
unstddat   = undat(:,1:2:ndet.*(ntt+1).*2-1).*undat(:,2:2:ndet.*(ntt+1).*2);

nonflux = zeros(9,ntt,ndet);
nonstd = zeros(9,ntt,ndet);
punflux = zeros(9,ntt,ndet);
punstd = zeros(9,ntt,ndet);
unflux = zeros(9,ntt,ndet);
unstd = zeros(9,ntt,ndet);

for i = 1:ndet
    for j = 1:9
        nonflux(j,:,i) = nonfluxdat(j,(i-1)*(ntt+1)+1:i*(ntt+1)-1);%./tscale;
        nonstd(j,:,i)  = nonstddat(j,(i-1) *(ntt+1)+1:i*(ntt+1)-1);%./tscale;
        punflux(j,:,i) = punfluxdat(j,(i-1)*(ntt+1)+1:i*(ntt+1)-1);%./tscale;
        punstd(j,:,i)  = punstddat(j,(i-1) *(ntt+1)+1:i*(ntt+1)-1);%./tscale;
         unflux(j,:,i) =  unfluxdat(j,(i-1)*(ntt+1)+1:i*(ntt+1)-1);%./tscale;
         unstd(j,:,i)  =  unstddat(j,(i-1) *(ntt+1)+1:i*(ntt+1)-1);%./tscale;
    end
end

% %  Create differential flux and error matrices
% punfluxdiff = punflux - nonflux;
% punstddiff  = (punstd.^2 + nonstd.^2).^0.5;
%  unfluxdiff =  unflux - nonflux;
%  unstddiff  = ( unstd.^2 + nonstd.^2).^0.5;
%

% Plot data for no SFM
figure(c), clf reset, c = c + 1;
surf(tt,ypos,sum(nonflux,3))
% colormap gray
title('No SFM Present, Scatter Rxns')
xlabel('Time - sec')
ylabel('Y-Pos of det along boat - cm')

figure(c), clf reset, c = c + 1;
surf(tt(:,2:ntt),ypos,sum(nonflux(:,2:ntt),3))
% colormap gray
title('No SFM Present, Scatter Rxns')
xlabel('Time - sec')
ylabel('Y-Pos of det along boat - cm')

% Plot data for WGPu
figure(c), clf reset, c = c + 1;
surf(tt,ypos,sum(punflux,3))
% colormap gray
title('PU Scatter Rxns')
xlabel('Time - sec')
ylabel('Y-Pos of det along boat - cm')

figure(c), clf reset, c = c + 1;
surf(tt(:,2:ntt),ypos,sum(punflux(:,2:ntt),3))
% colormap gray
title('PU Scatter Rxns')
xlabel('Time - sec')
ylabel('Y-Pos of det along boat - cm')

figure(c), clf reset, c = c + 1;
semilogy(tt,sum(punflux,1),'k-' ,tt,sum(punflux,1)+sqrt(sum(punstd.^2,1)),'kx:'); hold on
semilogy(tt,sum(nonflux,1),'k--',tt,sum(nonflux,1)+sqrt(sum(nonstd.^2,1)),'k+:');
```

```
legend('Pu scatters','Pu Error bounds','No SFM scatters','No SFM Error bounds',0)
semilogy(tt,sum(punflux,1)-sqrt(sum(punstd.^2,1)),'kx:');
semilogy(tt,sum(nonflux,1)-sqrt(sum(nonstd.^2,1)),'k+:');
title('PU vs None Scatter Rxns')
xlabel('Time - sec')
ylabel('Scatters')

figure(c), clf reset, c = c + 1;
semilogy(tt(:,2:ntt),sum(punflux(:,2:ntt),1),'k-'
,tt(:,2:ntt),sum(punflux(:,2:ntt),1)+sqrt(sum(punstd(:,2:ntt).^2,1)),'kx:'); hold on
semilogy(tt(:,2:ntt),sum(nonflux(:,2:ntt),1),'k--
',tt(:,2:ntt),sum(nonflux(:,2:ntt),1)+sqrt(sum(nonstd(:,2:ntt).^2,1)),'k+:');
legend('Pu scatters','Pu Error bounds','No SFM scatters','No SFM Error bounds',0)
semilogy(tt(:,2:ntt),sum(punflux(:,2:ntt),1)-sqrt(sum(punstd(:,2:ntt).^2,1)),'kx:');
semilogy(tt(:,2:ntt),sum(nonflux(:,2:ntt),1)-sqrt(sum(nonstd(:,2:ntt).^2,1)),'k+:');
title('PU vs None Scatter Rxns')
xlabel('Time - sec')
ylabel('Scatters')

for i = 1:9
    figure(c), clf reset, c = c + 1;
    semilogy(tt,punflux(i,:),'k-' ,tt,punflux(i,:)+punstd(i,:),'kx:'); hold on
    semilogy(tt,nonflux(i,:),'k--',tt,nonflux(i,:)+nonstd(i,:),'k+:');
    legend('Pu scatters','Pu Error bounds','No SFM scatters','No SFM Error bounds',0)
    semilogy(tt,punflux(i,:)-punstd(i,:),'kx:');
    semilogy(tt,nonflux(i,:)-nonstd(i,:),'k+:');
    str = sprintf('PU vs None Scatter Rxn Data for y = %3.0d cm',ypos(i));
    title(str);
    xlabel('Time - sec')
    ylabel('Scatters')
    figure(c), clf reset, c = c + 1;
    semilogy(tt(:,2:ntt),punflux(i,2:ntt),'k-'
,tt(:,2:ntt),punflux(i,2:ntt)+punstd(i,2:ntt),'kx:'); hold on
    semilogy(tt(:,2:ntt),nonflux(i,2:ntt),'k--
',tt(:,2:ntt),nonflux(i,2:ntt)+nonstd(i,2:ntt),'k+:');
    legend('Pu scatters','Pu Error bounds','No SFM scatters','No SFM Error bounds',0)
    semilogy(tt(:,2:ntt),punflux(i,2:ntt)-punstd(i,2:ntt),'kx:');
    semilogy(tt(:,2:ntt),nonflux(i,2:ntt)-nonstd(i,2:ntt),'k+:');
    str = sprintf('PU vs None Scatter Rxn Data for y = %3.0d cm',ypos(i));
    title(str);
    xlabel('Time - sec')
    ylabel('Scatters')
end

% Plot data for HEU

figure(c), clf reset, c = c + 1;
surf(tt,ypos,sum(unflux,3))
% colormap gray
title('HEU Scatter Rxns')
xlabel('Time - sec')
ylabel('Y-Pos of det along boat - cm')

figure(c), clf reset, c = c + 1;
surf(tt(:,2:ntt),ypos,sum(unflux(:,2:ntt),3))
% colormap gray
title('HEU Scatter Rxns')
xlabel('Time - sec')
ylabel('Y-Pos of det along boat - cm')

figure(c), clf reset, c = c + 1;
semilogy(tt,sum( unflux,1),'k-' ,tt,sum( unflux,1)+sqrt(sum( unstd.^2,1)),'kx:'); hold on
semilogy(tt,sum(nonflux,1),'k--',tt,sum(nonflux,1)+sqrt(sum(nonstd.^2,1)),'k+:');
legend('HEU scatters','HEU Error bounds','No SFM scatters','No SFM Error bounds',0)
semilogy(tt,sum( unflux,1)-sqrt(sum( unstd.^2,1)),'kx:');
semilogy(tt,sum(nonflux,1)-sqrt(sum(nonstd.^2,1)),'k+:');
title('HEU vs None Scatter Rxns')
```

```
xlabel('Time - sec')
ylabel('Scatters')

figure(c), clf reset, c = c + 1;
semilogy(tt(:,2:ntt),sum( unflux(:,2:ntt),1),'k-' ,tt(:,2:ntt),sum(
unflux(:,2:ntt),1)+sqrt(sum( unstd(:,2:ntt).^2,1)),'kx:'); hold on
semilogy(tt(:,2:ntt),sum(nonflux(:,2:ntt),1),'k--
',tt(:,2:ntt),sum(nonflux(:,2:ntt),1)+sqrt(sum(nonstd(:,2:ntt).^2,1)),'k+:');
legend('HEU scatters','HEU Error bounds','No SFM scatters','No SFM Error bounds',0)
semilogy(tt(:,2:ntt),sum( unflux(:,2:ntt),1)-sqrt(sum( unstd(:,2:ntt).^2,1)),'kx:');
semilogy(tt(:,2:ntt),sum(nonflux(:,2:ntt),1)-sqrt(sum(nonstd(:,2:ntt).^2,1)),'k+:');
title('HEU vs None Scatter Rxns')
xlabel('Time - sec')
ylabel('Scatters')

for i = 1:9
    figure(c), clf reset, c = c + 1;
    semilogy(tt, unflux(i,:),'k-' ,tt, unflux(i,:)+ unstd(i,:),'kx:'); hold on
    semilogy(tt,nonflux(i,:),'k--',tt,nonflux(i,:)+nonstd(i,:),'k+:');
    legend('HEU scatters','HEU Error bounds','No SFM scatters','No SFM Error bounds',0)
    semilogy(tt, unflux(i,:)- unstd(i,:),'kx:');
    semilogy(tt,nonflux(i,:)-nonstd(i,:),'k+:');
    str = sprintf('HEU vs None Scatter Rxn Data for y = %3.0d cm',ypos(i));
    title(str);
    xlabel('Time - sec')
    ylabel('Scatters')
    figure(c), clf reset, c = c + 1;
    semilogy(tt(:,2:ntt), unflux(i,2:ntt),'k-' ,tt(:,2:ntt), unflux(i,2:ntt)+
unstd(i,2:ntt),'kx:'); hold on
    semilogy(tt(:,2:ntt),nonflux(i,2:ntt),'k--
',tt(:,2:ntt),nonflux(i,2:ntt)+nonstd(i,2:ntt),'k+:');
    legend('HEU scatters','HEU Error bounds','No SFM scatters','No SFM Error bounds',0)
    semilogy(tt(:,2:ntt), unflux(i,2:ntt)- unstd(i,2:ntt),'kx:');
    semilogy(tt(:,2:ntt),nonflux(i,2:ntt)-nonstd(i,2:ntt),'k+:');
    str = sprintf('HEU vs None Scatter Rxn Data for y = %3.0d cm',ypos(i));
    title(str);
    xlabel('Time - sec')
    ylabel('Scatters')
end

figure(c), clf reset, c = c + 1;
semilogy(tt,sum( unflux,1),'k-o'); hold on
semilogy(tt,sum(punflux,1),'k-s');
title('HEU vs Pu Scatter Rxns')
legend('HEU','Pu',0)
xlabel('Time - sec')
ylabel('Scatters')

figure(c), clf reset, c = c + 1;
semilogy(tt(:,2:ntt),sum( unflux(:,2:ntt),1),'k-o'); hold on
semilogy(tt(:,2:ntt),sum(punflux(:,2:ntt),1),'k-s');
title('HEU vs Pu Scatter Rxns')
legend('HEU','Pu',0)
xlabel('Time - sec')
ylabel('Scatters')
```

The following script was for the calculation of the detector response function.

```
function [f] = fyt(y,t,opt)
%   Function 'fyt' is the fitted shape function of detector response.
%   'opt' is the numerical flag for the fit with respect Pu (opt = 1) or
%   HEU (opt = 2).
%
```

```
%  The form of the function is
%       fyt(y,t) = Y(y)*T(t)'

if opt == 1
    A = 158087.3309;
elseif opt == 2
    A = 55565.03464;
end

f = A.*Y(y,opt)'*T(t,opt);
```

The following script was for the dose response function.

```
function [f] = fytD(y,t,opt)
%   Function 'fytD' is the fitted shape function of detector response.
%   'opt' is the numerical flag for the fit with respect Pu (opt = 1) or
%   HEU (opt = 2).
%
%  This particular curve is for the dose rate to the ICRU sphere.
%
%  The form of the function is
%       fyt(y,t) = Y(y)*T(t)'

if opt == 1
    A = 158087.3309;
elseif opt == 2
    A = 55565.03464;
end

f = A.*Y(y,opt)'*T(t,opt);
```

The following script was for the calculation of the shape component of the detector response function.

```
function [yp] = Y(y,opt)
%
%  Function Y(y,opt) requires 2 input arguments, the first is the position
%  vector (may be vector or single valued).  'opt' is the numerical flag
%  for the fit with respect Pu (opt = 1) or HEU (opt = 2).
%
%  The form of the function is
%       Y(y) = 660*a/(y*pi)*exp(-c*(log(y*pi/660)-b)^2) ...
%                + m*exp(-n*(y*pi/660-o)^2)

if opt == 1
    a = 1.396e-6;
    b = 0.3082;
    c = 6.122;
    m = 3.809e-7;
    n = 3.028;
    o = 0.6955;
elseif opt == 2
    a = 3.336e-6;
    b = 0.361;
    c = 5.879;
    m = 1.943e-6;
    n = 1.975;
```

```
    o = 0.9621;
end

yp = 660.*a./y./pi.*exp(-c.*(log(y.*pi./660)-b).^2) ...
    + m.*exp(-n.*(y.*pi./660-o).^2);
```

The following script was for the calculation of the shape component of the dose response function.

```
function [yp] = YD(y,opt)
%
%  Function YD(y,opt) requires 2 input arguments, the first is the position
%  vector (may be vector or single valued).  'opt' is the numerical flag
%  for the fit with respect Pu (opt = 1) or HEU (opt = 2).
%
%  This particular curve is for the dose rate to the ICRU sphere.
%
%  The form of the function is
%       Y(y) = 660*a/(y*pi)*exp(-c*(log(y*pi/660)-b)^2) ...
%               + m*exp(-n*(y*pi/660-o)^2)

if opt == 1
    a = 0.0005044;
    b = 0.4102;
    c = 4.094;
    m = 0.0001954;
    n = 1.922;
    o = 0.6735;
elseif opt == 2
    a = 0.002661;
    b = 0.4092;
    c = 4.125;
    m = 0.001034;
    n = 1.989;
    o = 0.6747;
end

yp = 660.*a./y./pi.*exp(-c.*(log(y.*pi./660)-b).^2) ...
    + m.*exp(-n.*(y.*pi./660-o).^2);
```

The following script was for the calculation of the die-away component of the detector response function.

```
function [tr] = T(t,opt)
%
%  Function T(t,opt) requires 2 input arguments, the first is the time
%  vector (may be vector or single valued).  'opt' is the numerical flag
%  for the fit with respect Pu (opt = 1) or HEU (opt = 2).
%
%  The form of the function is
%      T(t) = A*exp(-B*t) + C*exp(-D*t)

if opt == 1
    a = -2.595e-6;
    b = 2915;
```

```
    c = 8.999e-6;
    d = 1597;
elseif opt == 2
    a = 3.102e-5;
    b = 2174;
    c = 4.258e-6;
    d = 1040;
end

tr = a.*exp(-b.*t) + c.*exp(-d.*t);
```

The following script was for the calculation of the die-away component of the dose response function.

```
function [tr] = TD(t,opt)
%
%  Function T(t,opt) requires 2 input arguments, the first is the time
%  vector (may be vector or single valued).  'opt' is the numerical flag
%  for the fit with respect Pu (opt = 1) or HEU (opt = 2).
%
%  This particular curve is for the dose rate to the ICRU sphere.
%
%  The form of the function is
%      T(t) = A*exp(-B*t) + C*exp(-D*t)

if opt == 1
    a = -0.0001149;
    b = 6141;
    c = 0.000109;
    d = 1648;
elseif opt == 2
    a = 0.0005744;
    b = 2115;
    c = 3.278e-5;
    d = 844.1;
end

tr = a.*exp(-b.*t) + c.*exp(-d.*t);
```

VITA

Norman Alfan Johansen, III, was born 13 June 1978, in Metairie, Louisiana, to Barbara and Norman Johansen, Jr. He grew up in the New Orleans suburb and attended Brother Martin High School in New Orleans, graduating in 1996. He earned his baccalaureate degree from The University of Tennessee, Knoxville, earning a B.S. in Nuclear Engineering in May 2002. He enrolled in graduate school at Texas A&M University in the Fall of 2002 to pursue a master's degree in Nuclear Engineering.

Norman may be reached via the Nuclear Engineering Department office at 129 Zachry Engineering Center, 3133 TAMU, College Station, TX 77843-3133. His e-mail address is TreyJohansen@TAMU.edu.